Integrated Ocean Drilling Program
Expedition 338 Preliminary Report

NanTroSEIZE Stage 3:
NanTroSEIZE plate boundary deep riser 2

1 October 2012–13 January 2013

Gregory Moore, Kyuichi Kanagawa, Michael Strasser, Brandon Dugan, Lena Maeda, Sean Toczko, and the Expedition 338 Scientists

Published by
Integrated Ocean Drilling Program Management International, Inc.,
for the Integrated Ocean Drilling Program

Publisher's notes

Citation:
Moore, G., Kanagawa, K., Strasser, M., Dugan, B., Maeda, L., Toczko, S., and the Expedition 338 Scientists, 2013. NanTroSEIZE Stage 3: NanTroSEIZE plate boundary deep riser 2. *IODP Prel. Rept.*, 338. doi:10.2204/iodp.pr.338.2013

Distribution:
Electronic copies of this series may be obtained from the Integrated Ocean Drilling Program (IODP) Scientific Publications homepage on the World Wide Web at **www.iodp.org/scientific-publications/.**

This publication was prepared by the Japanese Implementing Organization, Center for Deep Earth Exploration (CDEX) at the Japan Agency for Marine-Earth Science and Technology (JAMSTEC), as an account of work performed under the international Integrated Ocean Drilling Program (IODP), which is managed by IODP Management International (IODP-MI), Inc. Funding for the program is provided by the following agencies:

National Science Foundation (NSF), United States

Ministry of Education, Culture, Sports, Science and Technology (MEXT), Japan

European Consortium for Ocean Research Drilling (ECORD)

Ministry of Science and Technology (MOST), People's Republic of China

Korea Institute of Geoscience and Mineral Resources (KIGAM)

Australian Research Council (ARC) and GNS Science (New Zealand), Australian/New Zealand Consortium

Ministry of Earth Sciences (MoES), India

Coordination for Improvement of Higher Education Personnel, Brazil

Disclaimer

March 2013

Expedition 338 participants

Expedition 338 scientists

Brandon Dugan (2 Nov–21 Dec 2012)
Co-Chief Scientist
Department of Earth Sciences
Rice University
6100 Main Street, MS-126
Houston TX 77005
USA
dugan@rice.edu

Kyuichi Kanagawa (25 Nov–13 Dec 2012)
Co-Chief Scientist
Department of Earth Sciences
Chiba University
1-33 Yayoi-cho, Inage-Ku Chiba
Chiba 263-8522
Japan
kyu_kanagawa@faculty.chiba-u.jp

Gregory Moore (13 Oct–2 Nov 2012 and 21 Dec 2012–13 Jan 2013)
Co-Chief Scientist
Department of Geology and Geophysics
University of Hawaii
1680 East-West Road
Honolulu HI 96822
USA
gmoore@hawaii.edu

Michael Strasser (13 Oct–27 Nov 2012)
Co-Chief Scientist
Geological Institute
ETH Zurich
Sonneggstrasse 5
8092 Zurich
Switzerland
strasser@erdw.ethz.ch

Lena Maeda (3–17 Oct, 5–27 Nov, and 21 Dec 2012–13 January 2013)
Expedition Project Manager/Staff Scientist
Center for Deep Earth Exploration
Japan Agency for Marine-Earth Science and Technology
3173-25 Showa-machi
Kanazawa-ku, Yokohama
Kanagawa 236-0001
Japan
maedal@jamtec.go.jp

Sean Toczko (13 Oct–5 Nov, 27 Nov–21 Dec 2012, and 6–13 Jan 2013)
Expedition Project Manager/Staff Scientist
Center for Deep Earth Exploration
Japan Agency for Marine-Earth Science and Technology
3173-25 Showa-machi
Kanazawa-ku, Yokohama
Kanagawa 236-0001
Japan
sean@jamstec.go.jp

Yukari Kido (16 Oct–5 Nov and 27 Nov–14 Dec 2012)
Logging Staff Scientist
Center for Deep Earth Exploration
Japan Agency for Marine-Earth Science and Technology
3173-25 Showa-machi
Kanazawa-ku, Yokohama
Kanagawa 236-0001
Japan
ykido@jamstec.go.jp

Moe Kyaw Thu (26 Dec 2012–6 Jan 2013)
Logging Staff Scientist
Center for Deep Earth Exploration
Japan Agency for Marine-Earth Science and Technology
3173-25 Showa-machi
Kanazawa-ku, Yokohama
Kanagawa 236-0001
Japan
moe@jamstec.go.jp

Yoshinori Sanada (5–16 Nov, 4–13 Dec, and 21 Dec 2012–2 Jan 2013)
Logging Staff Scientist
Center for Deep Earth Exploration
Japan Agency for Marine-Earth Science and Technology
3173-25 Showa-machi
Kanazawa-ku, Yokohama
Kanagawa 236-0001
Japan
sanada@jamstec.go.jp

Lionel Esteban (25 Nov 2012–13 Jan 2013)
Physical Properties Specialist
Commonwealth Scientific and Industrial Research Organization-Earth Science and Resource Engineering, Australia-New Zealand IODP Consortium (CSIRO/ANZIC)
26 Dick Perry Avenue
Perth, Kensington
Western Australia 6151
Australia
lionel.esteban@csiro.au

Olivier Fabbri (25 Nov 2012–13 Jan 2013)
Structural Geologist
Chrono-Environment Laboratory
University of Franche-Comté
16 Route de Gray
25000 Besançon
France
olivier.fabbri@univ-fcomte.fr

Jacob Geersen (13 Oct–27 Nov 2012)
Structural Geologist
School of Ocean and Earth Science
National Oceanography Centre, Southampton
University of Southampton
European Way
Southampton SO14 3ZH
United Kingdom
j.geersen@noc.soton.ac.uk

Sebastian Hammerschmidt (16 Oct–1 Dec 2012)
Gas/Pore Water Geochemist
MARUM–Center for Marine Environmental Sciences
Leobener Strasse
28359 Bremen
Germany
hammerschmidt@uni-bremen.de

Katrien Heirman (25 Nov 2012–13 Jan 2013)
Sedimentologist
Department of Geology and Soil Science
Renard Centre of Marine Geology
Ghent University
Krijgslaan 281 S8 (WE13)
B-9000 Gent
Belgium
Katrien.Heirman@gmail.com

Andre Huepers (13 Oct–1 Dec 2012)
Physical Properties Specialist
MARUM–Center for Marine Environmental Sciences
Leobener Strasse
28359 Bremen
Germany
andre.huepers@uni-bremen.de

Maria José Jurado Rodriguez (13 Oct–1 Dec 2012)
Logging Specialist (sedimentology)
Instituto de Ciencias de la Tierra Jaume Almera (CSIC)
Lluis Sole Sabaris s/n
E-08028 Barcelona
Spain
mjjurado@ictja.csic.es

Hiroko Kitajima (25 Nov 2012–13 Jan 2013)
Physical Properties Specialist
Geological Survey of Japan
National Institute of Advanced Industrial Science and Technology
Central 7, 1-1-1 Higashi
Ibaraki 305-8567
Japan
h-kitajima@aist.go.jp

Harue Masuda (25 Nov 2012–13 Jan 2013)
Geochemist
Department of Geosciences
Osaka City University
3-3-138 Sugimoto, Sumiyoshi-ku
Osaka 558-8585
Japan
harue@sci.osaka-cu.ac.jp

Kitty Milliken (25 Nov 2012–13 Jan 2013)
Sedimentologist
Bureau of Economic Geology
University of Texas at Austin
Austin TX 78713
USA
kittym@utexas.edu

Ravi Mishra (13 Oct–1 Dec 2012)
Sedimentologist
National Centre for Antarctic and Ocean Research (NCAOR)
Ministry of Earth Sciences, Government of India, NCAOR, Headland Sada
Vasco
Goa 403 804
India
ravimishra@rediffmail.com

Katelyn Olcott (13 Oct–1 Dec 2012)
Physical Properties/Downhole Measurements Specialist
Department of Geosciences
Rock and Sediment Mechanics Laboratory
The Pennsylvania State University
312 Deike Building
University Park PA 16802
USA
katelyn@psu.edu

Kiyokazu Oohashi (25 Nov 2012–13 Jan 2013)
Structural Geologist
Graduate School of Science
Chiba University
1-33 Yayoi-cho
Chiba 263-8522
Japan
oohashik@earth.s.chiba-u.ac.jp

Kevin T. Pickering (13 Oct–27 Nov 2012)
Sedimentologist
Department of Earth Sciences
University College London
Gower Street
London WC1E 6BT
United Kingdom
ucfbktp@ucl.ac.uk

Sebastian G. Ramirez (25 Nov 2012–13 Jan 2013)
Sedimentologist
Institute for Geophysics
University of Texas at Austin
10100 Burnet Road, Building 196, 3.102J
Austin TX 78758
USA
sgramirez@utexas.edu

Harunur Rashid (13 Oct–1 Dec 2012)
Gas/Pore Water Geochemist
School of Earth Sciences
The Ohio State University
1090 Carmack Road
Columbus OH 43210
USA
rashid.29@osu.edu

Anja Schleicher (13 Oct–1 Dec 2012)
Sedimentologist
Department of Earth and Environmental Sciences
University of Michigan
1100 North University Avenue
Ann Arbor MI 48109
USA
aschleic@umich.edu

Yehua Shan (25 Nov 2012–13 Jan 2013)
Structural Geologist
Laboratory of Marginal Sea Geology
Guangzhou Institute of Geochemistry
Chinese Academy of Sciences
511 Kehua Street, Tiande District
Guangzhou 510640
China
shanyh@gig.ac.cn

Robert Skarbek (25 Nov 2012–13 Jan 2013)
Logging Specialist (physical properties)
Department of Geological Sciences
University of Oregon
1272 University of Oregon
Eugene OR 97403
USA
rskarbek@uoregon.edu

Insun Song (13 Oct–1 Dec 2012)
Physical Properties Specialist
Korea Institute of Geoscience and Mineral Resources
124 Gwahangno, Yuseong
Daejeon 305-350
Korea
isong@kigam.re.kr

Toru Takeshita (13 Oct–1 Dec 2012)
Structural Geologist
Natural History Sciences
Hokkaido University
N10 W8 Kita-Ku
Sapporo Hokkaido 060-0810
Japan
torutake@mail.sci.hokudai.ac.jp

Tomohiro Toki (25 Nov 2012–13 Jan 2013)
Geochemistry
Faculty of Science
University of the Ryukyus
1, Senbaru, Nishihara
Okinawa 903-0213
Japan
toki@sci.u-ryukyu.ac.jp

Joanne Tudge (25 Nov 2012–13 Jan 2013)
Logging Specialist (lithostratigraphy)
Department of Geoscience
University of Wisconsin-Madison
1215 West Dayton Street
Madison WI 53706
USA
jtudge@geology.wisc.edu

Susanna Webb (13 Oct–1 Dec 2012)
Logging Specialist (structural geology)
Department of Geoscience
University of Wisconsin-Madison
1215 West Dayton Street
Madison WI 53706
USA
siwebb@wisc.edu

Dean J. Wilson (25 Nov 2012–13 Jan 2013)
Logging Specialist (structural geology)
School of Ocean and Earth Science
National Oceanography Centre, Southampton
University of Southampton
European Way
Southampton SO14 3ZH
United Kingdom
d.j.wilson@soton.ac.uk

Hung-Yu (Sonata) Wu (25 Nov–14 Dec 2012)
Logging Specialist (structural geology)
Institute for Research on Earth Evolution
Japan Agency for Marine-Earth Science and Technology
3173-25 Showa-machi
Yokohama
Kanagawa 236-0001
Japan
sonata@jamstec.go.jp

Asuka Yamaguchi (13 Oct–1 Dec 2012)
Structural Geologist
Atmosphere and Ocean Research Institute
The University of Tokyo
5-1-5 Kashiwanoha
Kashiwa Chiba 277-8564
Japan
asuka@aori.u-tokyo.ac.jp

NanTroSEIZE chief project scientists

Masataka Kinoshita
Chief Project Scientist
Institute for Research on Earth Evolution
Japan Agency for Marine-Earth Science and Technology
2-15 Natsushima-cho, Yokosuka
Kanagawa 237-0061
Japan
masa@jamstec.go.jp

Harold Tobin
Chief Project Scientist
Department of Geology and Geophysics
University of Wisconsin-Madison
1215 West Dayton Street
Madison WI 53706
USA
htobin@wisc.edu

NanTroSEIZE specialty coordinators

Toshiya Kanamatsu (14 Dec 2012–2 Jan 2013)
Paleomagnetism/Biostratigraphy
Institute for Research on Earth Evolution
Japan Agency for Marine-Earth Science and Technology
2-15 Natsushima-cho, Yokosuka
Kanagawa 237-0061
Japan
toshiyak@jamstec.go.jp

Gaku Kimura
Structural Geology
Department of Earth and Planetary Science
Graduate School of Science
University of Tokyo
7-3-1 Hongo, Bunkyo-ku
Tokyo 113-0033
Japan
gaku@eps.s.u-tokyo.ac.jp

Gregory Moore (25–29 Nov 2012)
Core-Log-Seismic Integration
Department of Geology and Geophysics
University of Hawaii
1680 East-West Road
Honolulu HI 96822
USA
gmoore@hawaii.edu

Demian Saffer (27–29 Nov 2012)
Physical Properties
The Pennsylvania State University
Deike Building
University Park PA 16802
USA
dsaffer@psu.edu

Michael B. Underwood (23–29 Nov 2012)
Sedimentology
University of Missouri
307 Geology Building
Columbia MO 65211
USA
underwoodm@missouri.edu

Geoff Wheat (23–27 Nov 2012)
Geochemistry
School of Fisheries and Ocean Sciences
University of Alaska Fairbanks
PO Box 475
Moss Landing CA 99775
USA
wheat@mbari.org

Shore-based personnel and technical representatives

Micropaleontologists
Koji Kameo (Chiba University)
Isao Motoyama (Yamagta University)

Shipboard personnel and technical representatives

Captains (Mantle Quest Japan)
Yasushi Minoura
Yuji Onda

Offshore Installation Managers (Mantle Quest Japan)
Peter Hetherington
Masayuki Kawasaki

Operations Superintendents (CDEX)
Tomokazu Saruhashi
Ikuo Sawada

Drilling Engineers (CDEX)
Daiji Ikenomoto
Sho Kataoka
Tadashi Otani
Koji Takase
Takahiro Yokoyama

Downhole Tool Engineers (Schlumberger)
Fifai Achmad
Tomas Cosendey
Wang Feng
Kai Shao
Tan Chee Sing

Mud logging Engineers (Geoservices)
Pawan Kumar
U Myo Kyaw
Nguyen Quang Luc
Maung Ya Wai
Sorab Talati
Tasmin

Mud Engineers (Telnite)
Hiroki Ishikawa
Katsuki Mori
Masato Sawaguchi

Laboratory Officers (Marine Works Japan)
Satoshi Hirano
Hiroaki Muraki
Tomoyuki Tanaka

Curators (Marine Works Japan)
Yohei Arakawa
Toshikuni Yabuki
Masaru Yasunaga

Laboratory Technicians (Marine Works Japan)
Mitsuru Arata
Nobuhiro Anraku
Akihiko Fujihara
Chisato Fujita
Yuji Fuwa
Kazuki Harumoto
Kazeta Hashimoto
Kentaro Hatakeda
Hiroyuki Hayashi
Takehiro Higashi
Yuya Hitomi
Hiroshi Hoshino
Asuna Kamijo
Yasuhiro Kawaguchi
Tatsuya Kawai
Sayaka Kawamura
Yoshiki Kido
Shunsuke Miyabe
Ayako Miura
Yoshitomo Mochizuki
Soichi Moriya
Teina Nakashima
Masahiro Nishimura
Atsushi Ohashi
Satomi Saito
Masumi Sakaguchi
Kiyoshi Shiono
Hiromichi Soejima
Fuko Sugimoto
Takahiro Suzuki
Kazuma Takahashi
Yasumi Yamada
Nagisa Yamamoto
Kazuhiro Yoshida

Operations Geologists
Kan Aoike (CDEX)
Taiki Sawada (JGI)
Takamitsu Sugihara (CDEX)
Takanao Yoshii (JGI)

Coring Specialist (CDEX)
Yuichi Shinmoto

Technical Engineers (CDEX)
Eigo Miyazaki
Yasuyuki Yamazaki

Publications Assistants
Yoko Okamoto (Marine Works Japan)
Jean Wulfson (USIO)

Outreach Manager (CDEX)
Tadashi Yoshizawa

Tool Pushers/Coring Supervisors (Mantle Quest Japan)
Geoffrey Cook
Teruyuki Koyama
Atsushi Oikawa
Paul Thornton

Underreamer Engineers (NOV)
Glyn Christopher Edwards
Robert Hershberger

Abstract

The Nankai Trough Seismogenic Zone Experiment (NanTroSEIZE) is a multidisciplinary scientific project designed to investigate fault mechanics and seismogenesis along subduction megathrusts through reflection and refraction seismic imaging, direct sampling, in situ measurements, and long-term monitoring in conjunction with laboratory and numerical modeling studies. The fundamental scientific objectives of NanTroSEIZE include characterizing the nature of fault slip and strain accumulation, fault and wall rock composition, fault architecture, and state variables throughout an active plate boundary system. As part of the NanTroSEIZE program, operations during Integrated Ocean Drilling Program (IODP) Expedition 338 were planned to extend and case riser IODP Hole C0002F, begun during IODP Expedition 326 in 2010, from 856 to 3600 meters below the seafloor (mbsf). Riser operations extended the hole to 2005.5 mbsf, collecting a full suite of logging-while-drilling (LWD) and measurement-while-drilling, mud gas, and cuttings data. However, because of damage to the riser during unfavorable winds and strong current conditions, riser operations were cancelled. Hole C0002F was suspended at 2005.5 mbsf and left for reentry during future riser drilling operations, which will deepen the hole to penetrate the megasplay fault at ~5000 mbsf.

Contingency riserless operations included coring at Site C0002 (200–505, 902–940, and 1100.5–1120 mbsf), LWD at IODP Sites C0012 (0–709 mbsf) and C0018 (0–350 mbsf), and LWD and coring at IODP Sites C0021 (0–294 mbsf) and C0022 (0–420 mbsf). These sites and drilling intervals represent key targets not sampled during previous NanTroSEIZE expeditions but relevant to comprehensively characterize the alteration stage of the oceanic basement input to the subduction zone, the early stage of Kumano Basin evolution, gas hydrates in the forearc basin, and recent activity of the shallow megasplay fault zone system and submarine landslides.

Principal results of Expedition 338 include the following:

- LWD, mud-gas monitoring, and analyses of cuttings from the deep riser hole characterize two lithologic units within the inner wedge of the accretionary prism at Site C0002, separated by a prominent fault zone at ~1640 mbsf. Internal style of deformation, downhole increase of thermogenically formed gas, and evidence for mechanical compaction and cementation document a complex structural evolution and provide unprecedented insights into the mechanical state and behavior of the wedge at depth.

- Multiple samples of the boundary between the Kumano Basin section and the underlying accretionary prism at Site C0002 shed new light on this unconformity, the interpretation of which was debatable from previous samples and data. New samples suggest that variable erosional processes were active on small spatial scales.
- Geochemical data characterize the gas hydrate–bearing zone (200–400 mbsf) in the Kumano Basin at Site C0002 as a zone of disseminated, methane-dominated hydrate of microbial origin.
- Operations at Site C0012 included 178.7 m of detailed LWD characterization of the oceanic basement, indicating an upper ~100 m zone of altered pillow basalts and sheet flow deposits and a lower, presumably less altered basement unit.
- Cores recovered at Site C0021 improve our understanding of submarine landslides in the slope basins seaward of the splay fault. LWD data acquired at Sites C0018 and C0021 characterize in situ internal structures and properties of mass transport deposits, which relate to the dynamics and kinematics of submarine landslides.
- LWD resistivity images from Hole C0022A, located in the slope basin immediately seaward of the megasplay fault, show a conductive horizon where the tip of the megasplay fault is inferred from the 3-D seismic data. Although the fault itself was not sampled in Hole C0022B, structural and porosity data from cores as well as interstitial water data suggest that the conductive horizon is possibly the splay fault tip.

Introduction

The Integrated Ocean Drilling Program (IODP) drilling phase of the Nankai Trough Seismogenic Zone Experiment (NanTroSEIZE) is a multiexpedition, multistage project focused on understanding the mechanics of seismogenesis and rupture propagation along subduction plate boundary faults. The drilling program includes a coordinated effort to sample and instrument the plate boundary system at several locations offshore the Kii Peninsula (Tobin and Kinoshita, 2006) (Figs. **F1**, **F2**). The main objectives are to understand

- The mechanisms and processes controlling the updip aseismic–seismic transition of the megathrust fault system,
- The processes of earthquake and tsunami generation,
- The mechanics of strain accumulation and release,
- The absolute mechanical strength of the plate boundary fault, and
- The potential role of a major upper plate fault system (termed the “megasplay” fault) in seismogenesis and tsunamigenesis.

Along the Nankai margin, high-resolution seismic reflection profiles across the outer wedge of the accretionary prism clearly document a large out-of-sequence-thrust fault system (the megasplay fault, after Park et al., 2002) (Fig. **F2**) that branches from the plate boundary décollement close to the updip limit of inferred coseismic rupture in the 1944 Tonankai Mw 8.2 earthquake (Fig. **F1**). Several lines of evidence indicate the megasplay system is active and that it may accommodate an appreciable component of plate boundary motion. However, the partitioning of strain between the décollement zone and the megasplay system (Fig. **F2**) and the nature and mechanisms of fault slip as a function of depth and time on the megasplay are not understood. One of the main objectives of the NanTroSEIZE project is to document the role of the megasplay fault in accommodating plate motion (both seismically and interseismically) and to characterize its mechanical and hydrologic behavior.

IODP Expeditions 314, 315, and 316 were carried out as a unified drilling program collectively known as NanTroSEIZE Stage 1 (Tobin et al., 2009a). Eight sites were selected for riserless drilling to target the frontal thrust region, the midslope megasplay fault region, and the Kumano forearc basin (Figs. **F1, F2**). IODP Site C0002 was the preparatory pilot site for planned deeper riser drilling and operations, whereas the other sites primarily targeted fault zones in the shallow, presumed aseismic, portions of the accretionary complex (Kinoshita et al., 2009). Expedition 314 was dedicated to in situ measurement of physical properties and borehole imaging through logging while drilling (LWD) (Tobin et al., 2009b). Expedition 315 was devoted to core sampling and downhole temperature measurements at sites in the megasplay region and in the forearc basin (Ashi et al., 2009). Expedition 316 targeted the frontal thrust and megasplay fault in their shallow, aseismic portions (Screaton et al., 2009).

Stage 2 of NanTroSEIZE comprised four IODP expeditions (319, 322, 332, and 333), with the aims of building on the results of Stage 1, characterizing the subduction inputs on the Philippine Sea plate, and preparing for later observatory installations for long-term monitoring of deformation at the updip limit of the seismogenic zone (Expedition 319 Scientists, 2010; Underwood et al., 2010; Expedition 332 Scientists, 2011a; Expedition 333 Scientists, 2012a).

NanTroSEIZE Stage 3 started with IODP Expedition 326, during which the first casing string was installed in Hole C0002F to 860 meters below seafloor (mbsf) (Expedition 326 Scientists, 2011). IODP Expedition 338, the ninth NanTroSEIZE drilling expedition, was planned to deepen Hole C0002F to investigate the properties, structure, and state of stress within the hanging wall above the locked plate boundary at Site C0002.

Site C0002 is the centerpiece of the NanTroSEIZE project, as it is planned to access the plate interface fault system at a location where the fault system is believed to be capable of seismogenic locking and slip and to have slipped coseismically in the 1944 Tonankai earthquake (e.g., Ichinose et al., 2003). This zone also coincides with the location where a cluster of very low frequency (VLF) seismic events occurred in 2004–2005 (Ito and Obara, 2006) and the first tectonic tremor recorded in an accretionary prism setting has been found (Obana and Kodaira, 2009). To access, sample, and monitor these deeper zones, Hole C0002F will be further deepened later in 2013–2015, with the ultimate goal of penetrating the megasplay fault and for the future installation of a long-term observatory (Fig. **F3**).

Background

Geological setting

The Nankai Trough is formed by subduction of the Philippine Sea plate to the northwest beneath the Eurasian plate at a rate of ~4.1–6.5 cm/y (Fig. **F1**) (Seno et al., 1993; Miyazaki and Heki, 2001). The convergence direction is slightly oblique to the trench, and Shikoku Basin sediment is actively accreting at the deformation front. The Nankai Trough has been one of the focus sites for studies of seismogenesis by both IODP and the U.S. MARGINS initiative, based on the wealth of geological and geophysical data available. A better understanding of seismic and tsunami behavior at margins such as Nankai is highly relevant to heavily populated coastal areas.

Subduction zones like the Nankai Trough, where most of the great earthquakes (Mw > 8.0) occur, are especially favorable for study because the entire downdip width of the seismogenic zone ruptures in each event, suggesting that the zone of coseismic rupture in future large earthquakes may be more predictable than for smaller earthquakes. The Nankai Trough region has a 1300 year historical record of recurring great earthquakes that are typically tsunamigenic, including the 1944 Tonankai Mw 8.2 and 1946 Nankai Mw 8.3 earthquakes (Fig. **F1**) (Ando, 1975; Hori et al., 2004). The rupture area and zone of tsunami generation for the 1944 event (within which Site C0002 is located) are now reasonably well understood (Ichinose et al., 2003; Baba et al., 2005). Land-based geodetic studies suggest that currently the plate boundary thrust is strongly locked (Miyazaki and Heki, 2001). Similarly, the relatively low level of microseismicity near the updip limits of the 1940s earthquakes (Obana et al., 2001) implies significant interseismic strain accumulation on the megathrust. However, re-

cent observations of VLF earthquakes within or just below the accretionary prism in the drilling area (Obara and Ito, 2005) demonstrate that interseismic strain is not confined to slow elastic strain accumulation. Slow slip phenomena, referred to as episodic tremor and slip, including episodic slow slip events and nonvolcanic tremor (Schwartz and Rokosky, 2007), are also known to occur in the downdip part of the rupture zone (Ito et al., 2007). In the subducting Philippine Sea plate below the rupture zone, weak seismicity is observed (Obana et al., 2005). Seaward of the subduction zone, deformation of the incoming oceanic crust is suggested by microearthquakes as documented by ocean-bottom seismometer (OBS) studies (Obana et al., 2005).

The region offshore the Kii Peninsula on Honshu Island was selected for seismogenic zone drilling for several reasons. First, the rupture area of the 1944 Mw 8.2 Tonankai event is well constrained by recent seismic and tsunami waveform inversions (e.g., Tanioka and Satake, 2001; Kikuchi et al., 2003). Slip inversion studies suggest that only in this region did past coseismic rupture clearly extend shallow enough for drilling (Ichinose et al., 2003; Baba and Cummins, 2005), and an updip zone of large slip has been identified and targeted. Notably, coseismic slip during events like the 1944 Tonankai earthquake may have occurred on the megasplay fault in addition to the plate boundary décollement (Ichinose et al., 2003; Baba et al., 2006). The megasplay fault is therefore a primary drilling target equal in importance to the basal décollement. Second, OBS campaigns and onshore high-resolution geodetic studies (though of short duration) indicate significant interseismic strain accumulation (e.g., Miyazaki and Heki, 2001; Obana et al., 2001). Third, the region offshore the Kii Peninsula is typical of the Nankai margin in terms of heat flow and sediment on the incoming plate. This is in contrast to the area offshore Cape Muroto (the location of previous Deep Sea Drilling Project and Ocean Drilling Program drilling), where local stratigraphic variation associated with basement topography and anomalously high heat flow have been documented (Moore et al., 2001, 2005). Finally, the drilling targets are within the operational limits of riser drilling by the D/V *Chikyu* (i.e., maximum of 2500 m water depth and 7000 m subseafloor penetration). In the seaward portions of the Kumano Basin, the seismogenic zone lies <6000 m beneath the seafloor (Nakanishi et al., 2002).

Seismic studies and site survey data

A significant volume of site survey data has been collected in the drilling area over many years, including multiple generations of 2-D seismic reflection (e.g., Park et al., 2002), wide-angle refraction (Nakanishi et al., 2002), passive seismicity (e.g., Obana

et al., 2001, 2005), heat flow (Yamano et al., 2003), side-scan sonar, swath bathymetry, and submersible and remotely operated vehicle (ROV) dive studies (Ashi et al., 2002). In 2006, Japan and the United States conducted a joint, 3-D seismic reflection survey over an ~11 km × 55 km area, acquired by Petroleum GeoServices (Moore et al., 2009). This 3-D data volume is the first deep-penetration, fully 3-D marine survey ever acquired for basic research purposes and has been used to (1) refine selection of drill sites and targets in the complex megasplay fault region, (2) define the 3-D regional structure and seismic stratigraphy, (3) analyze physical properties of the subsurface through seismic attribute studies, and (4) assess drilling safety (Moore et al., 2007, 2009). These high-resolution, 3-D data will be used in conjunction with petrophysical and geophysical data obtained from core analyses and both wireline logging and LWD to allow extensive and high-resolution integration of core, logs, and seismic data.

Long-term observatories

In future IODP expeditions, a series of long-term borehole observatories will be installed at IODP Sites C0002, C0006 or C0007, and C0010. The three sites are located within and above regions of contrasting behavior of the megasplay fault zone and plate boundary as a whole (i.e., a site in the toe of the accretionary prism [Sites C0006 and C0007], a site above the updip edge of the locked zone [Site C0002], and a shallow site in the megasplay fault zone and footwall where slip is presumed to be aseismic [Site C0010]). These observatories have the potential of capturing seismic activity, slow slip behavior, and possibly interseismic strain accumulation on the plate boundary and megasplay faults across a range of seismogenic settings. These temporal and spatial observations are necessary to understand how each part of the plate boundary functions through the seismic cycle of megathrust earthquakes.

Currently, the planned observation system for the observatory boreholes consists of an array of sensors designed to monitor slow crustal deformation (e.g., strain, tilt, and pore pressure as a proxy for strain), seismic events including VLF earthquakes, hydrologic transients associated with strain events, ambient pore pressure, and temperature. To ensure the long-term and continuous monitoring necessary to capture events occurring over a wide range of timescales, these borehole observatories will be connected to a submarine cabled observation network called Dense Oceanfloor Network System of Earthquakes and Tsunamis (DONET) (**www.jamstec.go.jp/donet/e/**), which will be constructed in and around the drilling target area.

Scientific objectives

The primary drilling plan for Expedition 338 was to extend Hole C0002F from 860 (20 inch casing set point) to 3600 mbsf (13⅜ inch casing set point) through riser drilling. However, riser operations during Expedition 338 were suspended because of riser damage during unfavorable winds and strong current conditions. Contingency operations were then conducted for the remainder of Expedition 338.

Site C0002 objectives

At Site C0002, LWD data already exist from 0 to 1400 mbsf from Expeditions 314 and 332 (Expedition 314 Scientists, 2009a; Expedition 332 Scientists, 2011b) and core data exist for 0–204 and 475–1057 mbsf from Expedition 315 (Expedition 315 Scientists, 2009). The Kumano Basin sedimentary package composes the interval from 0 to ~940 mbsf, which is underlain by the inner accretionary wedge. The seismic reflection character of the entire zone from ~940 mbsf to the megasplay reflection at ~5000 mbsf exhibits virtually no coherent reflections that would indicate intact stratal packages, which is in contrast to the outer accretionary wedge seaward of the megasplay fault system (Fig. **F2**) (also see Moore et al., 2009).

The main research objectives for combined primary riser operations and contingency riserless operations at Site C0002 were to sample the upper part of the forearc basin sediment and gas hydrate zone, the basal Kumano Basin-to-accretionary prism unconformity, and the upper portion of the inner wedge with cores, drill cuttings, mud-gas sampling, and an extensive suite of LWD logs. Sampling these intervals, which are either previously unsampled or undersampled, allows the (1) determination of composition, age, stratigraphy, and internal style of deformation of the Pliocene–Recent Kumano forearc basin and underlying Miocene accretionary complex; (2) characterization of the gas hydrate zone in the forearc basin; (3) reconstruction of thermal, diagenetic, and metamorphic history and comparison with present pressure and temperature conditions; (4) determination of minimal horizontal stress within the inner wedge; (5) investigation of the mechanical state and behavior of the formation; (6) characterization of the overall structural evolution of the Nankai accretionary prism; and (7) characterization of the current state of the upper plate above seismogenic plate boundary thrust.

Site C0012 objectives

The primary objectives at IODP Site C0012 were to characterize the sedimentary section and the upper portion of the oceanic crust with a full suite of LWD logs. Site C0012 is located in the Shikoku Basin on the crest of a prominent basement high (Kashinosaki Knoll; Ike et al., 2008) on the subducting Philippine Sea plate (Figs. **F1, F2**). This location provides access to the uppermost igneous crust with modest penetration below the seafloor. Previously, Expedition 322 collected core samples to 576 mbsf, which included sampling sediment and basement (Expedition 322 Scientists, 2010b) and Expedition 333 sampled the sediment and igneous basement to 630.5 mbsf (Expedition 333 Scientists, 2012b). As part of contingency operations, Expedition 338 collected LWD logs to 709 mbsf.

LWD operations at Site C0012 were performed to provide key data to understand (1) how compressional velocity relates to compaction state and fluid sources, (2) how chemical profiles relate to physical and chemical properties, (3) how the structures of the sedimentary section relates to slumping, and (4) how structures in igneous basement relate to the alteration state. Ultimately, these analyses will help define the fluid and chemical budgets of subduction inputs, which are important toward the understanding of fluids in the accretionary prism and subducted materials.

Site C0018 and C0021 objectives

A slope basin seaward of the megasplay fault was drilled and sampled during Expedition 333 (IODP Hole C0018A) (Figs. **F2, F4**) targeting mass transport deposits (MTDs) to understand how submarine landslides relate to tectonic activity and evolution of the slope basin and shallow megasplay fault system and to evaluate deformation and transport mechanisms of MTDs (Expedition 333 Scientists, 2012c). Site C0018 is situated within a depocenter for downslope mass transport, and the sedimentary succession is dominated by stacked MTDs that are seismically imaged as acoustically transparent-to-chaotic bodies with ponded geometries (Fig. **F5**) (Strasser et al., 2011). Hole C0018A was drilled at a location where the MTD bodies wedge out and basal erosion is minimal. Coring to ~314.15 mbsf in Hole C0018A sampled six MTDs, which record more than 1 million years of submarine landslide history (Strasser et al., 2012).

The primary goals of Expedition 338 operations at IODP Sites C0018 and C0021 were (1) to characterize the sedimentary section and MTDs at Site C0018 with LWD logs and (2) to add LWD and coring at Site C0021, which is located ~2 km northwest of

Site C0018 at a more proximal site for MTDs observed at Site C0018 (Figs. F4, F5). Logging and coring at Site C0021 were designed to provide data for correlation to Site C0018. Together, the sites provide constraints on the lateral variability of MTDs within the basin. This variability relates to the nature, provenance, and kinematics of the landslides. Logging at Sites C0018 and C0021 enables us to correlate and integrate these data with core and seismic data, and hence, to understand the comprehensive nature of MTDs and their bearing on sliding dynamics and tsunamigenic potential.

Site C0022 objectives

LWD and coring were carried out at IODP Site C0022, located in the slope basin between previously drilled IODP Sites C0004 and C0008 (Figs. F1, F4) (Expedition 314 Scientists, 2009b; Expedition 316 Scientists, 2009a, 2009b) to target the uppermost 400 mbsf near the projected fault tip of the megasplay fault. The seismic reflection data had previously identified this region as the tip of the megasplay fault that emplaced the block drilled at Site C0004 over slope basin strata (Fig. F6) (Moore et al., 2009). This megasplay fault is thought to coincide with the rupture area of the 1944 Tonankai earthquake, and its slip was likely responsible for the associated devastating tsunami (Park et al., 2002; Moore et al., 2007).

Reconstruction of splay fault activity through time, however, indicates that the surface layers younger than ~1.24 Ma are not displaced by the megasplay fault (Fig. F6) (Strasser et al., 2009), which implies that this fault has been inactive recently. Alternatively, further work by Kimura et al. (2011) defined the lateral extent and characteristics of this fault zone and predicted that its tip should extend into the slope basin strata. According to the authors, ongoing splay fault activity may not only be inferred by stratal ages and architecture across the fault itself, but also by broader and distributed deformation, apparent in (1) deformation of the lower slope basin, (2) erosion and redeposition of slope sediment by successive oversteepening and mass transport, and (3) accumulation of MTDs overlying the fault. Thus, Site C0022 was cored and logged to test these ideas.

Operational strategy

To meet the scientific and engineering objectives of Expedition 338, primary operations in Hole C0002F were to drill from 860.3 to 2300 mbsf using LWD/measurement while drilling (MWD) and set 16 inch casing (Fig. F3). Wireline coring was to be con-

ducted in Hole C0002F between 2300 and 2400 mbsf using a rotary core barrel (RCB) to obtain the highest quality and most complete core samples. Then, LWD/MWD, cuttings, and mud-gas analyses were to continue to 3600 mbsf where 13⅜ inch casing was to be set.

Following suspension of riser drilling operations, a contingency riserless operations plan was formulated that allowed coring at Sites C0002 (200–505, 902–940, and 1100.5–1120 mbsf), C0021 (0–194.5 mbsf), and C0022 (0–419.5 mbsf) as well as LWD at Sites C0012 (0–709 mbsf), C0018 (0–350 mbsf), C0021 (0–294 mbsf), and C0022 (0–420.5 mbsf) (Table **T1**).

Logging/Downhole measurements strategy in Hole C0002F

LWD/MWD tools provide the ability to monitor drilling parameters and conditions and to collect gamma ray and resistivity logs to define major lithologic changes in real time (MWD) as well as record high-resolution borehole and formation conditions (LWD). The MWD tool suite included annular pressure while drilling (APWD), downhole weight on bit (WOB), downhole torque, hole inclination, and gamma radiation. The Power-V tool was run during drilling to maintain hole inclination <3°. The geoVISION LWD tool was added to this suite to obtain azimuthal resistivity data and borehole resistivity images in order to further define stratigraphic boundaries and to characterize bedding, fractures, and any compressional borehole breakouts or drilling-induced tensile fractures (DITFs). In addition, the sonicVISION LWD tool was included to provide *P*-wave velocity data during drilling. A leak-off test (LOT) was conducted at 872.5 mbsf to help define the least horizontal principal stress.

Sampling and coring strategy at Site C0002

A total of 35 cores were cut from the 200–505 mbsf depth interval in Holes C0002K and C0002L (Table **T1**): 2 with the hydraulic piston coring system (HPCS), 4 with the extended punch coring system (EPCS), and 29 with the extended shoe coring system (ESCS). This interval includes the gas hydrate zone and the bottom-simulating reflector (BSR), which were not cored during Expedition 315 (Expedition 315 Scientists, 2009).

Nine RCB cores were cut from depth intervals 902–940 and 1100.5–1120 mbsf in Holes C0002H and C0002J (Table **T1**). This interval covers the lower part of lithologic Unit III (basal Kumano forearc basin) and the uppermost part of Unit IV (upper accre-

tionary prism) according to the stratigraphy established during Expeditions 314 and 315 (Expedition 314 Scientists, 2009a; Expedition 315 Scientists, 2009).

During riser drilling in Hole C0002F (875.5–2005.5 mbsf), cuttings were collected every 5 m and mud gas was routinely sampled for geochemical analyses. Depth differences between LWD/MWD, mud gas, and cuttings data had to be carefully considered because of the mixing of cuttings caused by reaming while drilling (RWD). RWD technology allowed LWD/MWD analysis behind a 12¼ inch drill bit while simultaneously opening the hole above the LWD/MWD tool assembly with a 20 inch reamer bit.

Logging/Downhole measurements strategy in Hole C0012H

Logging operations in Hole C0012H used the same suite of LWD tools used for Hole C0002F LWD/MWD to 709 mbsf (Table **T1**). Logging data were collected from Shikoku Basin sediment overlying oceanic crust (~170 m crust penetration).

Logging/Downhole measurements strategy in Holes C0018B, C0021A, and C0022A

Logging with LWD/MWD tools in all three holes was conducted with the same suite of logging tools used in Holes C0002F and C0012H, with the exception of the sonicVISION tool (Table **T1**). Hole C0018B (0–350 mbsf) was designed to cover an interval cored during IODP Expedition 333 (Expedition 333 Scientists, 2012c). Holes C0021A (0–294 mbsf) and C0022A (0–420.5 mbsf) were logged to collect data from slope basin sediment.

Sampling and coring strategy in Holes C0022B and C0021B

A total of 55 cores were collected from Holes C0022B and C0021B (Table **T1**); however, only 41 cores from Hole C0022B were described on board the ship. Fourteen cores from Hole C0021B will be described and sampled in a shore-based sampling party at the Kochi Core Center. Both holes were cored using the HPCS (84.5 mbsf [or 8 cores in Hole C0022B] and 175.5 mbsf [or 12 cores in Hole C0021B]). After the formation consolidation state precluded further HPCS coring, EPCS coring was used for 3 cores and then ESCS was used for the final coring section in Hole C0022B (30 cores). In Hole C0021B, EPCS was used for the final 2 cores after the switch from HPCS.

Site summaries

Site C0002

Logging

Three logging units (III, IV, and V) (Fig. F7) were defined in Hole C0002F, with logging Units IV and V further divided into five and two subunits, respectively.

Logging Unit III (875.5–918.5 mbsf) is characterized by relatively consistent responses in the gamma ray, resistivity, and sonic logs (Fig. F7). The general logging character suggests this unit is mainly composed of clay- to silt-rich sediment, with occasional thin, interbedded sand layers. Logging Unit III identified in Hole C0002F correlates with Hole C0002A Unit III defined during Expedition 314 (Expedition 314 Scientists, 2009a).

Within logging Unit IV (918.5–1638 mbsf), the gamma ray and resistivity logs have generally higher variability than in the other logging units (Fig. F7). The general log character is interpreted to represent interbedding and alternating layers of thick sand-rich and clay-rich packages (lower to higher gamma ray values). In logging Unit IV, prominent highs in resistivity coincide with gamma ray lows, which are interpreted as sandier lithologies. This unit also shows two low-velocity zones. The fractures in logging Unit IV are mostly resistive and concentrated in an interval from 1500 to 1638 mbsf.

Logging Unit V (1638–2005.5 mbsf) is characterized by homogeneous, high gamma ray intervals and is interpreted as a homogeneous, clay-rich unit (Fig. F7). Sonic velocity is nearly constant in this interval. Resistivity data show some spikes and downhole variation. Logging Unit V contains the largest concentration of conductive fractures in the borehole.

Compressional borehole breakouts and DITFs observed in Hole C0002F suggest a northeast–southwest orientation of the maximum horizontal stress (σ_{Hmax}) throughout this hole, which is consistent with breakout data obtained in Hole C0002A during Expedition 314 (Expedition 314 Scientists, 2009a).

Lithology

Four lithologic units were identified at Site C0002 based on geological and geochemical characteristics of core and cuttings samples: Unit II (200–505 mbsf in Holes

C0002K and C0002L), Unit III (875.5–1025.5 mbsf in Hole C0002F and 902–926.7 mbsf in Hole C0002J), Unit IV (1025.5–1740.5 mbsf in Hole C0002F and 1100.5–1120 mbsf in Hole C0002H), and Unit V (1740.5–2004.5 mbsf in Hole C0002F) (Fig. **F8**). The difference of the lithologic Unit III/IV boundary between Holes C0002F and C0002J arises from RWD in Hole C0002F, which resulted in mixing of cuttings over an interval of as much as ~100 m. As a result of RWD, the logging Unit III/IV and IV/V boundaries in Hole C0002F are placed at 918.5 mbsf and 1638 mbsf, respectively (Fig. **F7**), which are ~100 m shallower than the corresponding lithologic unit boundaries (Fig. **F9**).

Lithologic Unit II in Holes C0002K and C0002L is dominated by silty claystone with subordinate sandstone, sandy siltstone, calcareous silty claystone, and fine ash. Similar to Unit II in Hole C0002B, this unit is interpreted to be the lower Kumano forearc basin sediment dominated by the hemipelagic mud of distal turbidites (Expedition 315 Scientists, 2009).

Lithologic Unit III in Hole C0002J is dominated by heavily bioturbated, calcareous silty claystone containing abundant glauconite. Cuttings from lithologic Unit III in Holes C0002F have similar lithologic features. These lithologic features are consistent with those observed in Unit III in Hole C0002B, which was interpreted as basal Kumano forearc basin sediment that accumulated above the carbonate compensation depth (CCD) at sediment-starved conditions (Expedition 315 Scientists, 2009).

The lithologic Unit III/IV boundary was sampled at 926.7 mbsf in Hole C0002J and is characterized by (1) a relatively sharp contact immediately overlain by a 15 cm thick interval with mixed fragments from both the calcareous glauconitic silty claystone above (Unit III) and less calcareous, nonglauconitic silty claystone below (Unit IV) (Fig. **F10A**); (2) an abrupt and substantial increase in the abundance of sand below this boundary; and (3) a substantial decrease in the amount of carbonate in silty claystone below this boundary. The nature of the Unit III/IV boundary suggests that this is an erosional unconformity.

Lithologic Unit IV in Holes C0002F, C0002H, and C0002J is dominated by noncalcareous silty claystone with subordinate sandstone and sandy siltstone (Figs. **F8, F11**). Lithologic Unit IV is divided into five subunits based on sand content (Fig. **F8**). Based on the sandstone-rich deposits recovered in Hole C0002F, lithologic Unit IV is interpreted as the upper accretionary prism sediment that accumulated either in a paleo-

trench or in the Shikoku Basin. Low carbonate concentration in silty claystone (Fig. F8) suggests deposition below the CCD.

Lithologic Unit V in Hole C0002F is composed almost entirely of silty claystone (Fig. F8). Its thickness of several hundred meters suggests that it may be correlatable with the hemipelagic Unit III drilled at the subduction input Sites C0011 and C0012 (Expedition 322 Scientists, 2010a, 2010b).

Structural geology

In the Kumano Basin sediment (lithologic Units II and III) in Holes C0002J, C0002K, and C0002L, bedding is subhorizontal to gently dipping (Fig. F11). At the base of lithologic Unit III, however, bedding is intensely disrupted and boudinaged (e.g., Fig. F10B). In Unit III in Hole C0002J, east-west–striking and north-dipping low- to moderate-angle faults are dominant. Vein structures (e.g., Fig. F10C) were observed in cores and cuttings exclusively from Unit III in Holes C0002F and C0002J (Fig. F8). Deformation bands (e.g., Fig. F10D) were also observed mostly in cores from Unit III in Hole C0002J (Fig. F11).

In the upper accretionary prism sediment (lithologic Unit IV) in Holes C0002H and C0002J, bedding dips at variable angles of 7°–64° (Fig. F11). Reoriented bedding in Unit IV is subhorizontal to steeply dipping toward the south or north. Four sets of faults were observed in Unit IV in Hole C0002H: north-south–striking and east-dipping high-angle faults, northwest-striking and northeast-dipping high-angle faults, east-west–striking high-angle faults, and north-south–striking and west-dipping low-angle faults.

Cuttings containing carbonate veins (Fig. F10E) occur throughout the accretionary prism Units IV and V (Fig. F8). Cuttings with slickenlined surfaces also occur throughout Units IV and V. Cuttings with slickenlined surfaces up to 10% occur at 1550.5–1675.5 mbsf. This interval is correlatable with the high fracture concentration interval of 1500–1550 mbsf identified by LWD resistivity images.

Geochemistry

Geochemical data of interstitial water and gas sampled from cores in Holes C0002H, C0002J, C0002L, and C0002K obtained during Expedition 338 complement the previous data in Holes C0002B and C0002D obtained during Expedition 315 (Expedition 315 Scientists, 2009), so continuous profiles of geochemical data to ~1100 mbsf are now available for Site C0002 (Figs. F12, F13).

Salinity, chlorinity, and Na^+ show similar changes with depth, reaching minimum concentrations at 300–500 mbsf (Fig. **F12**). These minimum concentrations of dissolved salts are attributable to freshwater derived from the dissociation of methane hydrate.

Methane shows a relatively high concentration at ~300 mbsf, and propane shows high concentration at 200–400 mbsf (Fig. **F13**). The methane- and propane-rich interval at 200–400 mbsf corresponds to the gas hydrate zone inferred from resistivity and sonic log data (Expedition 314 Scientists, 2009a). However, no massive gas hydrates were found in this interval, although gas-rich sands were common. This suggests that the methane hydrates are disseminated in porous sand layers. A prominent methane peak was observed in drilling mud gas data when passing the 918 mbsf boundary.

The ratio of methane to ethane and propane ($C_1/[C_2 + C_3]$) and $\delta^{13}C$ concentration in methane ($\delta^{13}C\text{-}CH_4$) suggest that the methane in the gas hydrate zone is mostly of microbial origin. Together with $C_1/(C_2 + C_3)$ and $\delta^{13}C\text{-}CH_4$ data of mud gas sampled during riser drilling in Hole C0002F, thermogenic methane is shown to gradually increase with depth up to ~50% at ~2000 mbsf (Fig. **F14**).

Physical properties

Discrete moisture and density (MAD) measurements were conducted on both cores and cuttings sampled from Holes C0002F, C0002H, C0002J, C0002K, and C0002L. Combined with MAD data obtained during Expedition 315 (Expedition 315 Scientists, 2009), a continuous profile of density and porosity data to 2005.5 mbsf is now available for Site C0002 (Fig. **F15**).

MAD data on cuttings (below 875.5 mbsf in Hole C0002F) show lower bulk density and higher porosity compared to measurements on discrete samples from cores (Fig. **F15**). This was also observed during previous riser drilling Expeditions 319 and 337 (Expedition 319 Scientists, 2010; Inagaki et al., 2012). Analyses on Expedition 338 cuttings revealed that these differences resulted from mixing of aggregates produced during the drilling process, termed drilling-induced cuttings aggregates. MAD data from discrete core samples and a few selected intact formation cuttings from lithologic Unit V suggest that bulk density increases continuously from 1.6 g/cm^3 at the seafloor to ~2.3 g/cm^3 at 2005.5 mbsf. Porosity decreases from ~65% at the seafloor to ~23% at the base of lithologic Unit V (2005.5 mbsf) (Figs. **F11, F15**).

A LOT to estimate the least principal stress was performed at 875.5 mbsf, which is 12.3 m below the 20 inch casing shoe. Two cycles of pressurization were conducted by injecting drilling mud at 31.8 and 47.7 L/min, respectively. The first cycle was not successful because of loss of a large volume of mud. The second cycle yielded an estimate of 32 MPa as the least horizontal principal stress (σ_{hmin}) at 875.5 mbsf.

Paleomagnetism

Remnant magnetization measurements were conducted on discrete samples from Holes C0002K and C0002L. The results show that magnetic inclinations at 200–505 mbsf (Unit II) are mostly negative, except for a positive interval at 240.72–299.37 mbsf. The data and results from Holes C0002B and C0002D during Expedition 315 (Expedition 315 Scientists, 2009) revealed that the 160–490 mbsf interval at Site C0002 ranges from 1.078 to 1.24 Ma and that the entire sampled intervals of Holes C0002K and C0002L should correspond to the middle part of the Matuyama reversed polarity interval. The normal polarity interval observed at 240.72–299.37 mbsf is therefore interpreted as the Cobb Mountain Subchron (1.173–1.185 Ma).

Anisotropy of magnetic susceptibility (AMS) measurements were conducted on discrete samples collected from Holes C0002J, C0002K, and C0002L. AMS data show that the samples from Holes C0002K and C0002L (200–505 mbsf) exhibit a subhorizontal, uniaxially oblate magnetic fabric, likely formed by subvertical compaction. In contrast, AMS data show that the samples from Hole C0002J (902–940 mbsf) exhibit more prolate magnetic fabric elongated in the northeast–southwest direction, suggesting a trench-normal compression in addition to subvertical compaction.

Site C0012

LWD in Hole C0012H was conducted from the seafloor to 709.0 mbsf and provided a suite of LWD data that can be combined with core analyses from previous expeditions (Expedition 322 Scientists, 2010b; Expedition 333 Scientists, 2012b) and seismic data (Park et al., 2008) to characterize the subduction zone inputs.

Log data and lithologic characterization

Based on variations of the gamma ray data from baselines and changes in trend and log character, seven primary logging units were identified: five within the sediment and two within the basement. The logging units were further divided into subunits based on more subtle variations in the resistivity and sonic velocity (Fig. **F16**).

Logging Unit I (0–188.1 mbsf) is characterized by a gradually increasing trend in gamma ray values from ~65 to ~95 gAPI and roughly constant low resistivity of ~0.7 Ωm (Fig. **F16**). The gamma ray values and resistivity through Unit I are interpreted to reflect sandy mud lithologies.

Logging Unit II (188.1–372.1 mbsf) is characterized by gamma ray values near ~95 gAPI with minor fluctuations (Fig. **F16**) that are interpreted to reflect changes in the relative proportions of silt and clay in the hemipelagic mud. Resistivity is roughly constant at ~0.9 Ωm. An increase in abundance of thin gamma ray and resistivity spikes below 339.6 mbsf suggests an increase in the number of ash and sand beds.

Logging Unit III (372.1–403.3 mbsf) is characterized by overall high gamma ray values (~115 gAPI) and a fairly constant resistivity of ~1 Ωm (Fig. **F16**). This is interpreted as a clay-dominated unit. The base of logging Unit III is placed at 403.3 mbsf, where a step down in gamma ray, resistivity, and sonic velocity values occurs.

Logging Unit IV (403.3–463.5 mbsf) has more variability in log character than logging Units I, II, and III, especially in *P*-wave velocity, which fluctuates between 1800 and 2000 m/s (Fig. **F16**). This is interpreted to be a heterogeneous mixture of hemipelagic mudstone, sand, and ash.

Logging Unit V (463.5–530.3 mbsf) exhibits a gradual decrease in gamma ray from ~95 to ~60 gAPI, whereas resistivity is fairly constant at ~0.85 Ωm (Fig. **F16**). The base of Unit V is placed where a significant change in the overall log character occurs, with a sharp decrease in gamma ray and corresponding sharp increase in resistivity and sonic velocity. This boundary is interpreted as the sediment/basement contact.

Logging Unit VI (530.3–626.6 mbsf) represents the uppermost part of the oceanic basement. Through logging Unit VI, the gamma ray log exhibits significant variation with depth (15–45 gAPI) (Fig. **F16**). These fluctuations in gamma ray value possibly represent changing sediment volume within the basement or alterations to the basalt.

Logging Unit VII (626.6–709 mbsf) is characterized by low gamma ray values of ~15 gAPI with only minor fluctuations (±5 gAPI) (Fig. **F16**), suggesting the presence of uniform or fresh basalt. Resistivity exhibits some variability with depth but remains high relative to all the other logging units.

Resistivity image analysis

In the Shikoku Basin sediment (logging Units I–V), bedding dips are 10°–30°. The dominant dip direction is bipolar, with strong clustering in west–northwest and east–northeast directions (Fig. **F16**).

In the basement (logging Units VI–VII), there are a wide variety of textures and fracture patterns that can broadly be summarized as (1) mottled texture, distinct from other regions of clear fracturing (Fig. **F17D**); (2) "turtleshell" texture as approximately circular regions of high-resistivity clasts within a lower resistivity network (Fig. **F17B, F17D, F17E**); and (3) zones of homogeneous background resistivity, often with subvertical fractures. The mottled texture can be interpreted to represent a multitude of small fractures or, alternatively, volcaniclastic sediment gravity flow deposits. The turtleshell texture possibly represents pillow basalts. The homogeneous zones containing subvertical fractures may represent sheet flows (Fig. **F17C, F17D**).

Four compressional borehole breakouts were observed in the Shikoku Basin sediment. The uppermost and lowermost breakouts (424.8 and 517.7 mbsf) agree with a north–south orientation of the maximum horizontal stress (σ_{Hmax}), whereas the central two breakouts (442.6 and 446.6 mbsf) demonstrate a northeast–southwest σ_{Hmax} orientation.

Core-Log-Seismic integration

Cores recovered from Holes C0012A–C0012E provided detailed lithologic information for the Shikoku Basin sediment; those intermittently recovered from Holes C0012A and C0012G provided some lithologic information about the underlying oceanic basement of the Philippine Sea plate (Expedition 322 Scientists, 2010b; Expedition 333 Scientists, 2012b). Hole C0012H provided detailed LWD data. Seismic Units A–G were identified on the Institute for Research on Earth Evolution (IFREE) 3-D prestack depth migration (PSDM) (Park et al., 2008) In-line 95 by the Expedition 322 Scientists (2010a, 2010b). Seismic Unit G represents the oceanic basement (Fig. **F18**).

Seismic Units A and B (0–120 mbsf) exhibit low-amplitude reflectivity with some irregular and discontinuous reflections (Fig. **F18**). In the cores, the same interval shows a dominant lithology of hemipelagic mud(stone) with a few volcanic ash/tuff beds (Expedition 322 Scientists, 2010b; Expedition 333 Scientists, 2012b). The upper sec-

tion of logging Unit I in Hole C0012H (0–140 mbsf) shows a slight increase in gamma ray values with minor fluctuations and likely correlates with these seismic units.

The lower section of logging Unit I (140–188 mbsf) has a greater variability in gamma ray values (Fig. **F18**). This interval corresponds to lithologic Unit II, which contains several volcanic sandstone beds (each ~5 m thick), and seismic Unit C, which contains a series of high-amplitude, continuous reflections.

Lithologic Units III and IV (215–415 mbsf) comprise hemipelagic mudstone and hemipelagic mudstone with interbedded siltstone sediment gravity flow deposits, respectively. Seismic Unit D, at the corresponding depth interval of 200–405 mbsf, is seismically transparent (Fig. **F18**). Lithologic Unit IV is correlatable with the base of logging Unit II (340–380 mbsf), where low spikes in gamma ray values (~30 gAPI) suggest an increasing number of siltstone turbidites.

Logging Units IV and V (403–530 mbsf) show a similar pattern of increasing gamma ray values with depth (Fig. **F18**). Lithologic Unit V (415–530 mbsf) contains a series of sandstone sediment gravity flow deposits and volcanic sandstone layers interbedded in hemipelagic mudstone. An increase in the ratio of mudstone to sandstone with depth may explain the observed increases in gamma ray values with depth. Seismic Unit E contains a series of strong reflections between 405 and 530 mbsf, corroborating the observation of sandstone layers interbedded in hemipelagic mudstone.

Lithologic Unit VI (~530–537 mbsf) was identified as thermally altered hemipelagic mudstone, resulting from contact with the basement rocks of lithologic Unit VII (seismic Unit G, logging Unit VI; Fig. **F18**). Finally, the oceanic basement is consistently observed at depths greater than ~530 mbsf.

Sites C0018 and C0021

LWD logs were collected in Holes C0018B and C0021A as well as cores in Hole C0021B for the purpose of characterizing the MTDs in the slope basin seaward of the megasplay fault zone.

Logging

During Expedition 333, which collected cores in Hole C0018A (Expedition 333 Scientists, 2012c), slope basin sediment was defined as Unit I. To maintain consistency, only one unit is defined encompassing the entire sections logged and cored at Sites

C0018 and C0021. The gamma ray log supports classification as one unit, as its character does not change significantly through the entire drilled section. However, based on changes in the character of resistivity logs, two subunits were identified in the Hole C0018B logs (Fig. **F19**) and four subunits were identified in the Hole C0021A logs (Fig. **F20**).

Logging units in Hole C0018B

Subunit IA (0.0–179.8 mbsf) is characterized by variable gamma ray and resistivity values (75 ± 30 gAPI and 1.0 ± 0.5 Ωm, respectively) (Fig. **F19**). Bedding is mostly subhorizontal, except for two intervals of high-angle dips (40°–80°) at 81.0–83.0 and 127.0–168.0 mbsf (Fig. **F18**), which correlate with MTDs observed in Hole C0018A cores (Expedition 333 Scientists, 2012a) (Fig. **F21**).

In contrast, Subunit IB (179.8–350.0 mbsf) is characterized by highly variable gamma ray and resistivity values (80 ± 40 gAPI and 1.5 ± 1.5 Ωm, respectively) (Fig. **F19**). From the gamma ray signature, coarsening- and fining-upward packages on a scale of tens of meters are interpreted throughout this subunit. Resistivity exhibits fluctuations over narrow (<2 m) horizons, possibly indicative of thin interbedded sand/ash and muddy sediment.

Log units in Hole C0021A

Subunit IA (0–144 mbsf) is characterized by variable gamma ray and resistivity values (75 ± 15 gAPI and 0.9 ± 0.3 Ωm, respectively) (Fig. **F20**). The majority of bedding dips moderately at 15°–40°, except for the 95–100 mbsf interval, where bedding dips >50° in variable directions. These variable dip directions reflect the expected chaotic nature of an MTD in this subunit.

Within Subunit IB (144–176.8 mbsf), the resistivity log exhibits two sharp peaks (154 and 163 mbsf) but no corresponding change is observed in the gamma ray log (Fig. **F20**). Bedding dips >50° in variable directions throughout this subunit, which implies that the whole of this subunit represents a thick MTD.

Subunit IC (176.8–276.5 mbsf) exhibits several increasing and decreasing cycles of gamma ray and resistivity values with some low spikes (Fig. **F20**). These cycles likely reflect lithologic coarsening- and fining-upward cycles.

Subunit ID (276.7–294 mbsf) exhibits two cycles of gamma ray and resistivity increases with depth (Fig. F20), which can be correlated with lithologic fining-upward cycles.

Lithology

In Hole C0018A, six MTDs were identified in cores between 0 and 190.0 mbsf (Expedition 333 Scientists, 2012a). The cored MTD section in Hole C0021B is different from that in Hole C0018A, but detailed description and sampling for Hole C0021B will be completed during a postexpedition sampling party. Strikingly, MTDs are unidentifiable from the gamma ray and resistivity logs alone (Figs. F21, F22), suggesting an intrabasin MTD source. Evidence seen in the resistivity images is mainly based on steep and chaotic bedding.

Core-Log-Seismic integration

We base our overall correlation between Sites C0018 and C0021 on the Kumano 3-D seismic reflection data (Fig. F21). A prominent regional seismic reflection identified by Kimura et al. (2011) and Strasser et al. (2011) marks the top of the thickest MTD (MTD 6) (Fig. F5), which was drilled both at Sites C0018 and C0021. The base of MTD 6 is not marked by one coherent single reflection, and regional correlation is affected by basal erosion of the MTD. At Site C0018, the logging Subunit IA/IB boundary has been defined at the base of MTD 6 (Fig. F21). At Site C0021, where the base of MTD 6 cuts deeper into the underlying subunit (Fig. F5), MTD 6 was assigned as a separate logging subunit (IB). Following successive ordering of subunits, therefore, logging Subunit IC at Site C0021 should be equivalent to Subunit IB at Site C0018 and correlates to the regional seismic Subunit IB defined by Kimura et al. (2011) and Strasser et al. (2011).

Site C0022

LWD data and cores were collected at Site C0022 to characterize the uppermost 400 m of sediment near the tip of the megasplay fault zone where the seaward-most branch of this fault system approaches the surface (Figs. F1, F4) (Moore et al., 2007, 2009).

Logging

As at Sites C0018 and C0021, the main slope sediment section was defined as a single lithologic and logging unit at Site C0022. The gamma ray log supports classification as one unit, as its value maintains a baseline near ~75 gAPI and the character does not

change significantly through the entire drilled section. However, three subunits were identified based on changes in the character of resistivity logs (Fig. F23).

Subunit IA (0.0–74.3 mbsf) is characterized by gradual increases in gamma ray and resistivity values with minor fluctuations (75–85 gAPI and 0.9–1.1 Ωm, respectively) (Fig. F23).

Throughout Subunit IB (74.3–212.9 mbsf), the gamma ray log exhibits repeated decimeter-scale decreases and increases, which are interpreted to reflect coarsening- and fining-upward cycles (Fig. F23). The resistivity fluctuates at ~1.1 Ωm with low (≤0.7 Ωm) and high (≥1.5 Ωm) anomalies. A high-resistivity (up to ~1.5 Ωm) interval at 85–88 mbsf, a low-resistivity (0.72 Ωm) peak at 100 mbsf, and a high-resistivity (up to ~1.7 Ωm) interval at 102–106 mbsf correspond to a highly fractured zone and are likely related to the megasplay faulting. In particular, the low-resistivity peak at 100 mbsf is likely the location of the megasplay fault because the fault zone is presumed to be more porous because of fracturing and therefore richer in pore fluid than its host rock.

Throughout Subunit IC (212.9–420.5 mbsf) the gamma ray log exhibits small-scale variations around the baseline of ~90 gAPI, whereas resistivity generally maintains minor fluctuations (±0.2 Ωm) around a constant baseline (~1.2 Ωm) (Fig. F23).

Lithology

Two lithologic subunits are recognized in Hole C0022B within the slope basin sedimentary section (Fig. F24). Subunit designations applied here are adopted with minor modification from Site C0008 (Expedition 316 Scientists, 2009b).

Subunit IA (0.0–383.5 mbsf) is dominated by silty clay with a variable component of calcareous nannofossils, foraminifers, siliceous biogenic debris, and volcanic ash. A trend toward diminishing carbonate content with depth is observed (Fig. F24).

Subunit IB (383.5–415.9 mbsf) consists of a series of interbedded mud clast gravels (Figs. F24, F25) with thin sand, clayey silt, and silty clay in the upper part and is dominated by silty clay in the lower part. This mud clast gravel is correlatable with a similar section in lithologic Subunit IB of Hole C0008A.

Structural geology

Bedding is subhorizontal with dip angles <15° throughout the entire section, except in the vicinity of the possible splay fault (shaded interval in Fig. F24). These higher-than-average bedding dip angles are likely affected by the splay faulting.

Minor faults are clustered in two intervals: 50–83 mbsf and 386–405 mbsf (Fig. F24). The faults of the megasplay hanging wall strike northwest–southeast, whereas those of the footwall preferentially strike north–south to northeast–southwest. Such a difference in fault orientation suggests different stress conditions on either side of the splay fault.

The interval of 100–101 mbsf is a plausible candidate for the location of the splay fault at Site C0022. Observations that support this hypothesis are (1) an increase in bedding dip in the vicinity of this interval; (2) the higher density of minor faults 20 m above this interval; (3) poor core recovery in this interval, suggesting highly fractured or disturbed material; and (4) the presence of three 2 cm thick intervals of claystone showing planar fabrics not encountered elsewhere in Hole C0022B.

Geochemistry

Although overall geochemical trends of interstitial water in Hole C0022B are similar to those in Holes C0004D, C0008A, and C0008D, changes in geochemical trends at ~100 mbsf are noticed (Fig. F26). For example, pH decreases from ~20 mbsf (>8.0) to ~100 mbsf (~7.5), below which it increases to the bottom of the hole (>8.0). Chlorinity and bromide concentrations increase to ~100 mbsf and then become roughly constant (~630 and ~1.2 mM, respectively) below that depth. Na^+ shows a trend similar to chlorinity and bromide. Ca^{2+} concentration increases rapidly to ~100 mbsf and then increases gently downward. Fe^{2+} concentration has a high peak at ~100 mbsf. Li^+ concentration decreases from the seafloor to ~100 mbsf and then increases to ~200 mbsf. Rb^+ concentration rapidly decreases from the seafloor to ~100 mbsf and then slightly decreases to ~350 mbsf. All these geochemical changes at ~100 mbsf are considered to be associated with the megasplay fault.

Hydrocarbon gas trends in Hole C0022B are similar to those in Holes C0004D, C0008A, and C0008D. Methane and ethane concentrations increase from the seafloor to ~30 mbsf, then decrease to ~100 mbsf, and gradually increase again with depth (Fig. F27). In addition, methane concentrations exhibit a high peak at ~100 mbsf, which may be associated with the megasplay fault.

Physical properties

MAD measurements on discrete samples show that porosity decreases quickly from 70% at the seafloor to 45%–50% at ~100 mbsf and then increases to 60% at 150 mbsf (Fig. **F24**). Interestingly, the minimum porosity occurs at 93.4–94.7 mbsf, which is close to the proposed location of the megasplay fault tip. Thus, this trend suggests that sediment near the splay fault have experienced shear-enhanced compaction.

Core-Log-Seismic integration

At Site C0022, a single unit was defined from analysis of both core samples and LWD data. Two subunits were identified based on core lithology, whereas three subunits identified from the LWD data (Fig. **F23**) correlate to seismic units defined by Kimura et al. (2011). According to this unit definition, lithologic Subunit IA correlates to logging/seismic Subunits IA and IB and the upper part of Subunit IC, whereas lithologic Subunit IB correlates to the lower part of seismic/logging Subunit IC. This is in agreement with the compiled stratigraphy by Kimura et al. (2011) and Strasser et al. (2011) in the slope basin.

Several shear zones and minor faults were observed in cores from 80 to 140 mbsf. The depth of this deformation zone correlates with offsets in the seismic reflections at this depth (Fig. **F23**), suggesting that it may represent the updip extension of the megasplay fault. A zone of high deformation and fracturing was also identified in the LWD resistivity images at 85–106 mbsf with a low-resistivity interval at ~100 mbsf, which is likely the location of the splay fault at Site C0022.

Preliminary scientific assessment

Expedition 338 was planned to extend riser Hole C0002F from 856 to 3600 mbsf beginning in early October 2012 and ending in early January 2013. The primary goals for Site C0002 were riser drilling, analyses of cuttings, mud gas, LWD data, and limited cores (2300–2400 mbsf). The hole was to be suspended after setting casing at 3600 mbsf. However, riser drilling operations were suspended at 2005.5 mbsf because of riser damage, so the following riserless contingency operations were conducted instead: coring in Holes C0002H (1100.5–1120 mbsf), C0002J (902–940 mbsf), C0002K (0–286.5 mbsf), C0002L (277–505 mbsf), C0021B (0–194.5 mbsf), and C0022B (0–419.5 mbsf) and LWD in Holes C0012H (0–709 mbsf), C0018B (0–350 mbsf), C0021A (0–294 mbsf), and C0022A (0–420 mbsf).

Overall success

Riser drilling was conducted in Hole C0002F to 2005.5 mbsf and suspended for future reoccupation and completion of the NanTroSEIZE project (i.e., drilling through and sampling the seismogenic part of the megasplay fault [~5000 mbsf] and installing a long-term observatory). LWD data, mud-gas analyses, and cuttings samples in Hole C0002F provided constraints on the lithologic and structural features, physical properties, and geochemistry of the previously unaccessed deeper part of the Nankai accretionary prism. Riserless coring in Holes C0002H, C0002J, C0002K, and C0002L provided core samples (1) across the gas hydrate zone including the BSR of the Kumano Basin, which was not cored during Expedition 315, (2) across the preliminary unconformity boundary between the Kumano Basin sediment and the underlying accretionary prism sediment, and (3) in the uppermost accretionary prism, which allowed constraints on the lithologic and structural features, physical properties, and fluid and gas chemistries of sediment in those intervals. Thus, these operations enabled not only exploration of the accretionary prism to ~2005 mbsf but also complemented current knowledge of Site C0002.

LWD at Sites C0012 and C0018 provided petrophysical data where coring had already been conducted during Expeditions 322 and 333. Integration of the LWD data with the core and the 3-D seismic data already obtained at or across these sites enabled us to comprehensively understand the nature of oceanic basement and its overlying sediment at a subduction input site (C0012) as well submarine landslide dynamics and MTD emplacement processes at a Nankai Trough Submarine Landslide History (NanTroSLIDE) site (C0018).

Site C0021 is located ~2 km northwest of Site C0018 and at a more proximal site for MTDs observed at Site C0018. LWD and coring at Site C0021 provided further information on the nature, provenance, and kinematics of the MTDs observed at Site C0018 and provided data on the lateral heterogeneity of MTDs.

Site C0022 is located ~350 m southeast of Site C0004, where the shallow portion of the megasplay fault was cored during Expedition 316. LWD and coring at Site C0022 provided logging data and samples across the tip of the megasplay fault, which provided additional information on the activity of the megasplay fault and its bearing on earthquakes and tsunamis.

Problems and challenges

On 17 November 2012, the passage of a cold front caused sudden changes in wind direction and strong winds (~27 m/s), which together with the strong Kuroshio Current (~4.8 kt) made it difficult for the *Chikyu* to maintain position. In order to ensure the safety of the ship and drilling equipment, an emergency disconnect of the blowout preventer (BOP) riser pipe was completed. This left the lower portion of the BOP on the seafloor, safely sealing off Hole C0002F, whereas the riser pipe and upper portion of the BOP remained connected to the *Chikyu*. After the disconnect, the strong Kuroshio Current caused the *Chikyu* to drift, creating drag on the riser pipe such that it was not vertical. This tilt in the riser pipe was accommodated primarily by the intermediate flex joint, which in turn suffered damage. Because of this damage, riser drilling was suspended and will resume with IODP Expedition 348. This series of events demonstrated the difficulty of riser operations under such bad weather and rough sea conditions; however, since such weather and sea conditions will also be encountered during future NanTroSEIZE expeditions, this is a major operational issue that needs to be properly addressed for future riser operations.

Riser drilling in Hole C0002F used RWD technology, which allowed LWD/MWD analysis behind a 12¼ inch drill bit while simultaneously opening the hole above the LWD/MWD tool assembly with a 20 inch reamer bit. The distance between the drill bit and the reamer bit was 42.8 m; therefore, RWD results in mixing of cuttings from an interval of at least 42.8 m. However, it was realized that unit boundaries defined by LWD data and those defined by cuttings observations and analyses varied by as much as ~100 m. Cuttings samples also limited lithology and structural observations, physical properties measurements, and pore fluid chemistry analyses. Mud gas was monitored during riser drilling in Hole C0002F. However, for unknown reasons, air contamination occurred in the shipboard gas monitoring system, which affected measurements of gas chemistry analyses.

During contingency riserless drilling, the drill pipe got stuck in the hole several times during drilling and coring the accretionary prism. This occurred because borehole cavings from the accretionary prism were circulated uphole to the base of the Kumano Basin sediment. This narrowed the annulus and choked the drill pipe. The drill pipe was freed after several hours of efforts in Hole C0002H but remained stuck for ~40 h until it was cut off at ~850 mbsf in Hole C0002I. Although similar drill pipe issues were experienced during IODP Expeditions 314 and 315, the extreme difficulty of drilling into the accretionary prism was again underlined during this expedition.

This expedition had one science party split into two groups. We had a week-long crossover time with the entire science party, four Co-Chief Scientists, and Specialty Coordinators in order to hand over the shipboard work and data analyses smoothly. However, because of the riser drilling cancellation, half of the science party worked exclusively on LWD and cuttings and mud-gas samples in Hole C0002F, whereas the other half worked on LWD and core samples at several different sites and holes. This aspect of Expedition 338 was extremely challenging for the Co-Chief Scientists, Expedition Project Managers, and science party. Issues that were particularly difficult were the unification of the two groups as well as integration of the scientific results and reports.

Operations

Methods

Site C0002

RWD was employed for the first time by IODP during Expedition 338 in order to allow cutting the 12¼ inch diameter pilot hole and opening the hole to 20 inches at the same time. This procedure was employed to facilitate the installation of casing strings; however, these strings were not installed because of the early termination of riser operations (see **"Site C0002"** operations below). There is a concentric hole opener between the bit and the underreamer. The underreamer used to enlarge the hole to 20 inches was the National Oilwell Varco Anderreamer. The design of the bottom-hole assembly (BHA) also included a complete LWD tool suite. During riserless coring, no underreamer was used and the bit had a 12¼ inch diameter and used the standard RCB coring system for Holes C0002H, C0002I, and C0002J. Holes C0002K and C0002L were cored with a HPCS, EPCS, and ESCS (Table **T2**).

Site C0012

Hole C0012H was drilled with an LWD tool string similar to that used for logging in Hole C0002F; however, no underreamer was used. The 12¼ inch polycrystalline diamond compact (PDC) bit was employed to allow drilling in soft and semi-indurated sediment and into basement.

Site C0018

Hole C0018B was drilled with an LWD tool string similar to that used for logging in Hole C0002F; however, neither the underreamer nor the sonicVISION tool were used. The 12¼ inch PDC bit was employed to allow drilling in soft and semi-indurated sediment and into basement.

Site C0021

Hole C0021A was drilled with the same LWD tool string that was used for logging in Hole C0018B. Hole C0021B was cored with HPCS and EPCS.

Site C0022

Hole C0022A was drilled with the same LWD tool string that was used for logging in Hole C0018B. Hole C0021B was cored with HPCS, EPCS, and ESCS.

Shimizu, Japan, port call

Expedition 338 officially began at 0000 h on 1 October 2012 while the *Chikyu* was north of Izu-Oshima, Japan, as part of the evacuation procedures for Typhoon Jelawat. The evacuation ended at 0400 h on 1 October, when the vessel began to return to port call in Shimizu, Japan. Port call began on 0550 h on 2 October, with all loading operations concluded by 2400 h on 3 October. The vessel departed Shimizu, Japan, for Site C0002 at 1035 h on 4 October.

Site C0002

Seabed survey and transponder deployment began at 1230 h on 5 October and were completed on 7 October 2012. After calibrating transponders, the *Chikyu* sailed to the BOP and riser running point 20.8 nmi northwest of Site C0002. A BOP and riser joints were set up in the moonpool and prepared for running beginning at 0400 h on 8 October. By 0400 h on 9 October, the BOP reached 490 m drilling depth below rig floor (DRF); however, because of the development of Typhoon Prapiroon, a decision was made to wait on weather (WOW) and follow the typhoon track at 0900 h on 9 October; subsequently, the BOP and riser began to be recovered for evacuation standby at 1300 h on 11 October, and recovery was completed at 0600 h on 12 October. The vessel moved 21 nmi northwest of Site C0002 to facilitate the arrival of the first scientists by helicopter transfer on 13 October and to avoid the strengthening current. The *Chikyu* continued to observe developing typhoon tracks, remaining in WOW status

until 0700 h on 19 October, when preparations to begin running the BOP into the moonpool commenced. Once the BOP was in the moonpool at ~1700 h, BOP pressure tests were run, ending at 1800 h when the BOP was run into the water. Careful attention was paid to the auxiliary (AUX) line and buoyant riser joints, all the while conducting a schedule of regular AUX pressure tests (six pressure tests in total). AUX line troubleshooting and buoyancy riser joint replacement was required on 21 October when one joint was replaced.

While running the BOP, several function tests and pressure tests found failures in the AUX line, conduit line, and hot line, which were subsequently repaired. The BOP finally landed on the wellhead at 2130 h on 26 October, and all function tests, repairs, and maintenance were complete by 1045 h on 29 October. The tests included a pickup test by increasing tensioner tension, slump tests by decreasing drawworks tension, function tests of the diverter, pressure tests of the wellhead connector and the 20 inch casing, function tests of the BOP from both the Blue Pod (driller's control panel) and the Yellow Pod (toolpusher's control panel), a pressure test of the BOP, a pressure test of the BOP with 20 inch casing and inside drill pipe, a function test of the remaining valves in block position, and confirmation of working time and flow rate of the BOP. The BHA for drill-out cement (DOC) was run into the hole at 1900 h on 30 October and tagged the bottom (842 mbsf) at 1415 h on 31 October. DOC with the 17 inch bit reached 872.5 mbsf, with an extension into the formation (to 875.5 mbsf) to confirm the cement layer was completely drilled through ended at 2045 h. After drilling was complete, the hole was swept with Hi-Vis mud, and then seawater, followed by KNPP mud. Methane (15.5%) was found in the drilling mud, and after monitoring, it was decided to move ahead with two LOTs of the 20 inch casing shoe starting at ~1100 h on 1 November. The DOC BHA was recovered and laid down, after which the LWD/MWD underreamer BHA was made up and run into the hole (Table **T3**) and tested at 0430 h on 2 November. All function tests (n = 4: shallow; 50 meters below sea level [mbsl]; 132.5 mbsf; and 778.5 mbsf) were successfully completed by 0100 h on 3 November, after which initial pilot hole drilling began. The BHA was picked up after drilling ahead to 915.19 mbsf, back to 905.8 mbsf at 0745 h on 4 November to activate the underreamer (total of six attempts made), which took ~2 h.

Drilling with 12¼ × 20 inch LWD/MWD with underreamer began at 1000 h on 4 November. Rate of penetration (ROP) was controlled at 40 m/h from 914.5 mbsf and changed to 20–26 m/h below 923.8 mbsf. Concerns with the large volume of cuttings, more than the waste mud control system could cope with, required careful control, sweeping, and sometimes suspension of drilling. Repeat logging was carried out three

times using these periods (~30 m/h): uplogging from 1495.5 to 1457.5 mbsf, downlogging from 1503.5 to 1538.5 mbsf, and downlogging from 1557.5 to 1615.5 mbsf. Expected rough weather caused drilling to be suspended at 1538.5 mbsf (2200 h on 5 November), and the BHA was pulled out of the hole above the BOP. Drilling resumed (ROP = 15 m/h) at 2100 h on November 6 but stopped again when 1604.5 mbsf was reached because black smoke flow was observed coming from one port on the BOP 36 inch pressure housing with subsequent hydrate accumulation around the wellhead (1230 h on 7 November). Observation for 6 h showed stable flow, so drilling was resumed (ROP = 10–15 m/h) at 2300 h on 7 November. From 1604.5 to 2005.5 mbsf (2300 h on 7 November to 0800 h on 11 November), drilling continued with some interruptions, mainly because of waste mud control system issues (e.g., mud pump problems, screw conveyer for mud transfer issues, and strong currents interfering with supply boats). Drilling was stopped again to standby for rough weather, and the BHA was pulled out of the hole above the BOP at 1515 h on 12 November.

During WOW, a critical function failure of the Double V Shear (DVS) ram (a key component of the BOP designed to close the hole while maintaining annular pressure after the BOP disconnects) was found. It was decided at 0530 h on 13 November to suspend the hole until the failure was resolved. Fortunately, the root cause of the failure was determined, and a mitigation plan was enacted for the BOP; therefore, at 0230 h on 14 November, the BOP disconnection plan was canceled. DOC began at 0115 h on 15 November and completed at 1630 h when the DOC BHA was pulled out of the hole to the surface. Subsequently, the Anderreamer BHA for reaming and enlarging the hole from 12¼ to 20 inches was run into the hole at 0000 h on 16 November. The Anderreamer was activated at 2848 m DRF at 0300 h; reaming was conducted from 0300 to 2300 h on 16 November. When bit depth reached 3955 m DRF (1990 mbsf) and the Anderreamer depth and 20 inch hole was at 3949 m DRF (1984 mbsf), an approaching weather system caused another WOW. Reaming and backreaming down to the final bit depth were performed over the next 5 h until the BHA was pulled out of the hole to 1576 m DRF by 1430 h on 17 November after performing backreaming in the hole and spotting high-viscosity mud water. As a standby operation, the kill line was flushed and the DVS ram was closed.

At 1730 h on 17 November, the vessel went into emergency disconnect as the current speed of ~4.5 kt from the west suddenly changed direction along with strong winds (~27 m/s), the combination of which forced the vessel 40 m from the well center, and control of the vessel was lost. The emergency disconnect was conducted both safely and efficiently as the vessel drifted 1300 m east of the wellhead at 4 kt. However,

while this was happening, the riser intermediate flex joints struck the hull of the vessel and sustained damage. Pulling out of the hole to the surface continued, ending at 0415 h on 18 November; whereupon the vessel recovered the ROV and moved to the low-current area (LCA) 13 nmi northwest of Hole C0002F to begin riser recovery. The tensioner ring was removed, and electrical cable connections were removed as well. Riser pullout began at 2300 h and termination joints were checked. The diverter was laid out from 0000 h on 19 November, and the riser termination joint was pulled out of the moonpool at 0430 h. The hot line was reterminated in the moonpool, and a pressure check from 1400 to 1800 h confirmed the BOP status was still good. The gooseneck was inspected, including welding points on the slip joint with magnetic particle inspection (MPI) for cracks from 2100 to 0030 h on 20 November. Riser sections continued to be pulled, stopping to perform pressure tests on the choke and kill lines for 3 hours from 0315 h. After the intermediate flex joint was pulled up, the termination joint weld was inspected via MPI, whereupon four cracks were found; advice on repair was sought from the manufacturer. The results of careful inspection and manufacturer advice led to the conclusion that the repairs needed could only be conducted on shore; accordingly, it was decided to end riser operations once it was clear that the time needed for repairs would exceed the total planned expedition duration. Meanwhile, a pressure test of the conduit and kill lines on the gooseneck passed inspection after several tests and leakage troubleshooting by 2315 h on 21 November. Once passed, the gooseneck was removed so the intermediate flex joint could be installed, finishing at 0600 h on 22 November. Once installed, the gooseneck and choke, booster, and kill moonpool hoses were made up, pressure-tested, and installed by 1515 h. The landing and riser joints were also picked up, connected, and lowered to the moonpool, where work began to couple the riser tensioners to the landing ring, finishing by 0330 h on 23 November. After the ROV was launched, a dummy-landing test 50 m from the well center was conducted successfully at 1730 h, and by 2030 h the lower marine riser package (LMRP) was landed on the lower BOP stack and locked in place. Riser running components were laid down by 0600 h on 24 November. The diverter assembly was made up and run into the hole to 2987 m DRF by 1700 h, and then was slowly pulled out of the hole to 2878 m DRF. The first cement plug was set at 2200 h, and then pulled out of the hole to 2460 m DRF while waiting for cement. At 0445 h on 25 November, the BHA was run into the hole back to 2805 m DRF to confirm the top of cement and begin the first cement plug pressure test. After confirming the cement plug, the BHA was pulled out of the hole to 2367 m DRF to set the second cement plug, pulled out of the hole to 2120 m DRF, and then pulled out of the hole to the surface by 1745 h. The Hydralift Power Swivel (HPS) was parked and

the riser running tool and riser guide head were installed, finishing at 2245 h. Once complete, the master bushing was removed while the ROV removed the hydrate build-up around the wellhead connector. The diverter and upper flex joint were picked up and laid down by 0400 h on 26 November, whereupon the BOP was disconnected, the wellhead was examined by the ROV, and the ROV was recovered to the surface by 0730 h. The vessel moved to the LCA ~15 nmi from Hole C0002F and began recovering riser joints and the BOP at 1200 h on 27 November. The intermediate flex joint was recovered at 0200 h on 28 November, after which riser joint and BOP recovery continued. Recovery was briefly halted on 30 November to load the guide horn from the supply boat *Shincho-Maru* and resumed at 1000 h. The riser joints were all recovered and laid down by 0930 h on 1 December, after which the BOP was pulled out to the surface, landed on the BOP cart, and moved to its storage position aft of the moonpool by 1815 h. Once the BOP was loaded on the cart, the HPS was rigged up again, and the vessel returned to Site C0002, arriving at 0630 h on 1 December. At Site C0002, the ROV dove at 0745 h, and the vessel shifted to the Hole C0002G long-term borehole monitoring system (LTBMS) observatory for ROV inspection. The vessel shifted back to Hole C0002F, and the ROV set the corrosion cap and checked the bull's eyes, finishing by 1145 h. Once complete, the ROV began simultaneously recovering and deploying transponders; 4 transponders were deployed and 10 were recovered, all completed by 0330 h on 2 December. The lower and middle guide horn sections were set on the BOP cart and connected by 0415 h; once connected, the vessel moved to Site C0012.

Hole C0002H

On 8 December at 0130 h, the ship moved 7 nmi north-northwest of Hole C0002H after preparations for coring began with the makeup of the RCB BHA. There was a short WOW lasting until 1600 h, after which the vessel moved to within 5 nmi west of the well center. Drifting in began at 1800 h while the BHA was run into the hole, with a 1 h standby as an internal blowout preventer ball valve malfunction was solved. We continued to drift in to the well center, dropping the center bit at 0300 h on 9 December. The seafloor was tagged and confirmed at 1965 m DRF (1936.5 mbsl) at 0345 h, as indicated by an increase in WOB. We washed down the first 36 m then began drilling a 10⅝ inch hole at 0430 h, reaching 752 mbsf by 2000 h. The sinker bar was run down to recover the center bit for a wear check at 2145 h and dropped again at 2330 h, landing 13 min later. We then drilled down to 1055 mbsf by 0730 h on 10 December. After a series of sweeping out the hole, drilling ahead, and sweeping again, the sinker bar was run at 1100 mbsf to recover the center bit in preparation for

dropping the inner core barrel before coring began. At 1430 h, the first coring began, advancing 9.5 m to 1110 mbsf before being recovered on deck at 1545 h. The BHA was stuck for the next 45 min, but after working and sweeping, the core barrel was dropped at 1845 h for the next coring advance. Coring to 1120 mbsf (9.5 m coring advance) began and was recovered on deck at 2105 h. After the core barrel was recovered, the drill pipe was stuck in the hole again, but constant work freed the pipe at 0145 h on 11 December. The BHA was pulled out of the hole with reaming and laid down on deck by 0715 h. No obvious overpull or packoff indication was seen on the drill string, so preparations to return to RCB coring began. The vessel was moved 2 nmi from the next well for preparation for running the RCB BHA into the hole.

Hole C0002I

Hole C0002I operations began with drifting in at 1100 h on 11 December and dropping the center bit at 1630 h prior to spudding in at 1964.5 m DRF (1936 mbsl) 9 min later. The first 33.5 m was washed down and drilling ahead began at 1800 h, reaching 818.5 mbsf at 0600 h on 12 December. Another series of drilling ahead, sweeping, and hole cleaning began once past 905 mbsf. On 13 December, the bit reached 1360 mbsf at 0430 h, continuing until 0445 h on 13 December, when the 4S azimuth thruster shut down and dynamic positioning (DP) status changed to "yellow." Once this occurred, the BHA was pulled out of the hole to 900 mbsf in preparation for emergency pulling out of the hole to the seafloor. The 4S azimuth thruster was restarted at 0600 h, and DP status returned to "green." Circulation and hole cleaning began once "green" status was recovered and drilling back to 1105.5 mbsf stopped at 1005 mbsf, whereupon the BHA became stuck at 1030 h on 13 December. Operations to free the stuck pipe began immediately. Attempts to recover the center bit at 1400 h on 14 December were unsuccessful; therefore, rig up of the Schlumberger wireline tool, the Free-Point Indicator Tool (FPIT), began on 1645 h. The stuck position was confirmed at 853 and 915 mbsf, after which the FPIT was rigged down for running the colliding tool to free the drill pipe on 0300 h on 15 December. The colliding tool was set and the explosive primed at 0700 h, when operations to install the colliding tool were suspended because of bad weather conditions, specifically high winds. The lower connection of the drill pipe on the rig floor was broken to run the colliding tool directly from the rig floor by 0745 h when the Schlumberger wireline winch failed. Troubleshooting began immediately, finishing at 2130 h. The colliding tool was rigged up and the explosive was reset by 2315 h. The tool was run at 0300 h on 16 December, and the drill pipe was cut at 0345 h. The colliding tool was rigged down by 0515 h, and pulling out of the hole began. After the tools were laid down, the *Chikyu* moved

to the LCA to load equipment and to perform maintenance on the HPS top drive, ending on 17 December. After pressure tests confirmed the integrity of the HPS repairs, we began making up and testing the RCB BHA for Hole C0002J.

Hole C0002J

The vessel moved to a position 3 nmi west of Hole C0002J, while the RCB BHA was made up and run into the hole from 1830 h on 17 December. Spudding in Hole C0002J was confirmed at 1966 m DRF (1937.5 mbsl) at 0830 h on 18 December, and the BHA immediately jetting in the first 35 mbsf before drilling began. By 2330 h, the bit reached 872.5 mbsf before stopping to space out a single joint. Drilling down continued until reaching 902 mbsf at 0045 h on 19 December, and after sweeping out the hole, coring began from 0430 h. A total of seven RCB cores were collected, finishing at a total depth (TD) of 940 mbsf at 1930 h. Once coring was completed, kill mud was spotted and the RCB BHA was pulled out of the hole to the surface, and tool lay down was completed by 0545 h on 20 December. The vessel moved upstream 2 nmi to Hole C0002K and began preparations for coring in Hole C0002K.

Hole C0002K

Preparations for HPCS/ESCS coring started from 0545 h on 20 December, and the BHA was run into the hole to 1966 m DRF (estimated water depth = 1937.5 mbsl) by 1645 h. The 11⅞ inch BHA washed down the first 30 mbsf by 1700 h then began drilling ahead to 200 mbsf. From 2230 h, coring began with the HPCS, ending after reaching 204.5 mbsf. The low recovery of the last HPCS core (n = 2) caused the drilling program to switch to the ESCS from 204.5 mbsf. The ESCS assembly preparation was completed by 0215 h on 21 December. The inner barrel was dropped 15 min later when ESCS coring began. A total of 11 ESCS cores were collected from 204.5 to 286.5 mbsf and the last core was cut at 2315 h on 21 December. Once coring was completed, the ESCS BHA was pulled out of the hole to 1780 m DRF by 0100 h on 22 December. Two stands of S-150 drill pipe were added, and then the BHA was run down to 1800 m DRF to WOW from 0300 to 0830 h on 22 December. Once the cold front had passed, the vessel was shifted to the Hole C0002L well center for more coring.

Hole C0002L

The ESCS was run down from 1800 to 1960 m DRF by 1030 h, just above the seafloor. Spudding in Hole C0002L began at 1045 h (water depth = 1937.5 mbsl) and proceeded to wash down to 42 mbsf, after which drilling down to 277 mbsf was completed by 1830 h. ESCS coring began at 277 mbsf from 2000 h on 22 December,

finishing at a TD of 505.0 mbsf with Core 338-C0002L-24X at 0215 h on 25 December. Once coring operations were completed, 35 m^3 of kill mud was spotted in the hole and the BHA was pulled out of the hole to 1932 m DRF (above the seabed) by 0400 h. The BHA was laid down by 1030 h, after which transponders were released and recovered (by 1230 h) by the watch boat, ending Hole C0002L operations. The vessel shifted 2 nmi upstream of Site C0018 in preparation for LWD drilling.

Hole C0012H

The *Chikyu* arrived at Site C0012 at 1045 h on 2 December; the ROV was prepared with four transponders and dove at 1230 h. The ROV dropped the transponders by 2100 h, after which it was recovered to the surface and the vessel moved to the planned Hole C0012H well center by 2200 h. DP calibration was complete by 2345 h, and the LWD assembly including the sonicVISION tool was made up for running into the hole. The LWD BHA began running into the hole at 0430 h on 3 December. After passing a series of mid-water tests, the LWD tools reached the seafloor when the real-time data signal was lost. After spending some time on troubleshooting operations, the tool was pulled out of the hole to the rig floor for examination and possible replacement, reaching the deck at 0245 h on 4 December. Although a jamming alert from the TeleScope was received and visual inspection found no issues were found with the tool, a spare TeleScope was swapped into the BHA and ran back into the hole at 0645 h on 4 December. A series of tests were again run as the BHA was run down to the seafloor, and once all tests had been completed successfully, the LWD BHA was ready to spud in. Using the LWD tools to determine the mudline, the seafloor was set at 3538 m DRF (3509.5 mbsl) and drilling ahead resumed from 1730 h. The Schlumberger logging engineers were concerned that the sonicVISION configuration should be changed by downlink because in their estimation the real-time sonic velocity was not reliable. After close consultations with the Co-Chief Scientists, it was decided to leave the sonicVISION configuration as is and continue drilling from 3686 m DRF at 2315 h on 4 December. At 0430 h on 6 December, the planned TD of 4238 m DRF (700 mbsf) was reached, after which an additional 10 m was drilled ahead to allow the sonicVISION tool to record an interval where resistivity was seen to increase. The final TD in Hole C0012H of 4248 m DRF (710 mbsf) was reached at 0515 h, when circulation, a spot of kill mud was set, before pulling out of the hole to 1994 m DRF began, ending at 1145 h. The BHA reached the surface at 2300 h, after which the tools were laid down and preparation for coring began. Transponders were released from the sea-

floor and all were recovered by the *Hakuryu-Maru* by 1500 h on 7 December. The vessel then began to move to Site C0002 for coring operations.

Hole C0018B

The *Chikyu* moved to Site C0018 (water depth = 3084.5 mbsl) after completing all operations at Site C0002. Making up and running the LWD BHA started at 1400 h on 25 December. The 12¼ inch LWD BHA components were similar to Hole C0012H operations with the exception of the sonicVISON tool. Function tests on the LWD were conducted at 76, 1060, 2006, and 3100 m DRF, respectively, while lowering the LWD BHA. Spud-in of Hole C0018B was confirmed by real-time resistivity data at 0430 h on 26 December. Washing down with a controlled ROP at an average of 40 m/h (maximum = 50 m/h) changed to drilling ahead from 40 mbsf at 0600 h. Rotation speed was gradually increased, step-wise, to TD (350 mbsf): 15 rotations per minute (rpm) × 1.8–2.5 kNm (40–45 mbsf), 30 rpm × 0–5.0 kNm (45–50 mbsf), 45 rpm × 0–5.0 kNm (50–67 mbsf), 60 rpm × 0–5.0 kNm (67–242 mbsf), and 80 rpm × 1.6–8.3 kNm (242–350 mbsf). The target depth was reached by 1130 h on 26 December. After spotting kill mud, the LWD BHA was pulled out of the hole to 2813 m DRF (300 m above the seafloor) by 2000 h on 26 December in preparation for operations at Site C0021.

Hole C0021A

The *Chikyu* shifted from Hole C0018B, where LWD/MWD operations had just been completed, and prepared to begin running the LWD drilling BHA into the hole from 2200 h on 26 December. The seabed was tagged (water depth = 2940.5 mbsl) at 2330 h, and washing down to 40 mbsf in Hole C0021A commenced. From 40 mbsf, drilling ahead began at 0100 h on 27 December, again increasing rotation speed in gradual stepped increases to TD (294.0 mbsf): 15 rpm × 1.8–2.5 kNm (40–45 mbsf), 30 rpm × 0–5.0 kNm (45–50 mbsf), 45 rpm × 0–5.0 kNm (50–60 mbsf), 60 rpm × 0–5.0 kNm (67–103 mbsf), and 80 rpm × 1.6–8.3 kNm (103–294 mbsf). TD was reached at 1100 h, and the hole was spotted with kill mud. While the LWD BHA was pulled out of the hole to the surface, overpull (80 kN) was observed from 88 to 101 mbsf; no other overpull was observed. The tools were broken and racked back to the derrick while the vessel moved to the next site by 2030 h in preparation for LWD at Site C0022.

Site C0022

Hole C0022A

Operations began with dropping transponders at Site C0022 from 2030 h on 27 December. The transponders were all confirmed on the seabed by 0143 h on 28 December, whereupon DP calibration began, finishing at 0530 h. The vessel moved 1.5 nmi upcurrent from the well center and began making up and running the LWD BHA into the hole from 0730 h. The LWD BHA was run to 260 m DRF by 1445 h, when time was taken to test the active heave compensator (AHC). After 30 min in standby mode, the AHC test was suspended because the cause of the malfunction could not be found. Running into the hole continued to the seabed, when Hole C0022A was spudded at 1600 h (water depth = 2675.5 mbsl) and the next 40.5 mbsf was washed down. From 1730 h, LWD drilling commenced following the same rotation speed increase with depth plan to TD as for Holes C0018B and C0021A (15 rpm × 0.6–2.5 kNm [40.5–45.5 mbsf], 30 rpm × 0.9–3.4 kNm [45.5–50.5 mbsf], 45 rpm × 0.5–4.7 kNm [50.5–60.5 mbsf], 60 rpm × 0.8–4.4 kNm [60.5–82.5 mbsf], 70 rpm × 1.1–7.9 kNm [82.5–111.5 mbsf], and 80 rpm × 0.9–14.1 kNm [111.5–136 mbsf]). Kill mud was spotted from 2200 h, and the LWD BHA was pulled out of the hole to 36 mbsf for WOW. At 0300 h on 29 December, the LWD BHA was run down to 96 mbsf and then reamed down from 0330 h to 136.0 mbsf. Once back at 136.0 mbsf, drilling ahead with the LWD BHA resumed to TD (420.5 mbsf), finishing at 1645 h. From 1715 h the LWD BHA was pulled out of the hole to 2692.6 m DRF (11 m above seabed), while a damaged drill pipe joint was laid down. Pulling out of the hole continued from 1930 h, reaching the surface by 0315 h on 30 December.

Hole C0022B

At 1800 h on 30 December, the vessel moved 10 nmi north of Site C0022, into the LCA, to begin loading bentonite and drilling equipment. From 2130 h, the HPCS/ESCS BHA was made up and tested. From 0115 h the BHA was run into the hole and the vessel began drifting toward the well center by 0300 h on 31 December. The HPCS BHA reached 2960 m DRF by 0745 h and for the next 2 h stood by while the core BOP ball valve was worked on. The bit was lowered to 2700 m DRF (2 m above seabed), the sinker bar was run down at 1130 h in preparation for cutting the first core, and spud-in and shooting took place at 1245 h (seafloor = 2674 mbsl). Washing down to 19.5 mbsf ended at 1500 h, and piston coring resumed at 1600 h. By 0515 h on 1 January, HPCS Core 338-C0022B-8H had been cut at 84.5 mbsf. At that point, coring operations switched from HPCS to EPCS, cutting the first EPCS core (9T) by 0945 h to 89.5

mbsf. At 1730 h, the coring system was changed from EPCS to ESCS, cutting from 99.5 mbsf. ESCS coring continued, pausing at 1315 h on 2 January to drill ahead from 171.5 to 190.5 mbsf. ESCS coring from 190.5 mbsf resumed at 1715 h. There was another pause in ESCS coring on 0315 h on 3 January, while drilling ahead from 228.5 to 266.5 mbsf (38 m advance) was completed. ESCS Core 338-C0022B-24X was cut from 0900 h, after which coring resumed. Coring in Hole C0022B finished at 0745 h on 5 January with the recovery of Core 41X. Kill mud was spotted, and the ESCS BHA was pulled out of the hole to the surface by 2330 h. As drill pipe was laid down, the transponders were released and recovered on the surface by the watch boat. The vessel began moving to Site C0021 in preparation for coring operations.

Hole C0021B

After coring operations were completed in Hole C0022B, preparations began for testing the small-diameter rotary core barrel (SD-RCB) system at 1515 h on 6 January; however, during make-up of the SD-RCB BHA, it was found that the head sub would not fit the other SD-RCB parts, so the test was cancelled at 1900 h. From that time, the HPCS/ESCS coring BHA making up and running into the hole began for coring at Site C0021. By 0300 h on 7 January, the BHA had reached 2930.7 m DRF while drifting in to Site C0021 (the well center was reached by 0145 h). From 0330 h, troubleshooting the crown-mounted heave compensator (CMC) began, during which operations continued in stand-by while the main HPS line was also cut and slip. Upon completion at 1030 h, the coring BHA continued to be run into the hole to 2946 m DRF. The coring BHA was set to capture the first core while still above the seafloor, so at 1145 h, while the BHA was at 2969 m DRF, the HPCS inner barrel was shot, penetrating 5.9 m. The seafloor was then determined as being 2972.5 m DRF (2944.0 mbsl). After the first core was taken, the BHA was washed down to 80 mbsf before coring resumed at 1515 h. There was a short pause in coring from 1845 to 2045 h while the wireline BOP hydraulic hose leak was fixed. Coring resumed from Core 338-C0021B-5H at 108.5 mbsf from 2100 h, and ended at Core 12H; Cores 10H, 11H, and 12H ended up becoming stuck in the inner core barrel to greater and lesser degrees; therefore, coring continued with the EPCS for the last two cores. Efforts to recover the stuck core liners continued on the rig floor until 9 January as coring continued. EPCS Core 338-C0021B-13T was cut at 1730 h from 175.5 mbsf, and coring finished with EPCS Core 14T to a final TD of 194.5 mbsf at 2100 h on 8 December. Kill mud was spotted at 2230 h and the EPCS BHA was pulled out of the hole to the surface, finishing at 0130 h on 10 January, ending operations related to Site C0021. The ship began

transit to Shimizu port, Japan, reaching port on the morning of 11 January 2013. The scientists disembarked on 12 January 2013; the official end of the expedition was 13 January.

References

Ando, M., 1975. Source mechanisms and tectonic significance of historical earthquakes along the Nankai Trough, Japan. *Tectonophysics,* 27(2):119–140. **doi:10.1016/0040-1951(75)90102-X**

Ashi, J., Kuramoto, S., Morita, S., Tsunogai, U., Goto, S., Kojima, S., Okamoto, T., Ishimura, T., Ijiri, A., Toki, T., Kudo, S., Asai, S., and Utsumi, M., 2002. Structure and cold seep of the Nankai accretionary prism off Kumano—outline of the off Kumano survey during YK01-04 Leg 2 cruise. *JAMSTEC J. Deep-Sea Res.,* 20:1–8. (in Japanese, with abstract in English)

Ashi, J., Lallemant, S., Masago, H., and the Expedition 315 Scientists, 2009. Expedition 315 summary. *In* Kinoshita, M., Tobin, H., Ashi, J., Kimura, G., Lallemant, S., Screaton, E.J., Curewitz, D., Masago, H., Moe, K.T., and the Expedition 314/315/316 Scientists, *Proc. IODP,* 314/315/316: Washington, DC (Integrated Ocean Drilling Program Management International, Inc.). **doi:10.2204/iodp.proc.314315316.121.2009**

Baba, T., and Cummins, P.R., 2005. Contiguous rupture areas of two Nankai Trough earthquakes revealed by high-resolution tsunami waveform inversion. *Geophys. Res. Lett.,* 32(8):L08305. **doi:10.1029/2004GL022320**

Baba, T., Cummins, P.R., and Hori, T., 2005. Compound fault rupture during the 2004 off the Kii Peninsula earthquake (*M* 7.4) inferred from highly resolved coseismic sea-surface deformation. *Earth, Planets Space,* 57(3):167–172. **http://www.terrapub.co.jp/journals/EPS/pdf/2005/5703/57030167.pdf**

Baba, T., Cummins, P.R., Hori, T., and Kaneda, Y., 2006. High precision slip distribution of the 1944 Tonankai earthquake inferred from tsunami waveforms: possible slip on a splay fault. *Tectonophysics,* 426(1–2):119–134. **doi:10.1016/j.tecto.2006.02.015**

Expedition 314 Scientists, 2009a. Expedition 314 Site C0002. *In* Kinoshita, M., Tobin, H., Ashi, J., Kimura, G., Lallemant, S., Screaton, E.J., Curewitz, D., Masago, H., Moe, K.T., and the Expedition 314/315/316 Scientists, *Proc. IODP,* 314/315/316: Washington, DC (Integrated Ocean Drilling Program Management International, Inc.). **doi:10.2204/iodp.proc.314315316.114.2009**

Expedition 314 Scientists, 2009b. Expedition 314 Site C0004. *In* Kinoshita, M., Tobin, H., Ashi, J., Kimura, G., Lallemant, S., Screaton, E.J., Curewitz, D., Masago, H., Moe, K.T., and the Expedition 314/315/316 Scientists, *Proc. IODP,* 314/315/316: Washington, DC (Integrated Ocean Drilling Program Management International, Inc.). **doi:10.2204/iodp.proc.314315316.116.2009**

Expedition 315 Scientists, 2009. Expedition 315 Site C0002. *In* Kinoshita, M., Tobin, H., Ashi, J., Kimura, G., Lallemant, S., Screaton, E.J., Curewitz, D., Masago, H., Moe, K.T., and the Expedition 314/315/316 Scientists, *Proc. IODP,* 314/315/316: Washington, DC (Integrated Ocean Drilling Program Management International, Inc.). **doi:10.2204/iodp.proc.314315316.124.2009**

Expedition 316 Scientists, 2009a. Expedition 316 Site C0004. *In* Kinoshita, M., Tobin, H., Ashi, J., Kimura, G., Lallemant, S., Screaton, E.J., Curewitz, D., Masago, H., Moe, K.T., and the Expedition 314/315/316 Scientists, *Proc. IODP,* 314/315/316: Washington, DC (Inte-

grated Ocean Drilling Program Management International, Inc.). **doi:10.2204/iodp.proc.314315316.133.2009**

Expedition 316 Scientists, 2009b. Expedition 316 Site C0008. *In* Kinoshita, M., Tobin, H., Ashi, J., Kimura, G., Lallemant, S., Screaton, E.J., Curewitz, D., Masago, H., Moe, K.T., and the Expedition 314/315/316 Scientists, *Proc. IODP,* 314/315/316: Washington, DC (Integrated Ocean Drilling Program Management International, Inc.). **doi:10.2204/iodp.proc.314315316.136.2009**

Expedition 319 Scientists, 2010. Expedition 319 summary. *In* Saffer, D., McNeill, L., Byrne, T., Araki, E., Toczko, S., Eguchi, N., Takahashi, K., and the Expedition 319 Scientists, *Proc. IODP,* 319: Tokyo (Integrated Ocean Drilling Program Management International, Inc.). **doi:10.2204/iodp.proc.319.101.2010**

Expedition 322 Scientists, 2010a. Site C0011. *In* Saito, S., Underwood, M.B., Kubo, Y., and the Expedition 322 Scientists, *Proc. IODP,* 322: Tokyo (Integrated Ocean Drilling Program Management International, Inc.). **doi:10.2204/iodp.proc.322.103.2010**

Expedition 322 Scientists, 2010b. Site C0012. *In* Saito, S., Underwood, M.B., Kubo, Y., and the Expedition 322 Scientists, *Proc. IODP,* 322: Tokyo (Integrated Ocean Drilling Program Management International, Inc.). **doi:10.2204/iodp.proc.322.104.2010**

Expedition 326 Scientists, 2011. NanTroSEIZE Stage 3: plate boundary deep riser: top hole engineering. *IODP Prel. Rept.,* 326. **doi:10.2204/iodp.pr.326.2011**

Expedition 332 Scientists, 2011a. Expedition 332 summary. *In* Kopf, A., Araki, E., Toczko, S., and the Expedition 332 Scientists, *Proc. IODP,* 332: Tokyo (Integrated Ocean Drilling Program Management International, Inc.). **doi:10.2204/iodp.proc.332.101.2011**

Expedition 332 Scientists, 2011b. Site C0002. *In* Kopf, A., Araki, E., Toczko, S., and the Expedition 332 Scientists, *Proc. IODP,* 332: Tokyo (Integrated Ocean Drilling Program Management International, Inc.). **doi:10.2204/iodp.proc.332.104.2011**

Expedition 333 Scientists, 2012a. Expedition 333 summary. *In* Henry, P., Kanamatsu, T., Moe, K., and the Expedition 333 Scientists, *Proc. IODP,* 333: Tokyo (Integrated Ocean Drilling Program Management International, Inc.). **doi:10.2204/iodp.proc.333.101.2012**

Expedition 333 Scientists, 2012b. Site C0012. *In* Henry, P., Kanamatsu, T., Moe, K., and the Expedition 333 Scientists, *Proc. IODP,* 333: Tokyo (Integrated Ocean Drilling Program Management International, Inc.). **doi:10.2204/iodp.proc.333.105.2012**

Expedition 333 Scientists, 2012c. Site C0018. *In* Henry, P., Kanamatsu, T., Moe, K., and the Expedition 333 Scientists, *Proc. IODP,* 333: Tokyo (Integrated Ocean Drilling Program Management International, Inc.). **doi:10.2204/iodp.proc.333.103.2012**

Heki, K., 2007. Secular, transient, and seasonal crustal movements in Japan from a dense GPS array: implication for plate dynamics in convergent boundaries. *In* Dixon, T.H., and Moore, J.C. (Eds.), *The Seismogenic Zone of Subduction Thrust Faults:* New York (Columbia Univ. Press), 512–539.

Hori, T., Kato, N., Hirahara, K., Baba, T., and Kaneda, Y., 2004. A numerical simulation of earthquake cycles along the Nankai Trough in southwest Japan: lateral variation in frictional property due to the slab geometry controls the nucleation position. *Earth Planet. Sci. Lett.,* 228(3–4):215–226. **doi:10.1016/j.epsl.2004.09.033**

Ichinose, G.A., Thio, H.K., Somerville, P.G., Sato, T., and Ishii, T., 2003. Rupture process of the 1944 Tonankai earthquake (M_s 8.1) from the inversion of teleseismic and regional seismograms. *J. Geophys. Res., [Solid Earth],* 108(B10):2497. **doi:10.1029/2003JB002393**

Ike, T., Moore, G.F., Kuramoto, S., Park, J.-O., Kaneda, Y., and Taira, A., 2008. Variations in sediment thickness and type along the northern Philippine Sea plate at the Nankai Trough. *Isl. Arc,* 17(3):342–357. **doi:10.1111/j.1440-1738.2008.00624.x**

Inagaki, F., Hinrichs, K.-U., Kubo, Y., and the Expedition 337 Scientists, 2012. Deep coalbed biosphere off Shimokita: microbial processes and hydrocarbon system associated with deeply buried coalbed in the ocean. *IODP Prel. Rept.,* 337. **doi:10.2204/iodp.pr.337.2012**

Ito, Y., and Obara, K., 2006. Very low frequency earthquakes within accretionary prisms are very low stress-drop earthquakes. *Geophys. Res. Lett.,* 33(9):L09302. **doi:10.1029/2006GL025883**

Ito, Y., Obara, K., Shiomi, K., Sekine, S., and Hirose, H., 2007. Slow earthquakes coincident with episodic tremors and slow slip events. *Science,* 315(5811):503–506. **doi:10.1126/science.1134454**

Kikuchi, M., Nakamura, M., and Yoshikawa, K., 2003. Source rupture processes of the 1944 Tonankai earthquake and the 1945 Mikawa earthquake derived from low-gain seismograms. *Earth, Planets Space,* 55(4):159–172. **http://www.terrapub.co.jp/journals/EPS/pdf/2003/5504/55040159.pdf**

Kimura, G., Moore, G.F., Strasser, M., Screaton, E., Curewitz, D., Streiff, C., and Tobin, H., 2011. Spatial and temporal evolution of the megasplay fault in the Nankai Trough. *Geochem., Geophys., Geosyst.,* 12:Q0A008. **doi:10.1029/2010GC003335**

Kinoshita, M., Tobin, H., Ashi, J., Kimura, G., Lallemant, S., Screaton, E.J., Curewitz, D., Masago, H., Moe, K.T., and the Expedition 314/315/316 Scientists, 2009. *Proc. IODP,* 314/315/316: Washington, DC (Integrated Ocean Drilling Program Management International, Inc.). **doi:10.2204/iodp.proc.314315316.2009**

Miyazaki, S., and Heki, K., 2001. Crustal velocity field of southwest Japan: subduction and arc-arc collision. *J. Geophys. Res., [Solid Earth],* 106(B3):4305–4326. **doi:10.1029/2000JB900312**

Moore, G.F., Bangs, N.L., Taira, A., Kuramoto, S., Pangborn, E., and Tobin, H.J., 2007. Three-dimensional splay fault geometry and implications for tsunami generation. *Science,* 318(5853):1128–1131. **doi:10.1126/science.1147195**

Moore, G.F., Mikada, H., Moore, J.C., Becker, K., and Taira, A. 2005. Legs 190 and 196 synthesis: deformation and fluid flow processes in the Nankai Trough accretionary prism. *In* Mikada, H., Moore, G.F., Taira, A., Becker, K., Moore, J.C., and Klaus, A. (Eds.), *Proc. ODP, Sci. Results,* 190/196: College Station, TX (Ocean Drilling Program), 1–25. **doi:10.2973/odp.proc.sr.190196.201.2005**

Moore, G.F., Park, J.-O., Bangs, N.L., Gulick, S.P., Tobin, H.J., Nakamura, Y., Sato, S., Tsuji, T., Yoro, T., Tanaka, H., Uraki, S., Kido, Y., Sanada, Y., Kuramoto, S., and Taira, A., 2009. Structural and seismic stratigraphic framework of the NanTroSEIZE Stage 1 transect. *In* Kinoshita, M., Tobin, H., Ashi, J., Kimura, G., Lallemant, S., Screaton, E.J., Curewitz, D., Masago, H., Moe, K.T., and the Expedition 314/315/316 Scientists, *Proc. IODP,* 314/315/316: Washington, DC (Integrated Ocean Drilling Program Management International, Inc.). **doi:10.2204/iodp.proc.314315316.102.2009**

Moore, G.F., Taira, A., Klaus, A., Becker, L., Boeckel, B., Cragg, B.A., Dean, A., Fergusson, C.L., Henry, P., Hirano, S., Hisamitsu, T., Hunze, S., Kastner, M., Maltman, A.J., Morgan, J.K., Murakami, Y., Saffer, D.M., Sánchez-Gómez, M., Screaton, E.J., Smith, D.C., Spivack, A.J., Steurer, J., Tobin, H.J., Ujiie, K., Underwood, M.B., and Wilson, M., 2001. New insights into deformation and fluid flow processes in the Nankai Trough accretionary prism: results of Ocean Drilling Program Leg 190. *Geochem., Geophys., Geosyst.,* 2(10):1058. **doi:10.1029/2001GC000166**

Nakanishi, A., Takahashi, N., Park, J.-O., Miura, S., Kodaira, S., Kaneda, Y., Hirata, N., Iwasaki, T., and Nakamura, M., 2002. Crustal structure across the coseismic rupture zone of the 1944 Tonankai earthquake, the central Nankai Trough seismogenic zone. *J. Geophys. Res., [Solid Earth],* 107(B1). **doi:10.1029/2001JB000424**

Obana, K., and Kodaira, S., 2009. Low-frequency tremors associated with reverse faults in a shallow accretionary prism. *Earth Planet. Sci. Lett.,* 287(1–2):168–174. **doi:10.1016/j.epsl.2009.08.005**

Obana, K., Kodaira, S., and Kaneda, Y., 2005. Seismicity in the incoming/subducting Philippine Sea plate off the Kii Peninsula, central Nankai Trough. *J. Geophys. Res.,* 110(B11):B11311. **doi:10.1029/2004JB003487**

Obana, K., Kodaira, S., Mochizuki, K., and Shinohara, M., 2001. Micro-seismicity around the seaward updip limit of the 1946 Nankai earthquake dislocation area. *Geophys. Res. Lett.,* 28(12):2333–2336. **doi:10.1029/2000GL012794**

Obara, K., and Ito, Y., 2005. Very low frequency earthquakes excited by the 2004 off the Kii Peninsula earthquakes: a dynamic deformation process in the large accretionary prism. *Earth, Planets Space,* 57(4):321–326. **http://www.terrapub.co.jp/journals/EPS/pdf/2005/5704/57040321.pdf**

Park, J.-O., Tsuru, T., Kodaira, S., Cummins, P.R., and Kaneda, Y., 2002. Splay fault branching along the Nankai subduction zone. *Science,* 297(5584):1157–1160. **doi:10.1126/science.1074111**

Park, J.-O., Tsuru, T., No, T., Takizawa, K., Sato, S., and Kaneda, Y., 2008. High-resolution 3D seismic reflection survey and prestack depth imaging in the Nankai Trough off southeast Kii Peninsula. *Butsuri Tansa,* 61:231–241. (in Japanese, with abstract in English)

Schwartz, S.Y., and Rokosky, J.M., 2007. Slow slip events and seismic tremor at circum-Pacific subduction zones. *Rev. Geophys.,* 45(3):RG3004. **doi:10.1029/2006RG000208**

Screaton, E.J., Kimura, G., Curewitz, D., and the Expedition 316 Scientists, 2009. Expedition 316 summary. *In* Kinoshita, M., Tobin, H., Ashi, J., Kimura, G., Lallemant, S., Screaton, E.J., Curewitz, D., Masago, H., Moe, K.T., and the Expedition 314/315/316 Scientists, *Proc. IODP,* 314/315/316: Washington, DC (Integrated Ocean Drilling Program Management International, Inc.). **doi:10.2204/iodp.proc.314315316.131.2009**

Seno, T., Stein, S., and Gripp, A.E., 1993. A model for the motion of the Philippine Sea plate consistent with NUVEL-1 and geological data. *J. Geophys. Res., [Solid Earth],* 98(B10):17941–17948. **doi:10.1029/93JB00782**

Strasser, M., Henry, P., Kanamatsu, T., Moe, K.T., Moore, G.F., and the IODP Expedition 333 Scientists, 2012. Scientific drilling of mass-transport deposits in the Nankai accretionary wedge: first results from IODP Expedition 333. *In* Yamada, Y., Kawamura, K., Ikehara, K., Ogawa, Y., Urgeles, R., Mosher, D., Chaytor, J., and Strasser, M. (Eds.), *Submarine Mass Movements and Their Consequences*. Adv. Nat. Technol. Hazard Res., 31(8):671–681. **doi:10.1007/978-94-007-2162-3_60**

Strasser, M., Moore, G.F., Kimura, G., Kitamura, Y., Kopf, A.J., Lallemant, S., Park, J.-O., Screaton, E.J., Su, X., Underwood, M.B., and Zhao, X., 2009. Origin and evolution of a splay fault in the Nankai accretionary wedge. *Nat. Geosci.,* 2(9):648–652. **doi:10.1038/ngeo609**

Strasser, M., Moore, G.F., Kimura, G., Kopf, A.J., Underwood, M.B., Guo, J., and Screaton, E.J., 2011. Slumping and mass-transport deposition in the Nankai forearc: evidence from IODP drilling and 3-D reflection seismic data. *Geochem., Geophys., Geosyst.,* 12:Q0AD13. **doi:10.1029/2010GC003431**

Tanioka, Y., and Satake, K., 2001. Detailed coseismic slip distribution of the 1944 Tonankai earthquake estimated from tsunami waveforms. *Geophys. Res. Lett.,* 28(6):1075–1078. **doi:10.1029/2000GL012284**

Tobin, H.J., and Kinoshita, M., 2006. NanTroSEIZE: the IODP Nankai Trough Seismogenic Zone Experiment. *Sci. Drill.*, 2:23–27. **doi:10.2204/iodp.sd.2.06.2006**

Tobin, H., Kinoshita, M., Ashi, J., Lallemant, S., Kimura, G., Screaton, E.J., Moe, K.T., Masago, H., Curewitz, D., and the Expedition 314/315/316 Scientists, 2009a. NanTroSEIZE Stage 1 expeditions: introduction and synthesis of key results. *In* Kinoshita, M., Tobin, H., Ashi, J., Kimura, G., Lallemant, S., Screaton, E.J., Curewitz, D., Masago, H., Moe, K.T., and the Expedition 314/315/316 Scientists, *Proc. IODP,* 314/315/316: Washington, DC (Integrated Ocean Drilling Program Management International, Inc.). **doi:10.2204/iodp.proc.314315316.101.2009**

Tobin, H., Kinoshita, M., Moe, K.T., and the Expedition 314 Scientists, 2009b. Expedition 314 summary. *In* Kinoshita, M., Tobin, H., Ashi, J., Kimura, G., Lallemant, S., Screaton, E.J., Curewitz, D., Masago, H., Moe, K.T., and the Expedition 314/315/316 Scientists, *Proc. IODP,* 314/315/316: Washington, DC (Integrated Ocean Drilling Program Management International, Inc.). **doi:10.2204/iodp.proc.314315316.111.2009**

Underwood, M.B., Saito, S., Kubo, Y., and the Expedition 322 Scientists, 2010. Expedition 322 summary. *In* Saito, S., Underwood, M.B., Kubo, Y., and the Expedition 322 Scientists, *Proc. IODP,* 322: Tokyo (Integrated Ocean Drilling Program Management International, Inc.). **doi:10.2204/iodp.proc.322.101.2010**

Yamano, M., Kinoshita, M., Goto, S., and Matsubayashi, O., 2003. Extremely high heat flow anomaly in the middle part of the Nankai Trough. *Phys. Chem. Earth,* 28(9–11):487–497. **doi:10.1016/S1474-7065(03)00068-8**

Table T1. Expedition 338 coring summary.

Hole	Latitude	Longitude	Water depth (mbsl)	Cores (*N*)	Interval cored (m)	Core recovered (m)	Recovery (%)	Drilled interval (m)	Total penetration (m)	Time on site (days)
338-										
C0002F	33°18.0507′N	136°38.2029′E	1939.00	0	LWD/MWD	—	—	842–2005.5	2005.5	6.2
C0002H	33°18.0252′N	136°38.2152′E	1936.50	2	19.0	3.91	20.6	0–1120.0	1120.0	3.5
C0002I	33°18.0362′N	136°38.2077′E	1936.00	0	—	—	—	—	1360.5	5
C0002J	33°18.0173′N	136°38.2312′E	1937.50	7	38.0	22.19	58.4	0–940.0	940.0	3.5
C0002K	33°18.0063′N	136°38.2103′E	1937.50	11	86.5	60.29	69.7	0–286.5	286.5	3
C0002L	33°17.9970′N	136°38.2200′E	1937.50	24	228.0	186.4	81.8	0–505.0	505.0	3
			Site C0002 totals:	44	371.5	272.79	73.4	0–2005.5	6217.5	80
C0012H	32°44.8783′N	136°55.0351′E	3509.50	0	LWD/MWD	—	—	0–710.0	710.0	6
			Site C0012 totals:	0	—	—	—	0–710.0	710.0	6
C0018B	33°09.4319′N	136°40.8826′E	3084.5	0	LWD/MWD	—	—	0–350	350.0	1.5
			Site C0018 totals:	0	—	—	—	0–350	350.0	1.5
C0021A	33°10.0482′N	136°39.4854′E	2940.50	0	LWD/MWD	—	—	0–294.0	294.0	1
C0021B	33°10.0555′N	136°39.8610′E	2944.00	14	120.4	129.91	107.90	0–194.5	194.5	4
			Site C0021 totals:	14	120.4	129.91	107.90	0–294.0	488.5	5
C0022A	33°13.0680′N	136°43.4540′E	2675.50	0	LWD/MWD	—	—	0–420.5	420.5	3
C0022B	33°13.0833′N	136°43.4667′E	2674.00	41	345.0	305.5	88.6	0–419.5	419.5	6.5
			Site C0022 totals:	41	345.0	305.5	88.6	0–420.5	840.0	9.5
			Expedition 338 totals:	198	836.9	708.2	84.6		8606.0	102

LWD = logging while drilling, MWD = measurement while drilling. — = not applicable.

Table T2. Summary of all BHAs from Expedition 338 holes.

Hole	Drilling Type	Water depth (mbsl)	Total depth (mbsf)	Bottom-hole assembly
338-				
C0002F	LWD/MWD	1939.0	2005.5	12-1/4 inch bit × GVR × ARC-8 × TeleScope × 12-1/8 inch ILS × sonicVISION × 12-1/8 inch stab × 8-1/2 inch DC(1) × CST × Anderreamer × float sub × 9-1/2 inch DC(2) × 17 inch stab × 9-1/2 inch DC(1) × XO
C0002H	RCB	1936.5	1120.5	10-5/8 inch RCB core bit × bit sub with 10-5/8 inch stab × RCB core barrel × top sub × head sub × 10-5/8 inch stab × 8-1/2 inch core DC(11) × 8-1/2 inch coring jar × 8-1/2 inch core DC(6) × XO × 5.68 inch HWDP(12) × XO
C0002I	RCB	1936.0	1360.3	10-5/8 inch RCB core bit × bit sub w/ 10-5/8 inch stab × RCB core barrel × top sub × head sub × 10-5/8 inch stab × 8-1/2 inch core DC(11) × 8-1/2 inch coring jar × 8-1/2 inch DC(6) × XO × 5.68 HWDP(12) × XO × 5 inch DP S-140(42 stds) × 5-1/2 inch DP S-150.
C0002J	RCB	1937.5	940.0	10-5/8 inch RCB core bit × bit sub w/ 10-5/8 inch stab × RCB core barrel × top sub × head sub × 10-5/8 inch coring stab × 8-1/2 inch core DC(11) × XO × 5-1/2 inch DP S-150(12) × XO × 5 inch DP S-140(42 stds) × 5-1/2 inch DP S-150.
C0002K	HPCS/ESCS	1937.5	286.5	11-7/16 inch core bit × bit sub × core barrel × landing sub × top sub × head sub × 8-1/2 inch core DC(11) × XO × 5-1/2 inch DP S-150(3 stds) × XO × 5 inch DP S-140(42 stds) × 5-1/2 inch DP S-150
C0002L	HPCS/ESCS	1937.5	505.0	11-7/16 inch core bit × bit sub × core barrel × landing sub × top sub × head sub × 8-1/2 inch core DC(11) × XO × 5-1/2 inch DP S-150(3 stds) × XO × 5 inch DP S-140(42 stds) × 5-1/2 inch DP S-150.
C0002L	ESCS	1937.5	505.0	11-7/16 inch core bit × bit sub × core barrel × landing sub × top sub × head sub × 8-1/2 inch core DC(11) × XO × 5-1/2 inch DP S-150(3 stds) × XO × 5 inch DP S-140(41 stds) × 5-1/2 inch DP S-150.
C0012H	LWD	3509.5	710.0	12-1/4 inch bit × GVR × ARC-8 × TeleScope × 12-1/8 inch ILS × sonicVISION × 12-1/8 inch stab × 8-1/2 inch DC(9) × 7-3/4 inch jar × 8-1/2 inch DC(3) × 5.68 HWDP(12) × 5 inch DP S-140(46 stds) × 5-1/2 inch DP S-150
C0018B	LWD/MWD	3084.5	350.0	12-1/4 inch bit × GVR-8 with 12-1/8 inch stab (with float valve) × ARC-8 × TeleScope 825HF × NM XO sub × NMDC × 12-1/8 inch stab × 8-1/2 inch DC(9) × 7-3/4 inch LI jar × 8-1/2 inch DC(3) × XO × 5-1/2 inch DP S-150(12) × XO × 5 inch DP S-140(42 stds) × XO × 5-1/2 inch DP S-150.
C0021A	LWD/MWD	2940.5	294.0	12-1/4 inch bit × GVR-8 with 12-1/8 inch stab (with float valve) × ARC-8 × TeleScope 825HF × NM XO sub × NMDC × 12-1/8 inch stab × 8-1/2 inch DC(9) × 7-3/4 inch LI jar × 8-1/2 inch DC(3) × XO × 5-1/2 inch DP S-150(12) × XO × 5 inch DP S-140(42 stds) × XO × 5-1/2 inch DP S-150.
C0021B	HPCS/ESCS	2940.5	194.5	11-7/16 inch core bit × bit sub × core barrel × landing sub × top sub × head sub × 8-1/2 inch DC(11) × XO × 5-1/2 inch DP S-150(12) × 5 inch DP S-140(27 stds) × 5-1/2 inch DP S-150
C0022A	LWD/MWD	2675.5	420.5	12-1/4 inch bit × GVR-8 with 12-1/8 inch stab (with float valve) × ARC-8 × TeleScope 825HF × NM XO sub × NMDC × 12-1/8 inch stab × 8-1/2 inch DC(9) × 7-3/4 inch LI jar × 8-1/2 inch DC(3) × XO × 5-1/2 inch DP S-150(12) × XO × 5 inch DP S-140(42 stds) × XO × 5-1/2 inch DP S-150.
C0022B	HPCS/ESCS	2674.0	419.5	11-7/16 inch core bit × bit sub × core barrel × landing sub × top sub × head sub × 7 inch DC(15) × XO × 5-1/2 inch DP S-150(12) × 5 inch DP S-140(42 stds) × 5-1/2 inch DP S-150

LWD = logging while drilling, MWD = measurement while drilling. RCB = rotary core barrel, HPCS = hydraulic piston coring system, ESCS = extended shoe coring system. GVR = geoVISION resistivity tool, ILS = instrument landing system, CST = concentric reamer. Stab = stabilizer, XO = crossover. DC = drill collar, NMDC = nonmagnetic drill collar. HWDP = heavy weight drill pipe, DP = drill pipe.

Table T3. BHA components of 12-1/4 inch × 20 inch LWD with underreamer.

BHA component	Length of tool (m)	Total length of the top of tool from the bit (m)
12-1/4 inch PDC bit	0.290	0.290
GVR-8 w/2 × 12-1/8 inch stabilizer	3.882	4.172
ARC-8	5.644	9.816
TeleScope 825	8.435	18.251
12-1/8 inch ILS (stabilizer)	0.830	19.081
sonicVISION 825	7.299	26.380
12-1/8 inch stabilizer	2.375	28.755
8-1/2 inch drill collar	9.223	37.978
CST 10-5/8 inch × 16-1/2 inch	1.310	39.288
Cutter part of CST	0.340	38.318
Anderreamer 16-3/8 inch × 20 inch	7.500	46.788
Cutter part of Anderreamer	4.500	43.788
Float sub	1.085	47.873
9-1/2 inch drill collar	9.308	57.181
9-1/2 inch drill collar	9.246	66.427
17 inch stabilizer	1.706	68.133
9-1/2 inch drill collar	9.310	77.443
Crossover	1.000	78.443
8-1/2 inch drill collar	9.310	87.753
8-1/2 inch drill collar	8.930	96.683
8-1/2 inch drill collar	9.310	105.993
7-3/4 inch drilling jar	10.635	116.628
8-1/2 inch drill collar	9.220	125.848
8-1/2 inch drill collar	9.310	135.158
8-1/2 inch drill collar	9.305	144.463
Crossover	0.508	144.971
5.68 inch heavy weight drill pipe	9.050	154.021
5.68 inch heavy weight drill pipe	9.042	163.063
5.68 inch heavy weight drill pipe	9.042	172.105
5.68 inch heavy weight drill pipe	9.043	181.148
5.68 inch heavy weight drill pipe	9.043	190.191
5.68 inch heavy weight drill pipe	9.050	199.241
5.68 inch heavy weight drill pipe	9.050	208.291
5.68 inch heavy weight drill pipe	9.050	217.341
5.68 inch heavy weight drill pipe	9.042	226.383
5.68 inch heavy weight drill pipe	9.050	235.433
5.68 inch heavy weight drill pipe	8.963	244.396
5.68 inch heavy weight drill pipe	9.050	253.446
Crossover	1.002	254.448

PDC = polycrystalline diamond compact. GVR = geoVISION resistivity tool. ILS = instrument landing system. CST = concentric reamer.

Figure F1. Map of the NanTroSEIZE region showing all Stage 1, 2, and 3 drill sites. Red = Expedition 338 sites, blue = NanTroSEIZE Stage 1 and 2 sites. Black outline = region with 3-D seismic data, yellow arrows = estimated far-field vectors between Philippine Sea plate and Japan (Seno et al. 1993; Heki, 2007). Stars = epicenter locations of 1944 and 1946 tsunamigenic earthquakes.

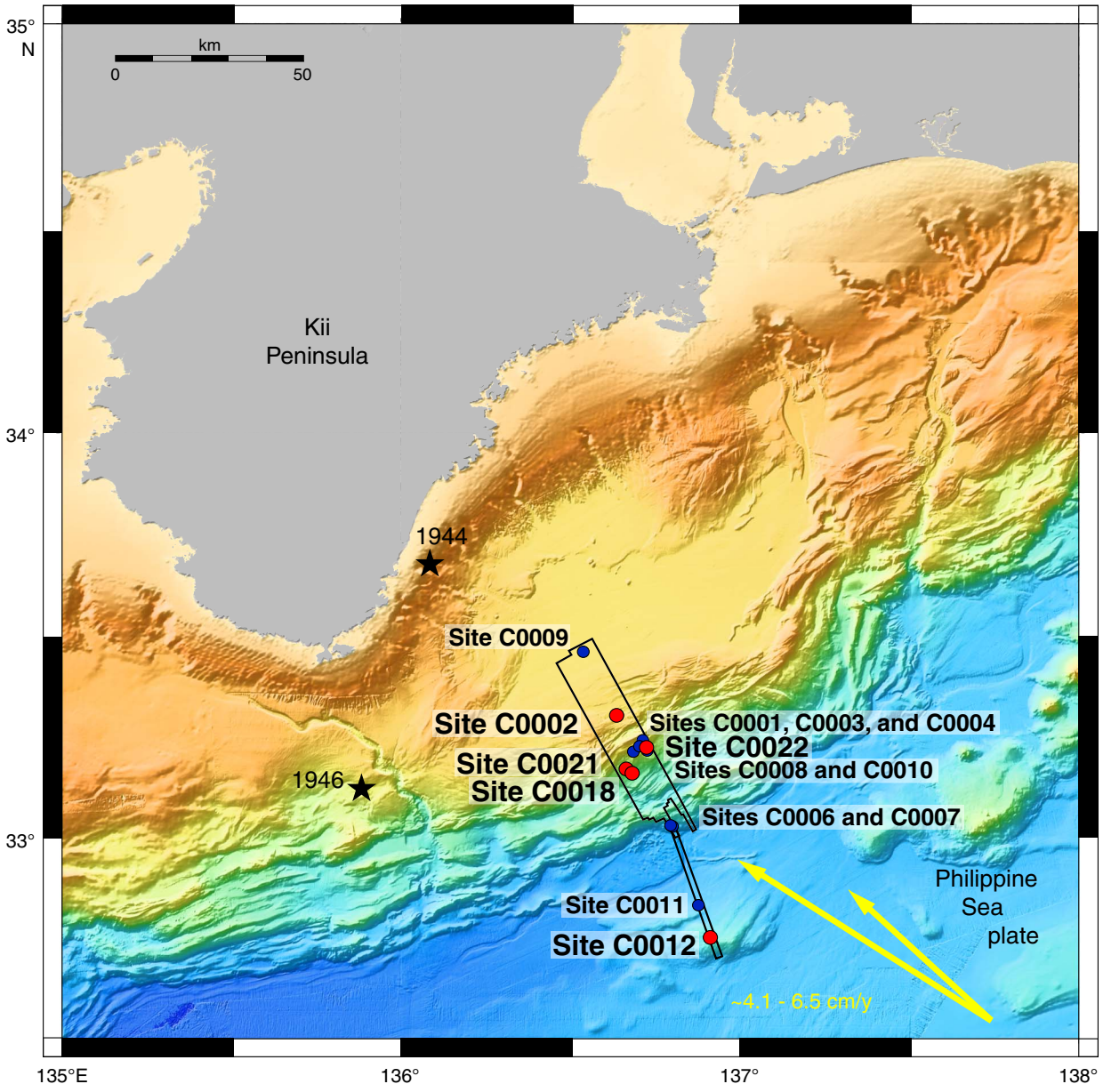

Figure F2. Composite seismic line extracted from the 3-D seismic volume, showing Expedition 338 sites (red), in relation to NanTroSEIZE Stage 1 and 2 sites (black).

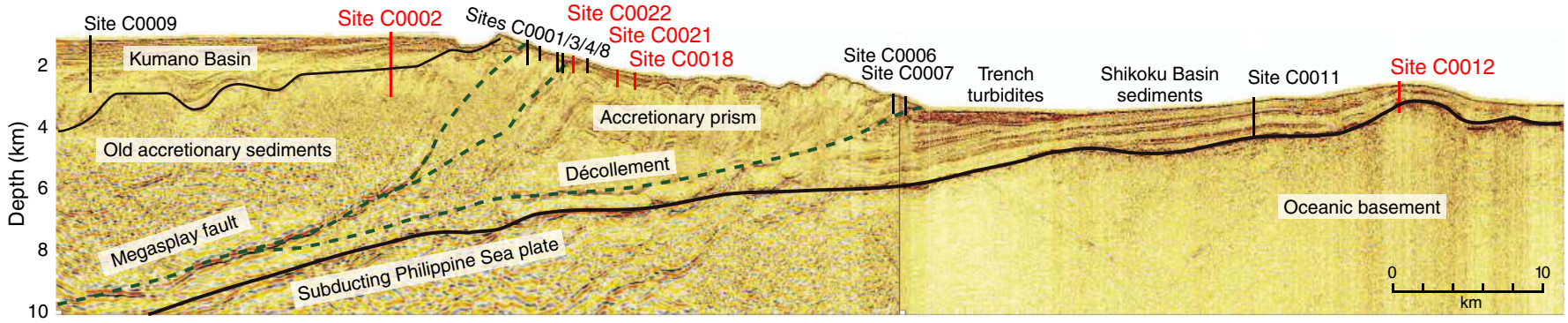

Figure F3. In-line (IL) 2529 extracted from the 3-D seismic volume, showing Site C0002 in relation to Stage 1 Sites C0001, C0003, C0004, and C0008. Green box = extent of LWD and cuttings obtained in Hole C0002F, red boxes = sections of cores obtained from Holes C0002H, C0002J, C0002K, and C0002L, dashed extension below the green box = ultimate planned plate boundary interception at ~5200 mbsf. VE = vertical exaggeration.

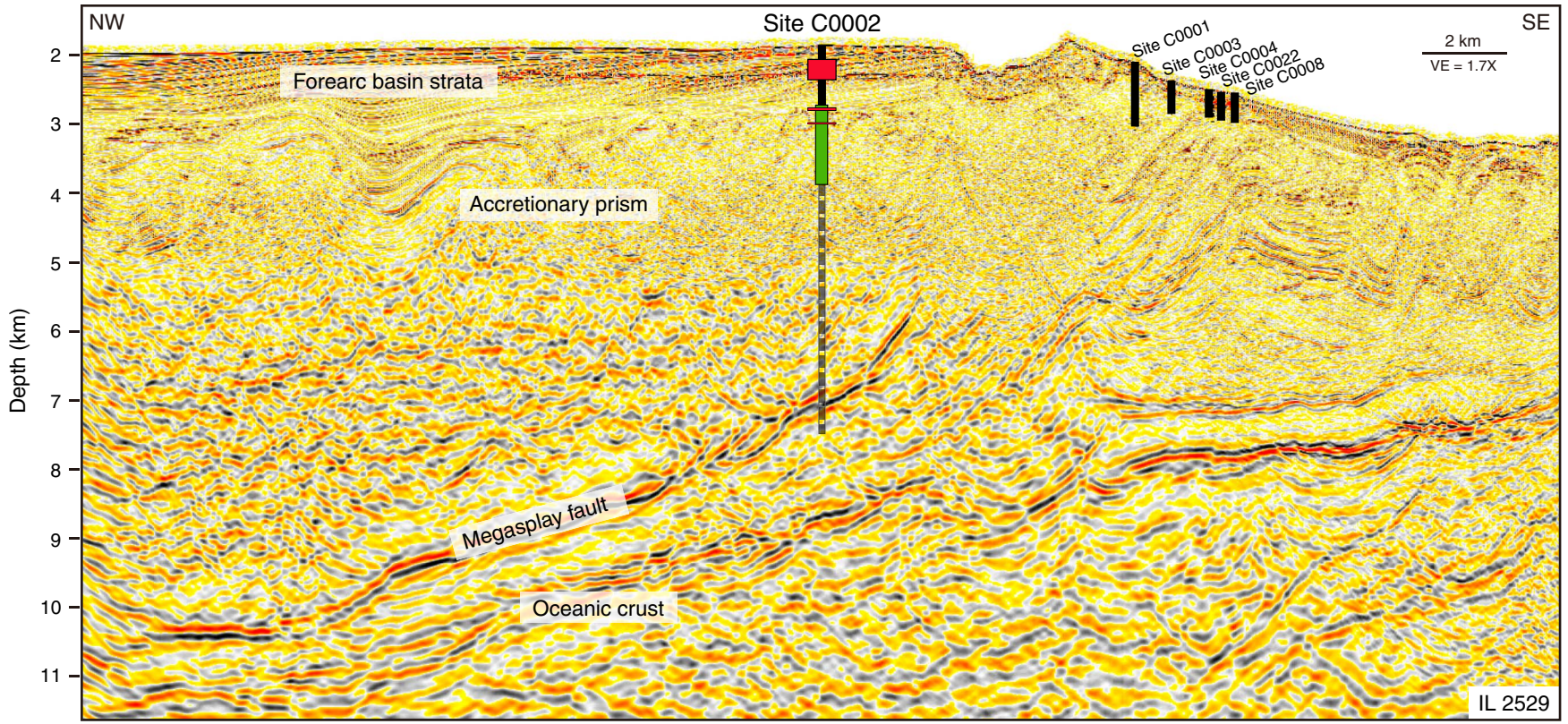

Figure F4. Detailed bathymetry and structure of the slope basin at the footwall of the splay fault (Strasser et al., 2011) showing Expedition 338 sites (red) in relation to NTS Stage 1 and 2 sites. Solid black lines = locations of seismic lines A–A′ and B–B′ in Figures F5 and F6, respectively. MTD = mass transport deposit, IL = in-line, XL = cross-line.

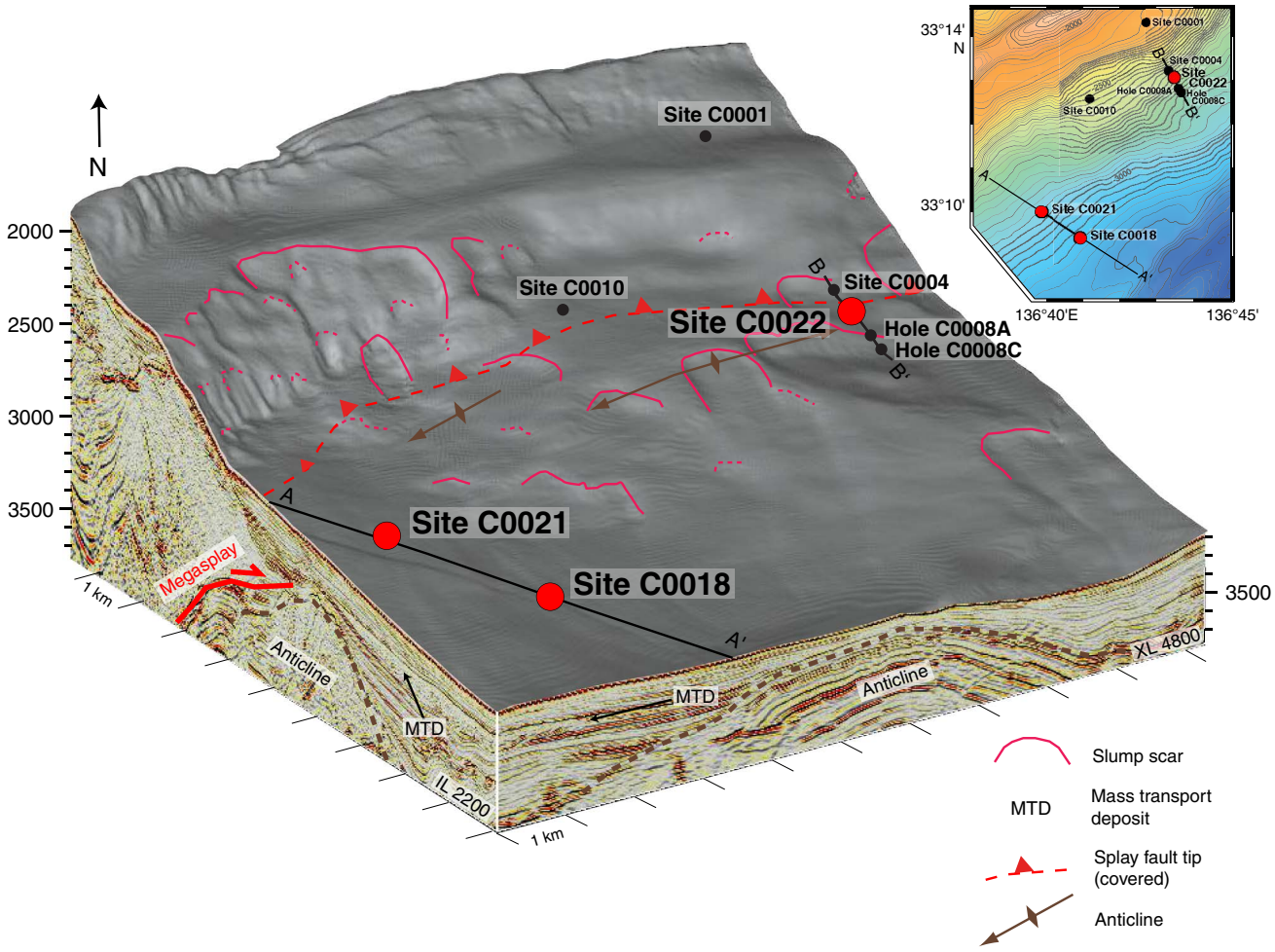

Figure F5. Arbitrary seismic line A–A′ through Sites C0018 and C0021. Location shown in Figure F4. VE = vertical exaggeration.

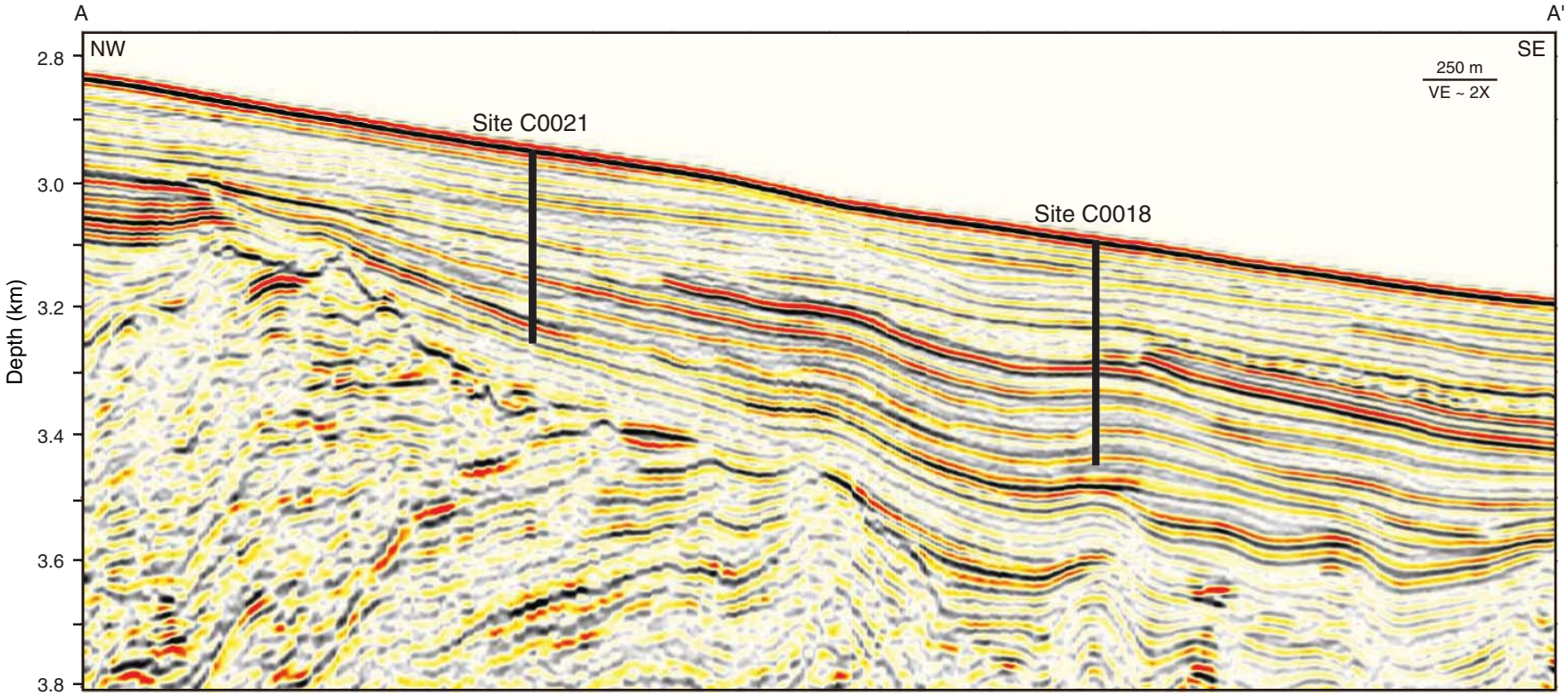

Figure F6. In-line 2675 (B–B′) extracted from 3-D seismic volume, showing Sites C0004, C0008, and C0022 (Moore et al., 2009). Location shown in Figure **F4.** VE = vertical exaggeration.

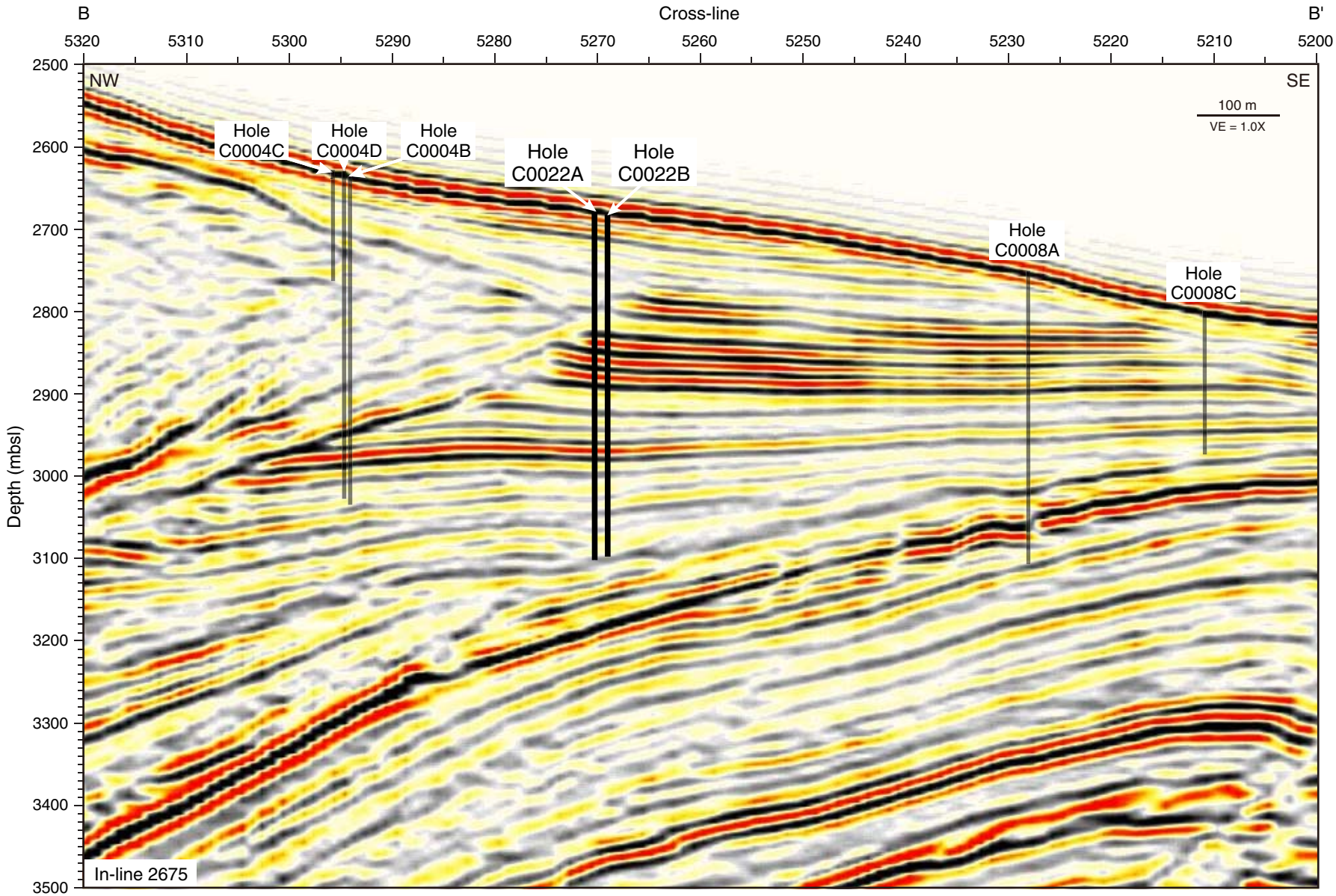

Figure F7. Composite of LWD data, Hole C0002F. Log units and subunits defined in Hole C0002F.

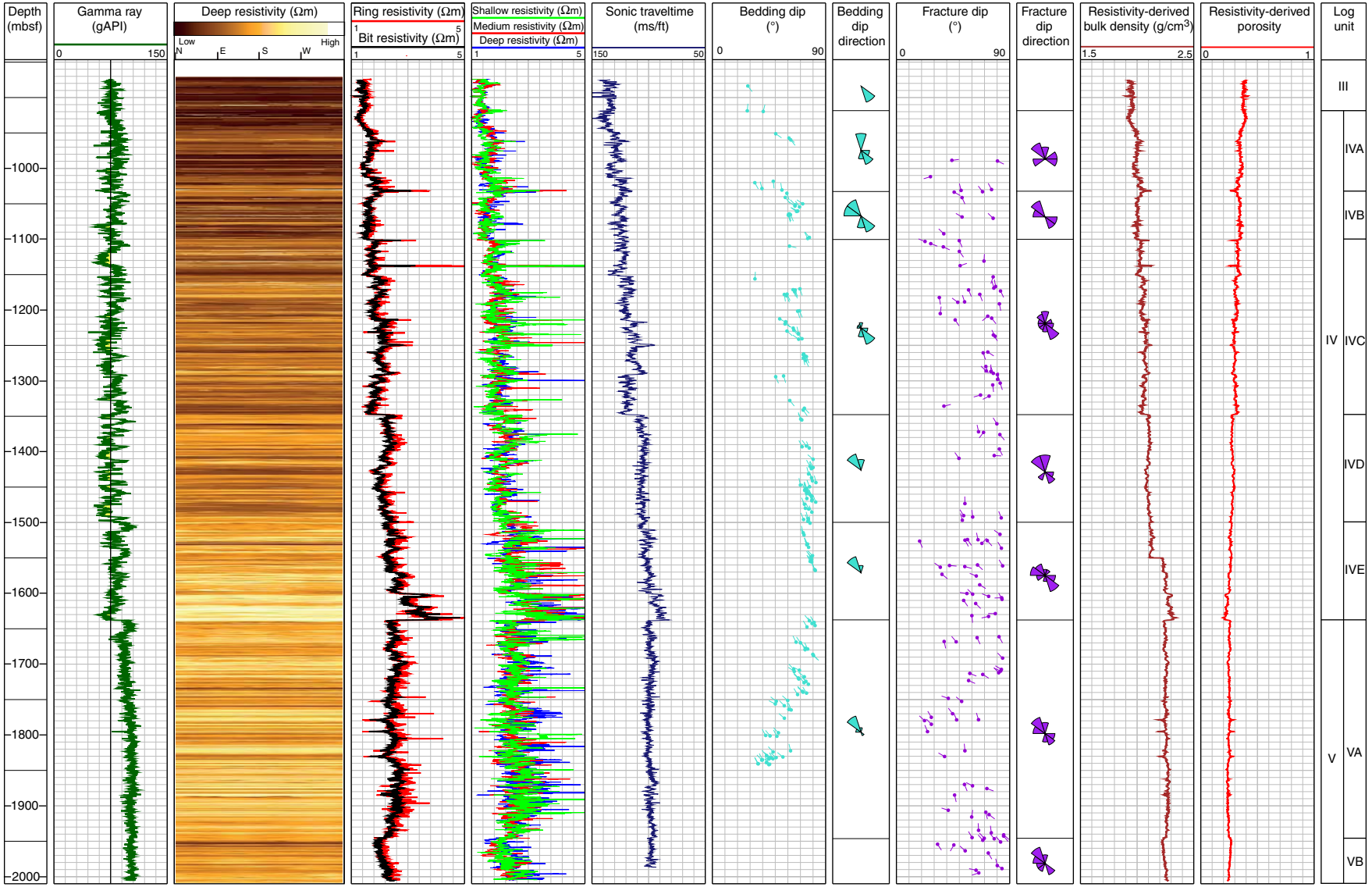

Figure F8. Cuttings analyses, Hole C0002F: XRD (1–4 and >4 mm fractions of silty claystones), deformation structures, and MAD bulk density and porosity. Number of deformation structures is derived from number of grains showing deformation relative to total number of investigated grains. Note that the method of counting deformation structures in the >4 mm size fraction changed at 1415.5 mbsf, and observations on 1–4 mm cuttings were only routinely performed at depths deeper than 1375.5 mbsf (gray shaded area = interval with only spot counting). Plag = plagioclase, Qtz = quartz.

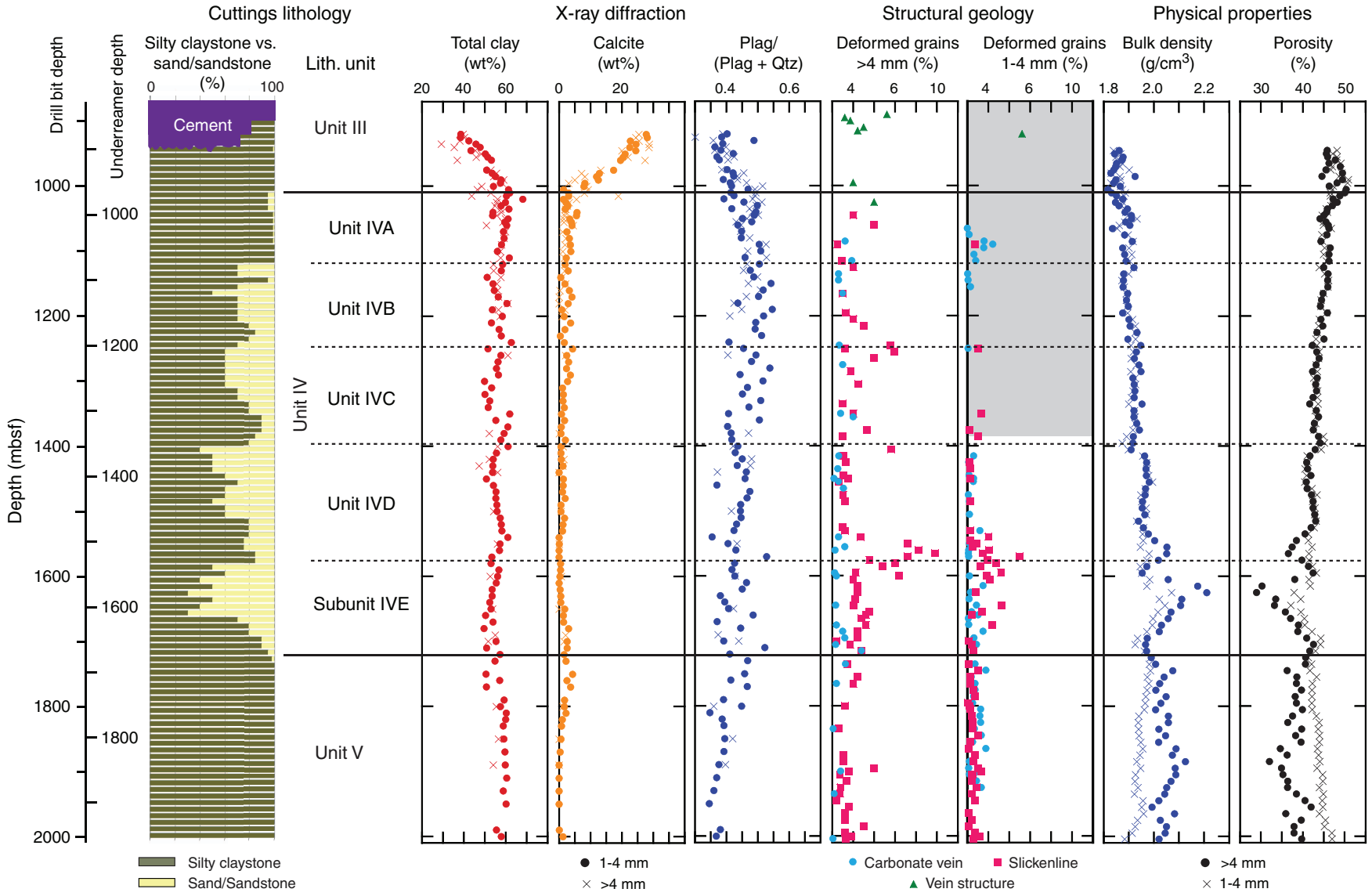

Figure F9. Cuttings-core-log-seismic integration, Site C0002: composite medium button static resistivity, In-line 2532 seismic data (Kumano 3-D PSDM volume; Moore et al., 2009), composite core lithology, cuttings-derived units, logging units from Holes C0002A and C0002G, and composite logging-while-drilling (LWD) data.

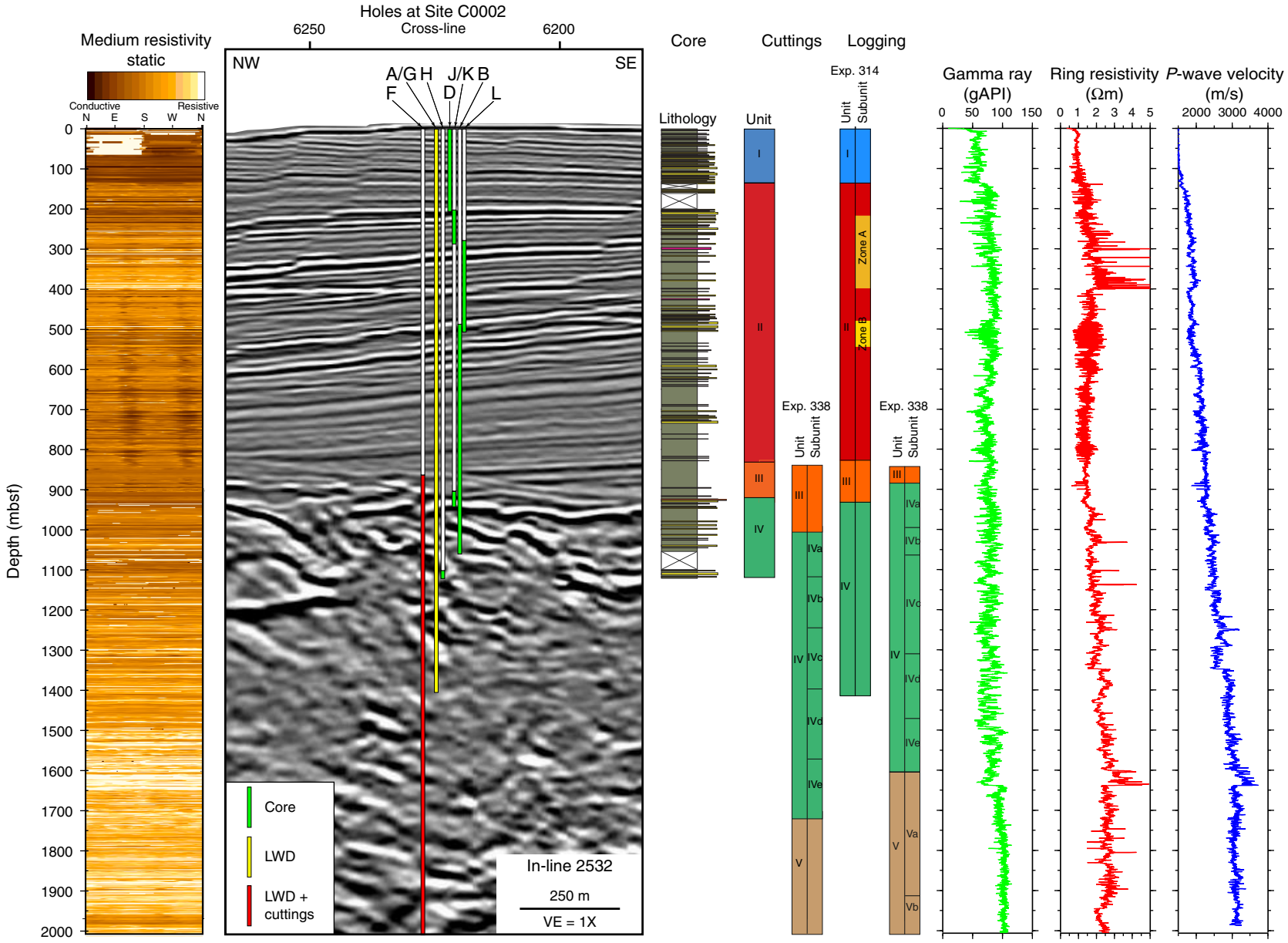

Figure F10. A. Detailed view of possible lithologic unit boundary (interval 338-C0002J-5R-8, 98–126 cm). **B.** Disrupted bedding observed close to the Unit III/IV boundary (interval 338-C0002J-5R-6, 13–25 cm). **C.** Vein structures (interval 338-C0002J-1R-8, 30–34 cm). **D.** Deformation bands (interval 338-C0002J-1R-7, 92–105 cm). **E.** Carbonate veins in cuttings (Sample 338-C0002F-56-SMW, >4 mm; 1085.5 mbsf).

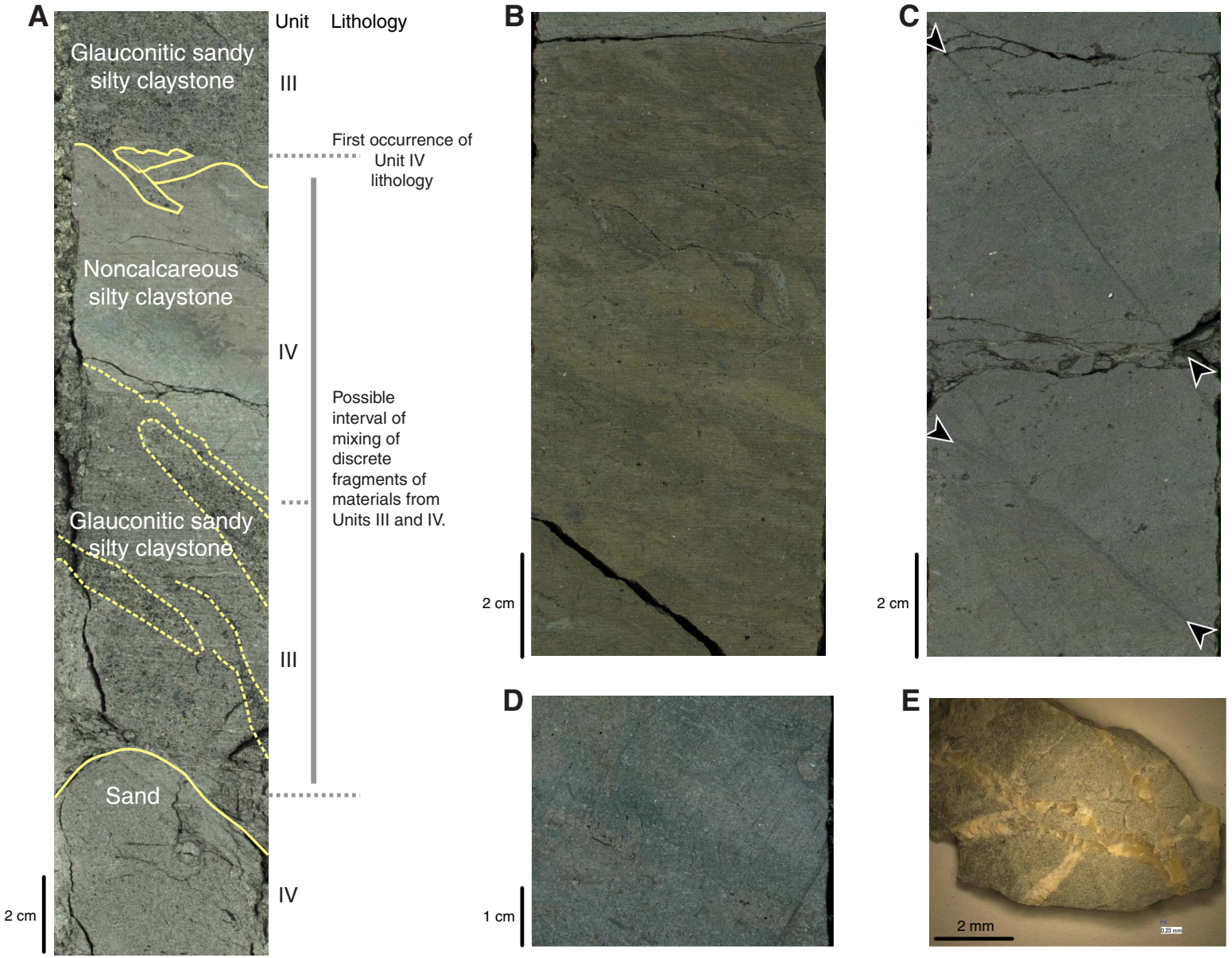

Figure F11. Composite summary of core analyses, Site C0002, from Expedition 315 (Holes C0002B and C0002D [small symbols]; Expedition 315 Scientists, 2009) and this expedition (Holes C0002H, C0002J, C0002K, and C0002L [larger symbols]). In XRD data gray shaded area = no data for Hole C0002D). Bulk density and porosity are from MAD measurements.

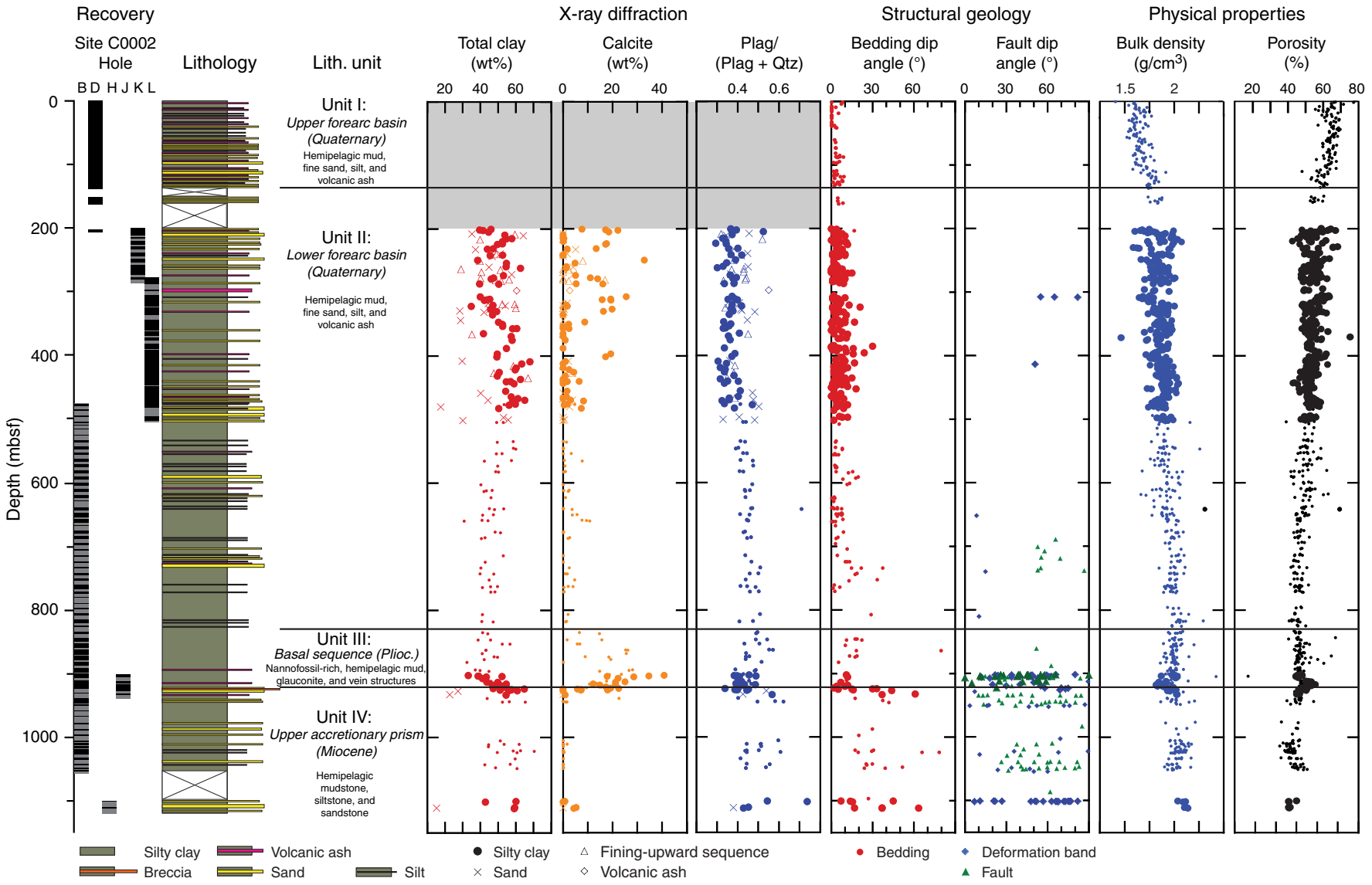

Figure F12. Interstitial water profiles of pH, salinity, chlorinity, and Na^+, Holes C0002J, C0002K, C0002L, C0002B, and C0002D. Refractive salinity is unitless.

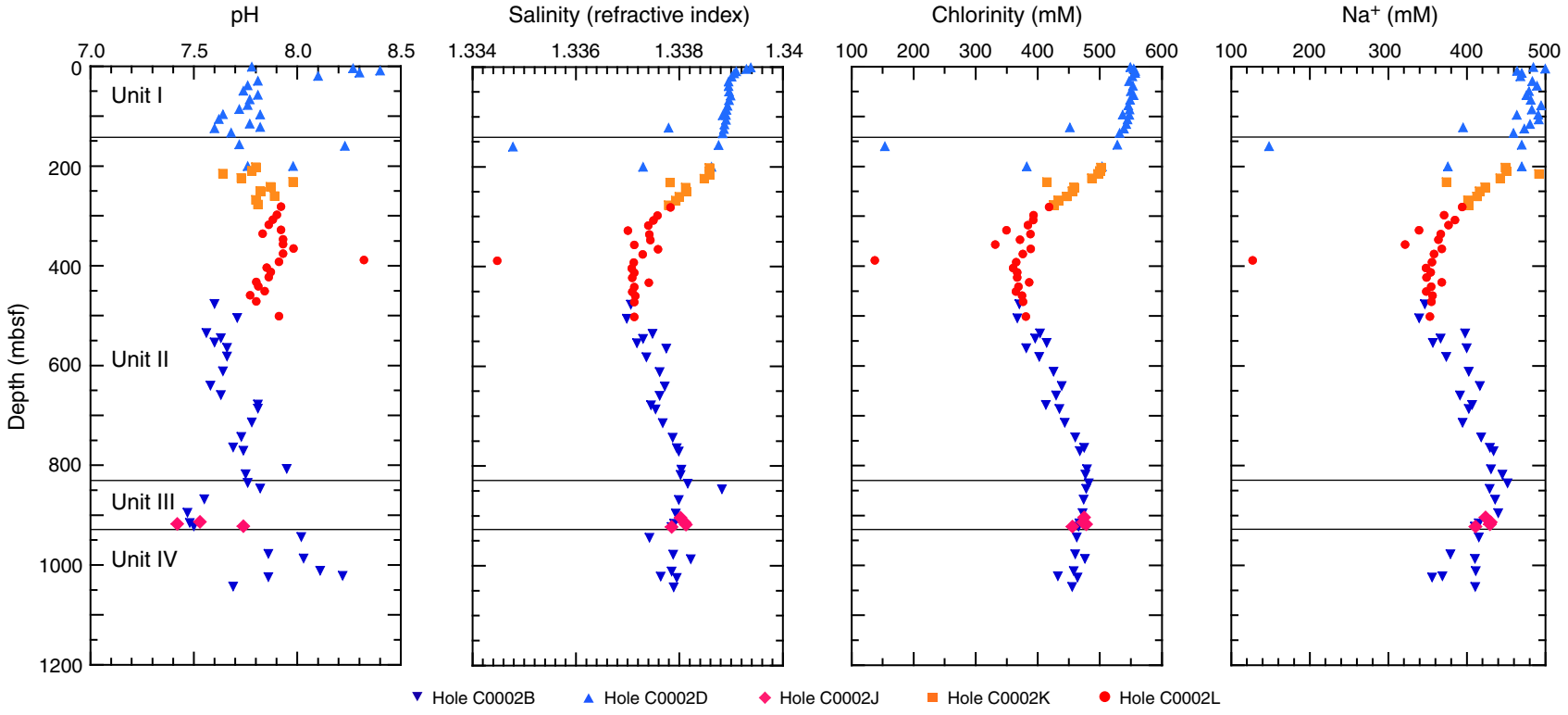

Figure F13. Headspace gas profiles of methane, ethane, and propane, Site C0002.

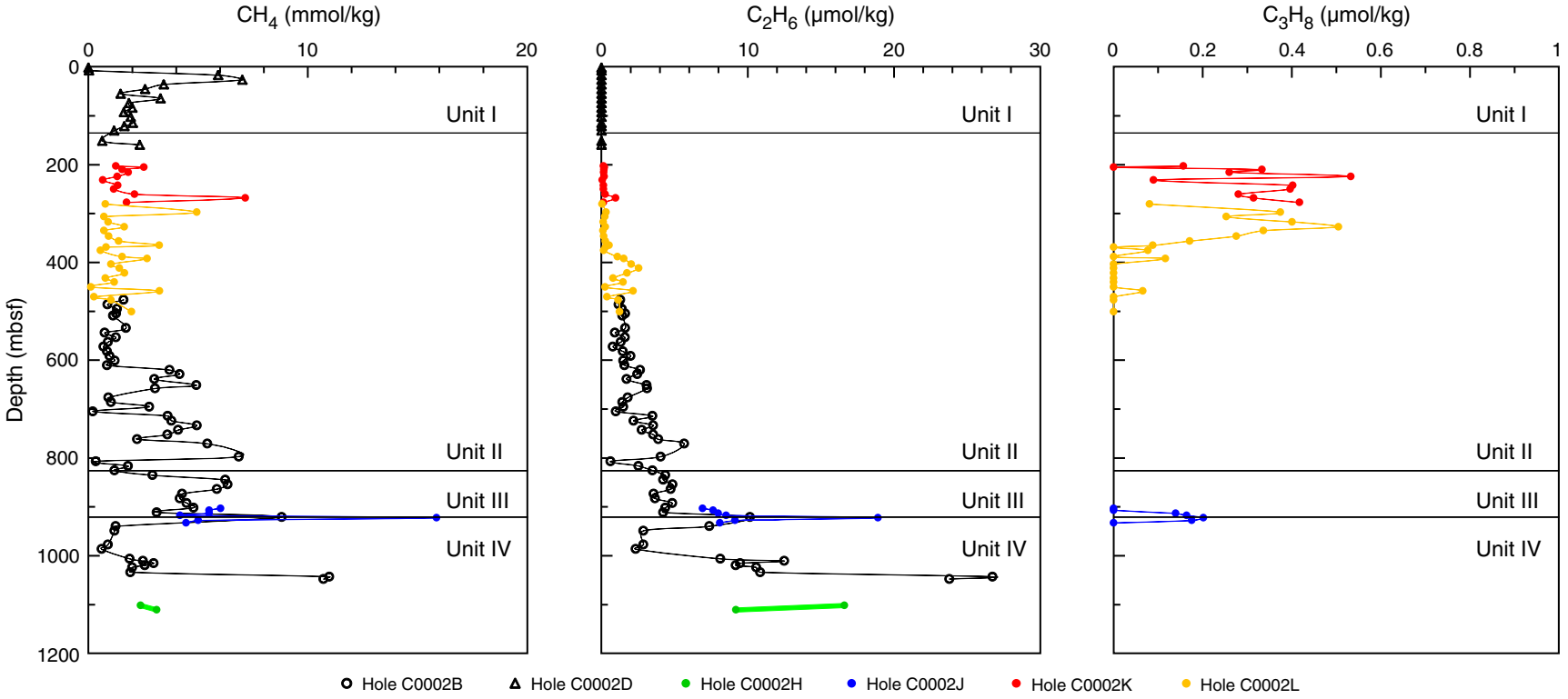

Figure F14. Selected results from mud-gas monitoring during riser drilling, Hole C0002F. Total hydrocarbon gas and $C_1/(C_2 + C_3)$ data are provided by Geoservices. $\delta^{13}C$ values were measured using the methane carbon isotope analyzer (MCIA). For better visualization, only $C_1/(C_2 + C_3)$ based on significant amounts of ethane and/or propane (i.e., >0.0001%) are plotted. Red dotted line in the $\delta^{13}C$ plot = beginning of a thermogenic signature (greater than –60‰ at ~1700 mbsf). A clear boundary at 918 mbsf is defined in the gas data and correlates to the logging Unit III/IV boundary.

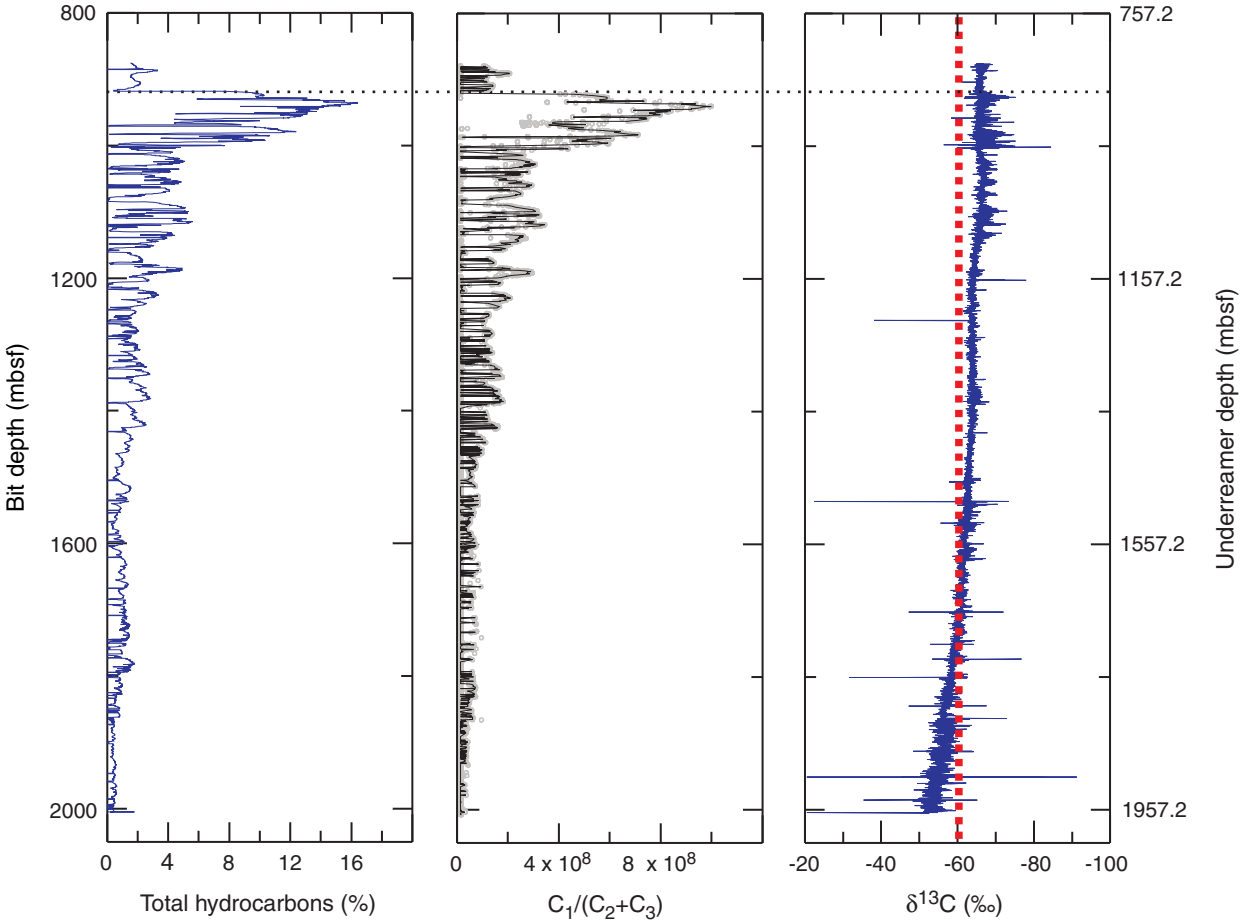

Figure F15. A. Compiled MAD porosity data from Hole C0002B (blue diamonds; Expedition 315 Scientists, 2009), Hole C0002H and C0002J core data and hand-picked samples of intact formation cuttings >4 mm compared with porosity determined from Hole C0002F bulk cuttings >4 mm (red dots). Black line = Athy model best fit to Expedition 315 and hand-picked data. **B.** MAD bulk density data from bulk cuttings >4 mm (red dots) in comparison with bulk density calculated from Athy model porosity (yellow circles). Lithologic units and underreamer depth are shown as a reference.

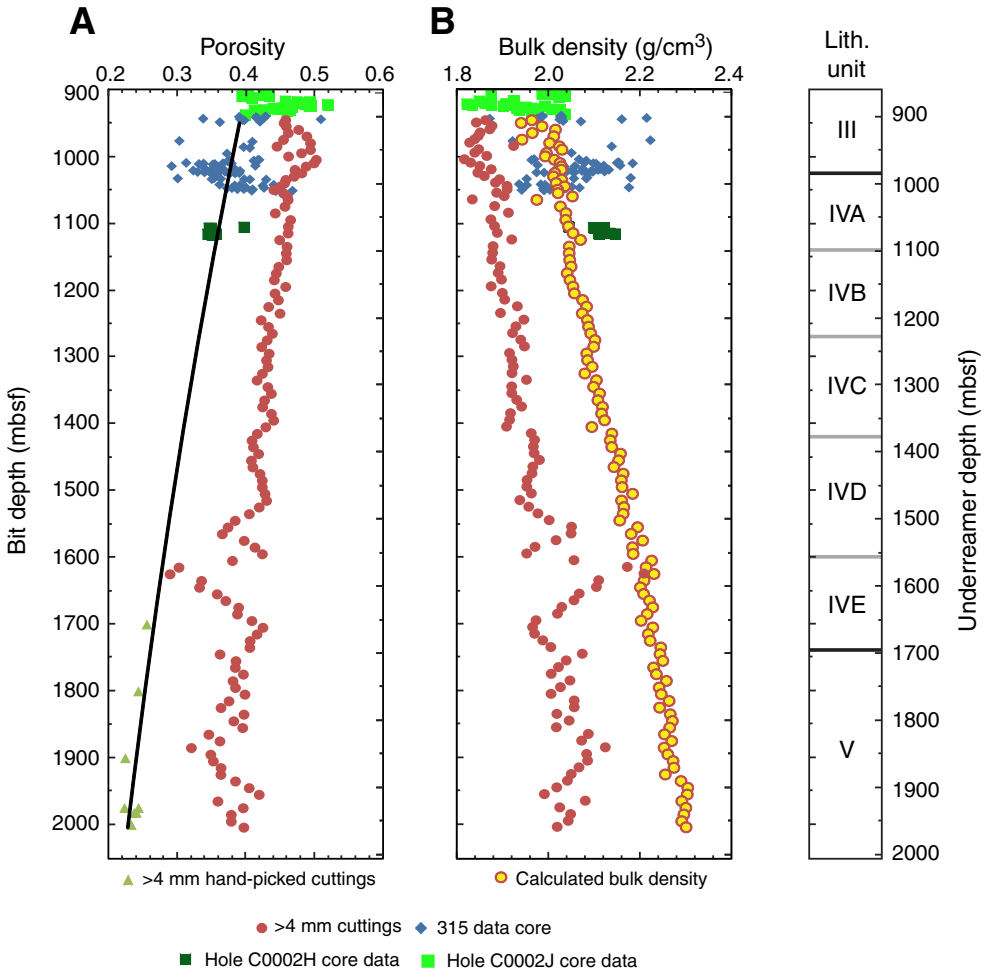

Figure F16. Composite logging plot, Hole C0012H: LWD data, deep resistivity image, bedding and fracture dips and orientations, resistivity-derived porosity, bulk density, and seismic data.

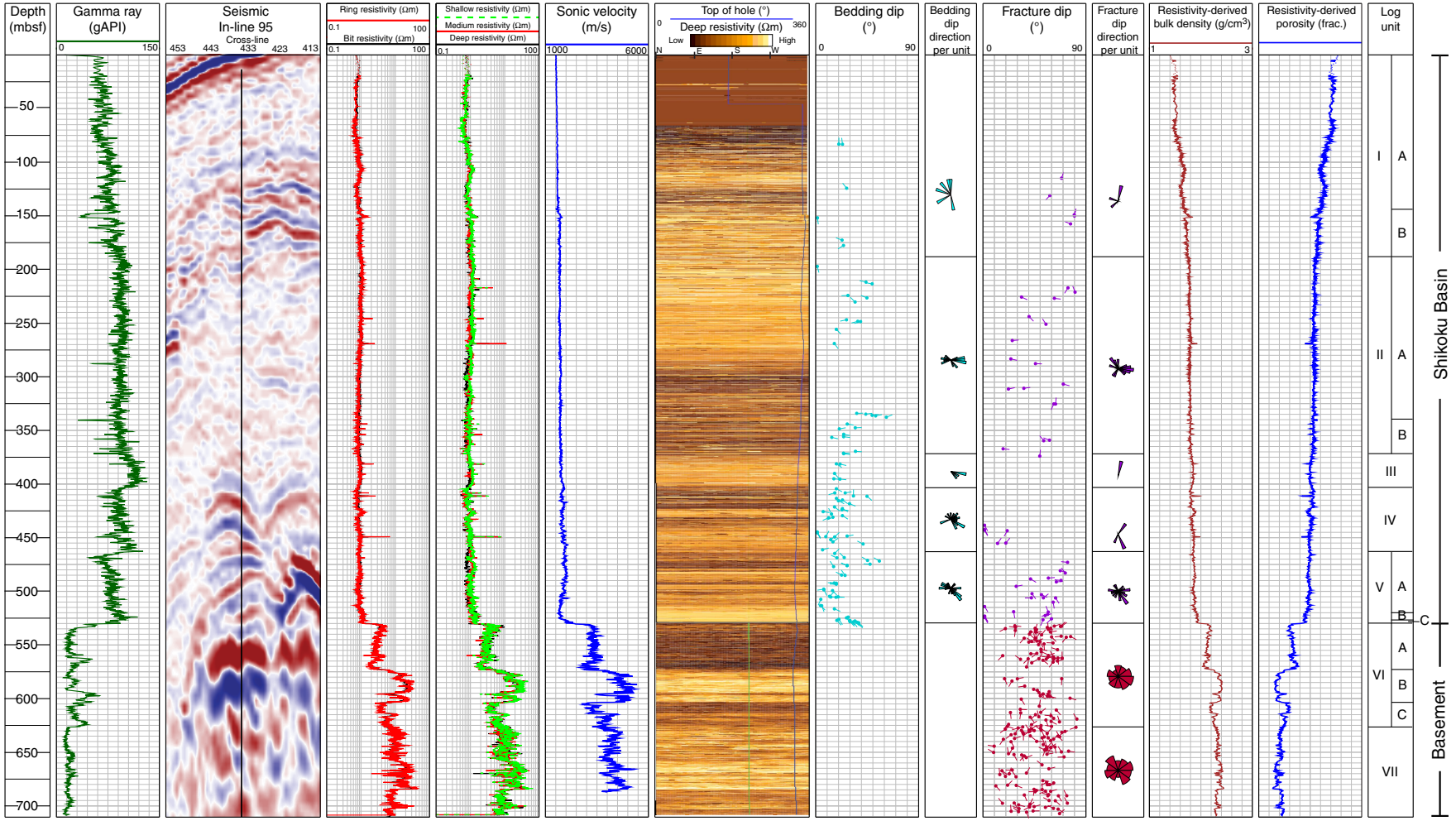

Figure F17. Static deep button resistivity images showing textures and fractures observed in oceanic basement, Hole C0012H. **A.** Irregular surface (i.e., nonplanar) at the sediment/basement interface (~530 mbsf). **B.** Logging Subunit VIA contains frequent variations in textural patterns (every 5 m or less), showing pillow basalt and a sheet flow with subvertical fractures. **C.** Large, high-angle (~75°) low-resistivity (<7 Ωm) fracture bisecting a homogeneous sheet flow in logging Subunit VIB. **D.** All three basement textures (mottled, turtleshell, and homogeneous zones) observed in logging Subunit VIC. **E.** A sharp drop in resistivity marks the transition from a homogeneous zone to a region of turtleshell texture at ~684 mbsf in logging Unit VII. This is interpreted as the basal surface of the sheet flow, and several other (less distinct) surfaces are observed throughout both basement units. A and B are plotted on the medium range resistivity scale (0–10 Ωm); C–E are plotted on the high range resistivity scale (2–50 Ωm).

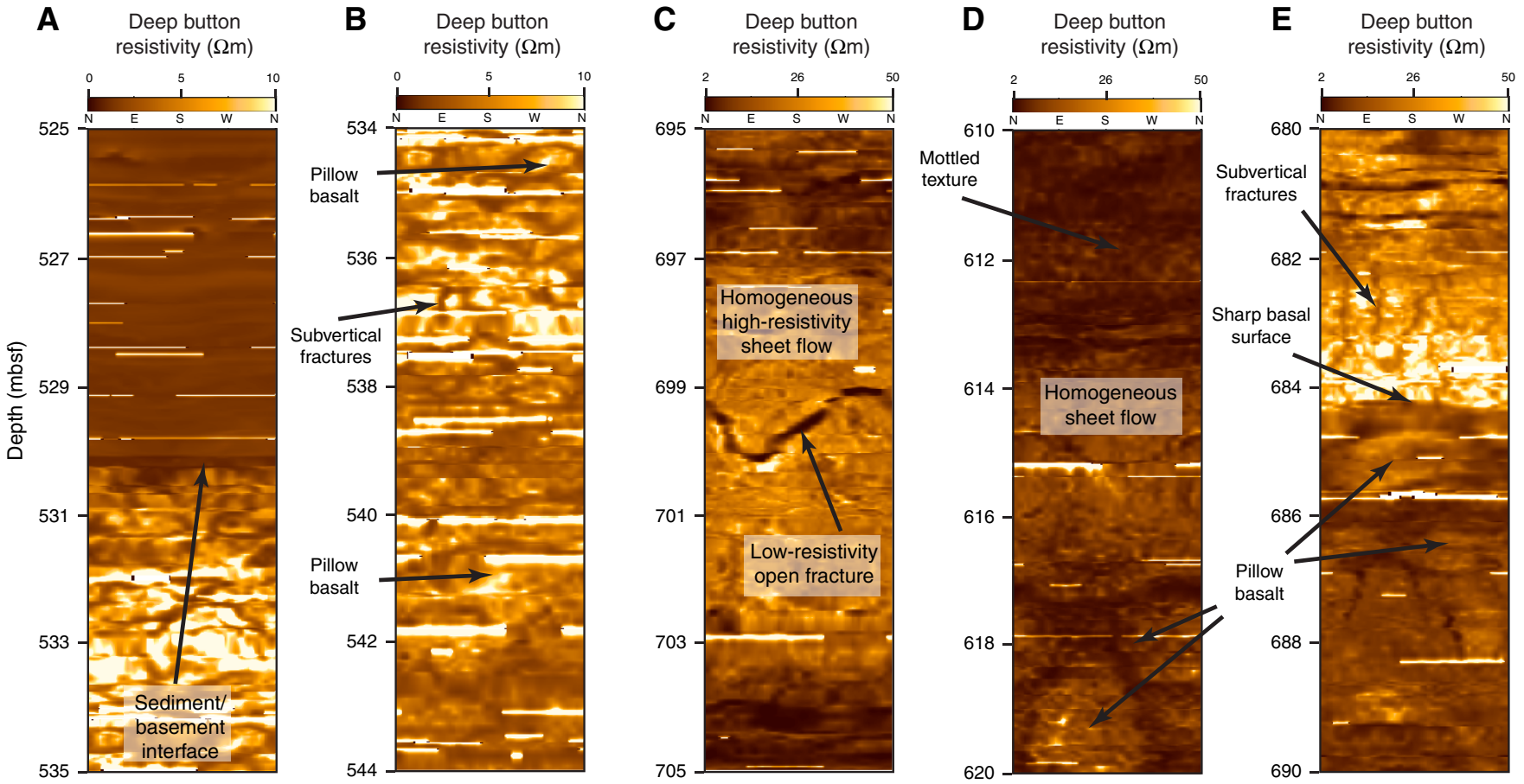

Figure F18. Core-log-seismic integration, Site C0012: LWD data from Hole C0012H with unit boundaries, composite lithologic column (Holes C0012A–C0012G; Expedition 333 Scientists, 2012b), and seismic data from In-line 95 (IFREE 3-D PSDM volume; Park et al., 2008) showing the interpretation of Expedition 322 Scientists (2010b). Black dashed lines = correlations ("?" = tentative) between unit boundaries identified for each data set. VE = vertical exaggeration.

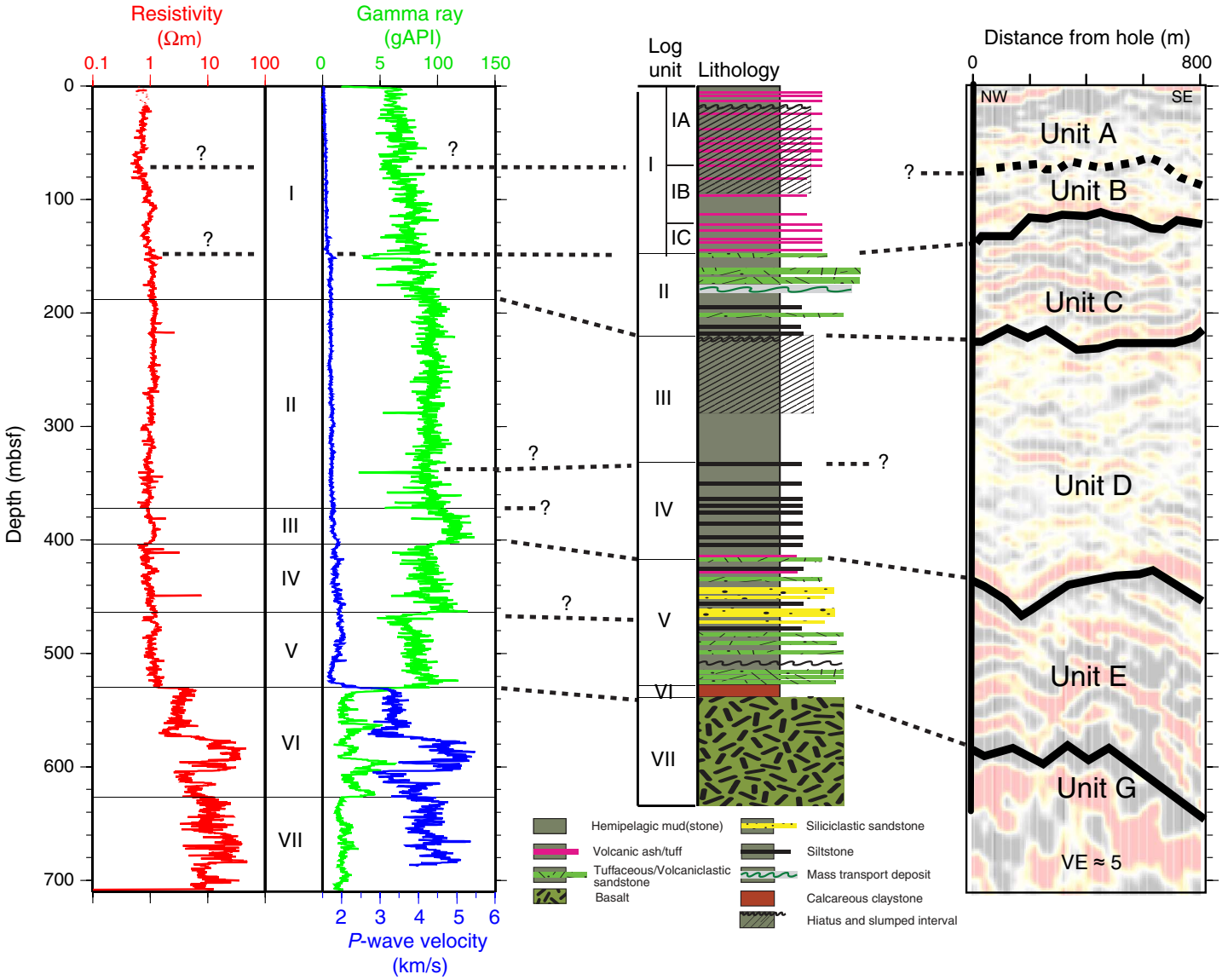

Figure F19. Composite plot, Hole C0018B: LWD, deep resistivity image, and seismic data, resistivity-derived porosity (red = Expedition 314, blue = Hole C0018A MAD data) and bulk density, and bedding and fracture dips.

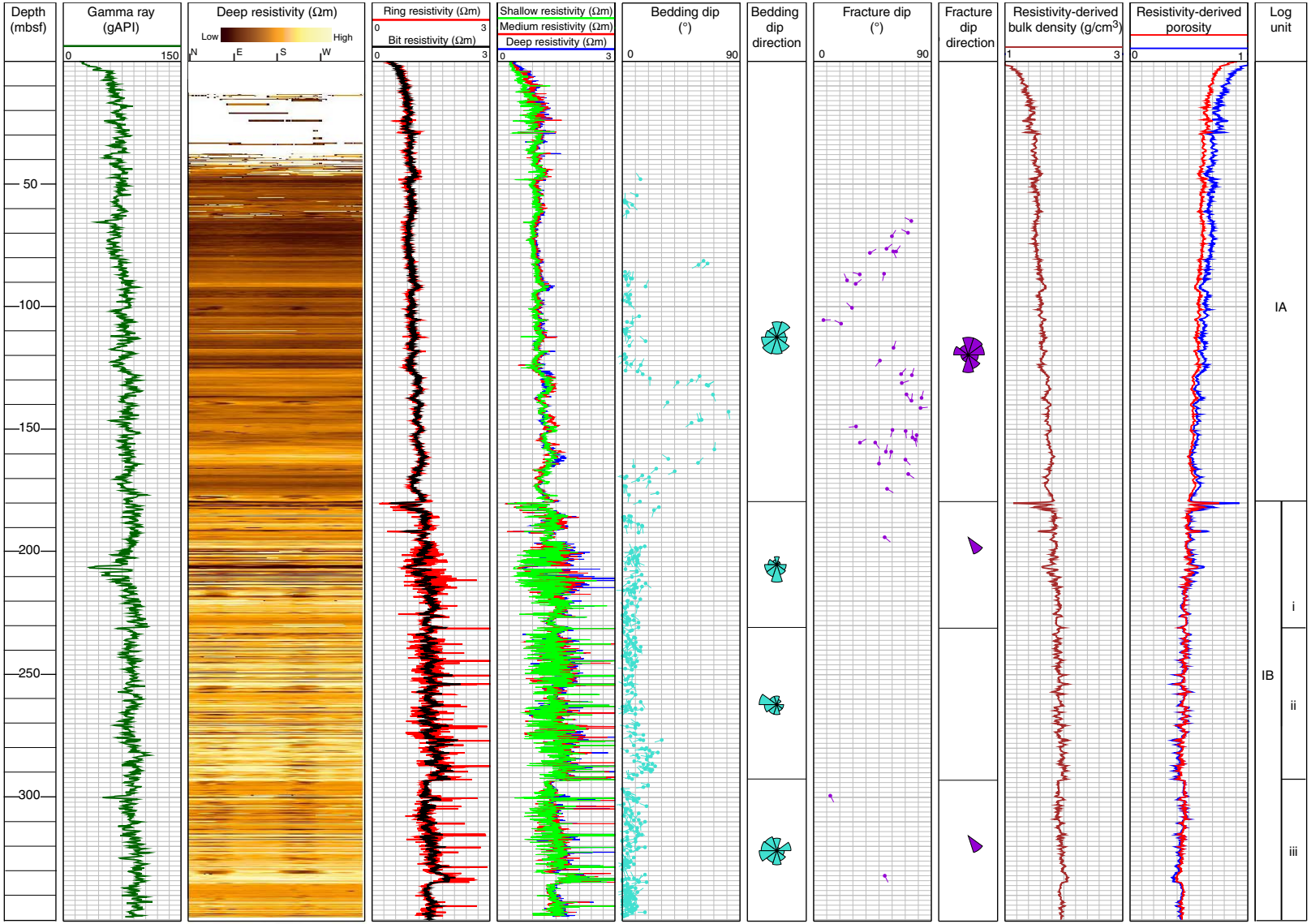

Figure F20. Composite plot, Hole C0021A: LWD, deep resistivity image, resistivity-derived porosity (red = Expedition 314 Archie parameters a = 1, m = 2.4; blue = Hole C0018A core-based Archie parameters a = 1, m = 3.2), calculated bulk density, and bedding and fracture dips.

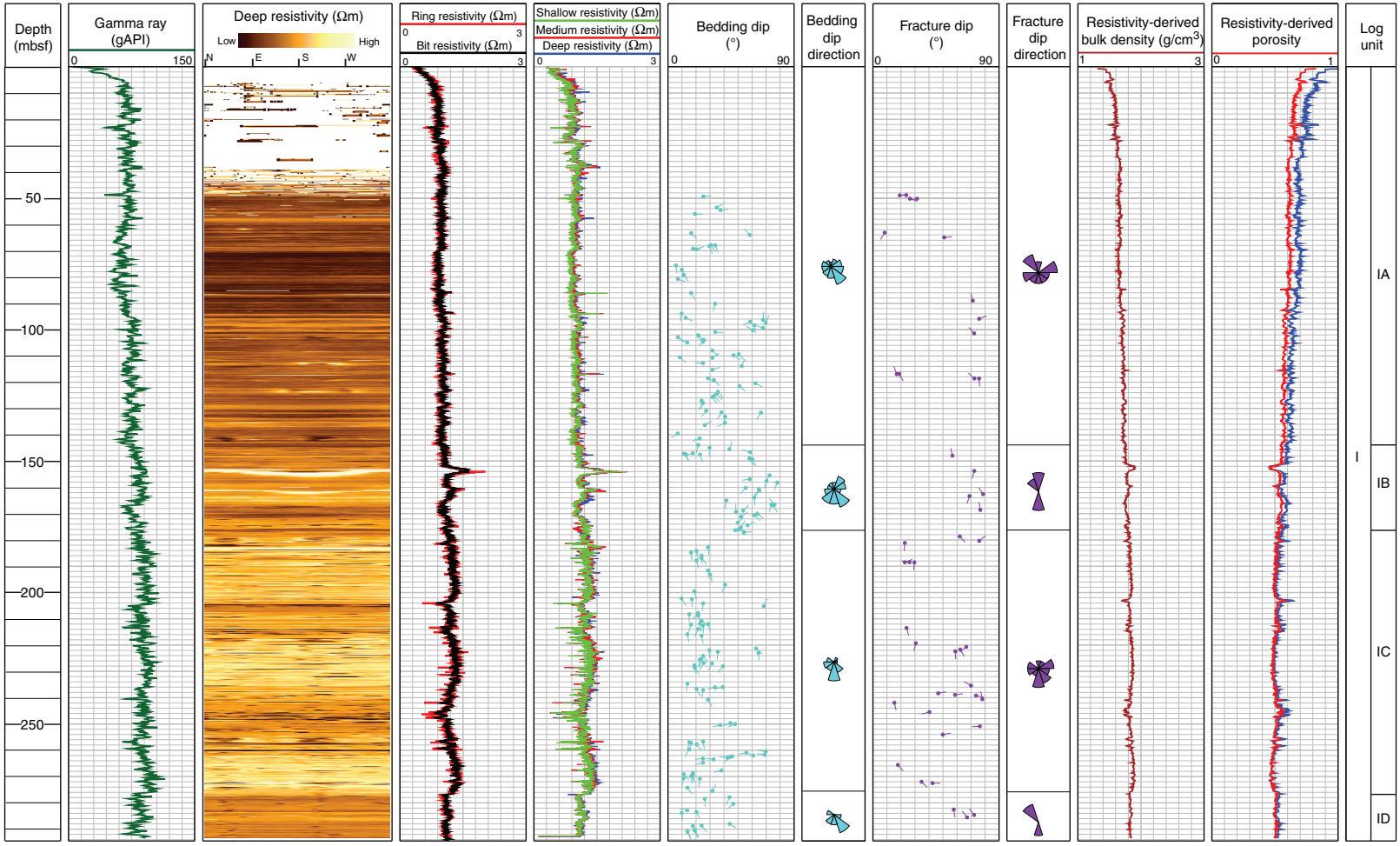

Figure F21. Core-log-seismic integration, Site C0018: LWD data from Hole C0018B, unit boundaries and mass transport deposit (MTD) intervals, seismic data from In-line 2315 (Kumano 3-D PSDM volume; Moore et al., 2009), bedding dips, and medium button static resistivity. Core lithologic column is from Hole C0018A (Expedition 333 Scientists, 2012c).

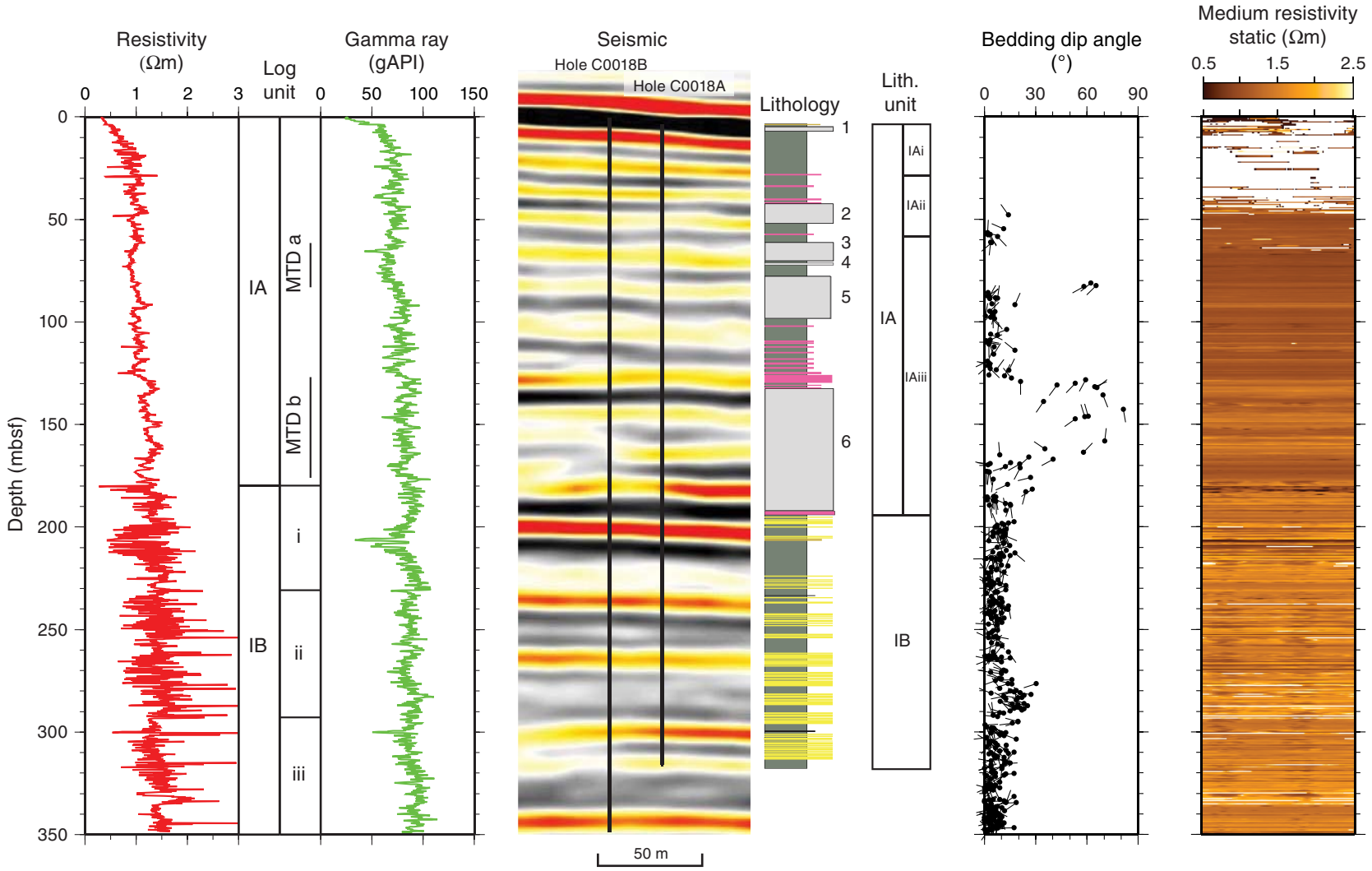

Figure F22. Core-log-seismic integration, Site C0021: LWD data, seismic data from In-line 2270 (Kumano 3-D PSDM volume; Moore et al., 2009), bedding dips, and medium button static resistivity. Dashed lines = correlations discussed in text ("?" = tentative).

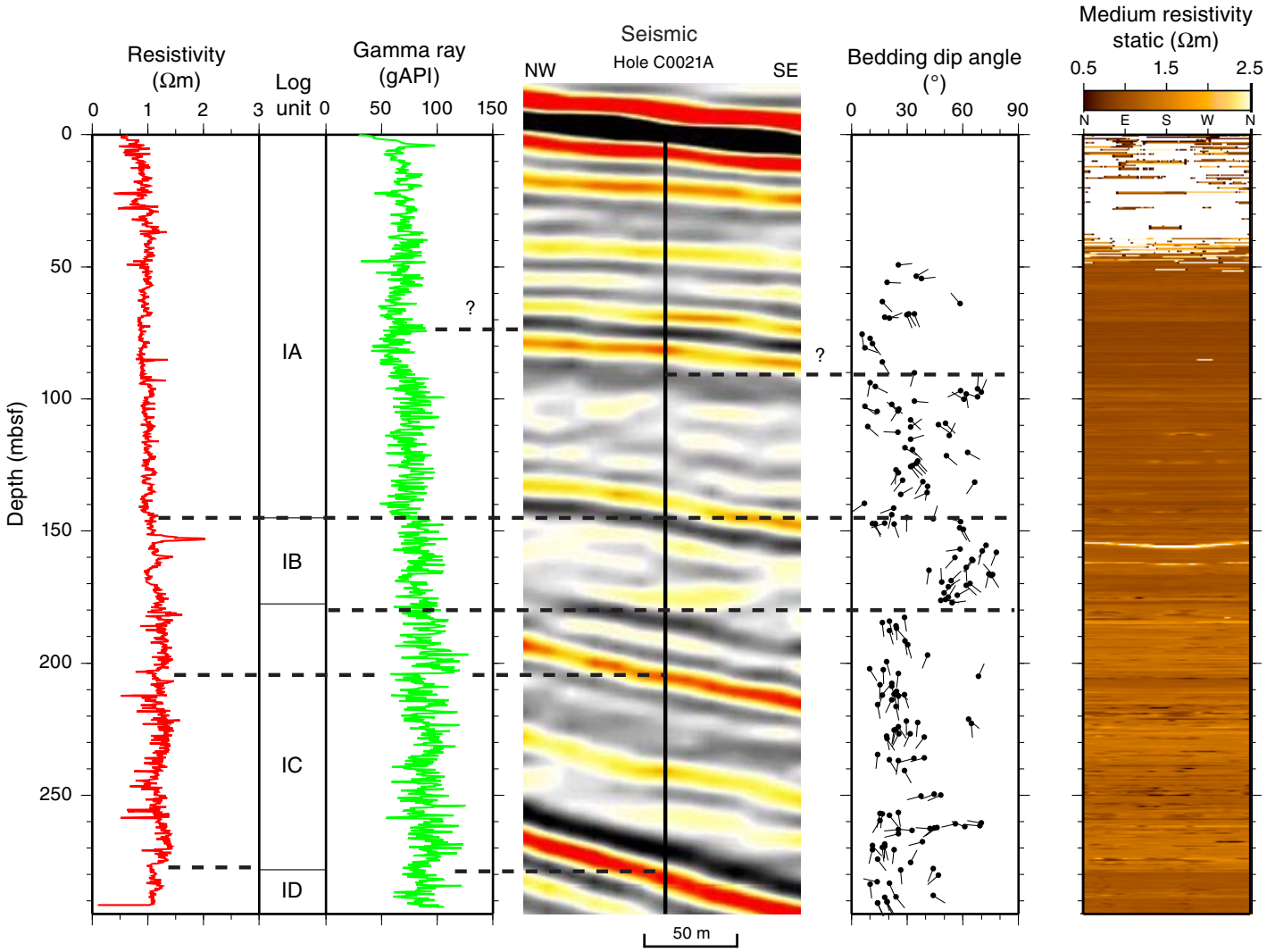

Figure F23. Core-log-seismic integration, Site C0022: LWD data from Hole C0022A, seismic data from In-line 2315 (Kumano 3-D PSDM volume; Moore et al., 2009) with seismic units defined by Kimura et al. (2011), fracture dips, and medium button static resistivity. Core lithologic column from Hole C0022B (see **"Lithology"**). Dashed black lines = correlations ("?" = tentative), shaded box = fault and wider deformation zone, identified from fractures in resistivity images and shear zones in cores. FZ = fracture zone.

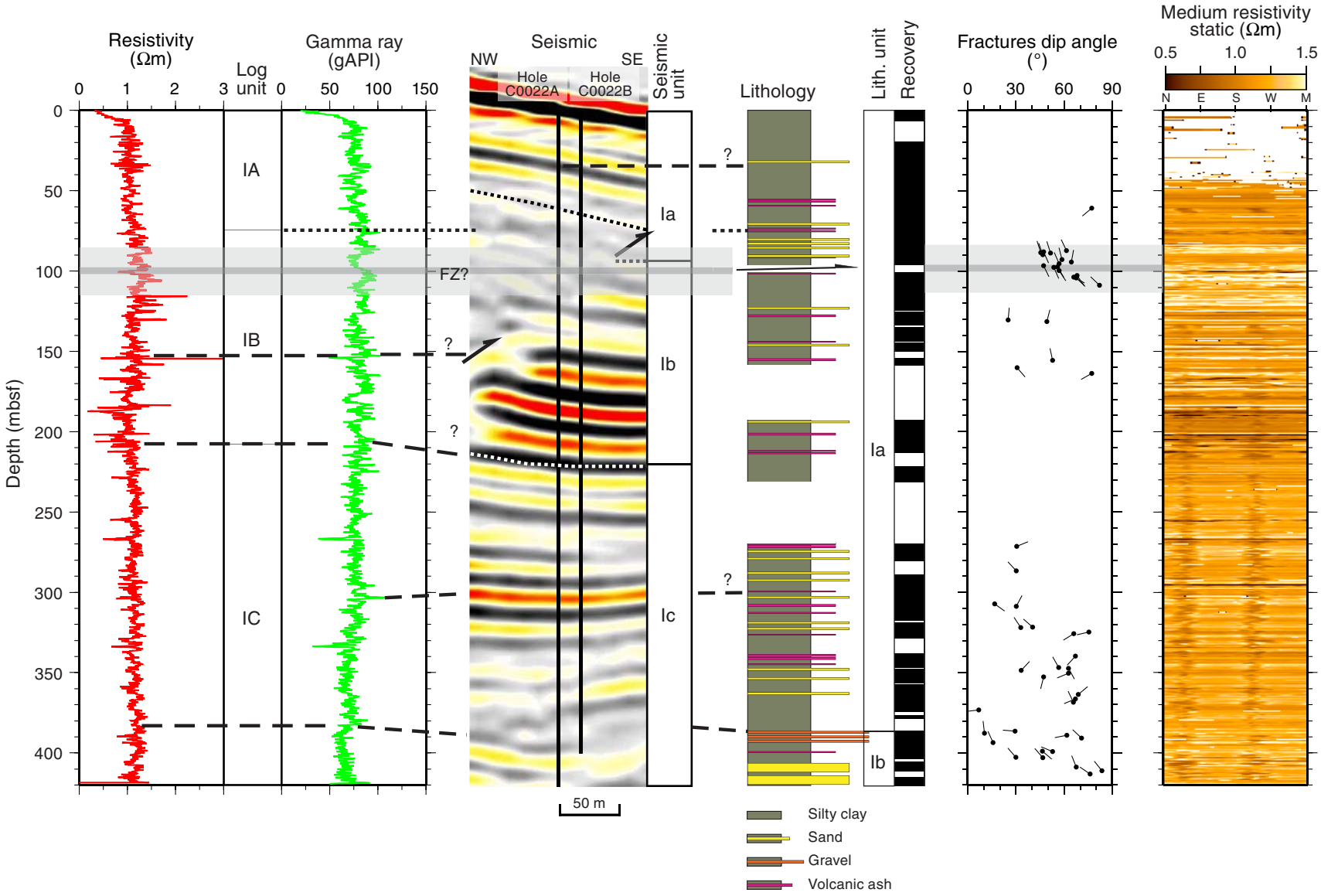

Figure F24. Composite summary of core results, Hole C0022B. Bulk density and porosity are from MAD measurements. Gray shaded zone in the structural geology data corresponds to intervals with dips >15°, including possible location of splay fault (yellow line) as deduced from LWD data in Hole C0022A.

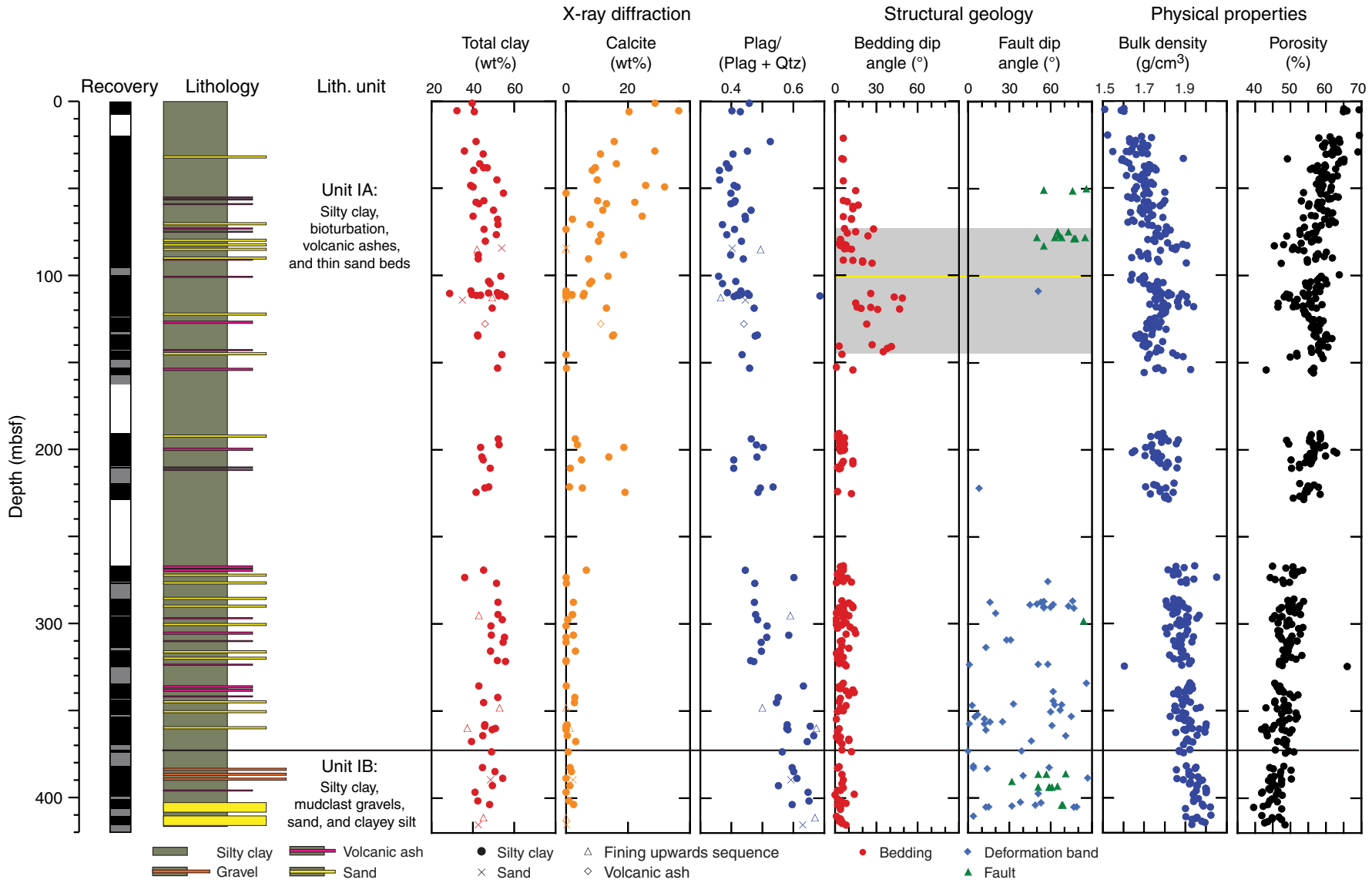

Figure F25. Images of textural and compositional variations of the mud clast gravels. **A.** Gravel of well-rounded pebble-size mud clasts (interval 338-C0022B-38X-4, 115.5–132.5 cm). Possible cobble of brownish silty clay is labeled. Arrows = compactional deformation of a clast that suggests the presence of contrasting hardness among the gravel population. **B.** Granule-size mud clast gravel (interval 338-C0022B-38X-2, 56–62 cm) [top of Unit II]). **C.** Mud clast pebbles distributed along possible erosion surfaces (dashed yellow lines; possible lag layers) (interval 338-C0022B-38X-5, 8–19 cm).

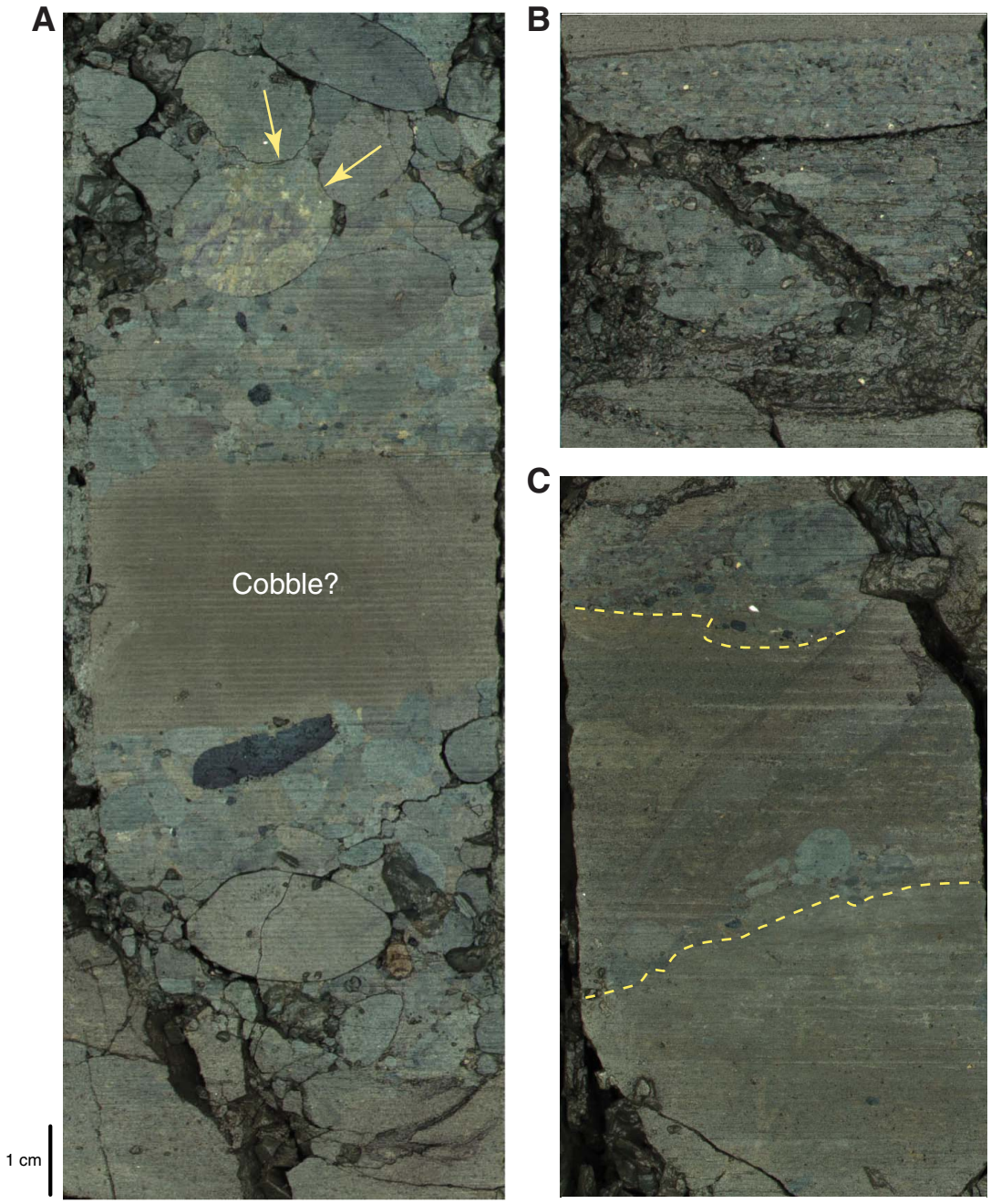

Figure F26. Interstitial water geochemistry, Hole C0022B showing lithologic units. Shaded zone = highly fractured interval of 85–105 mbsf.

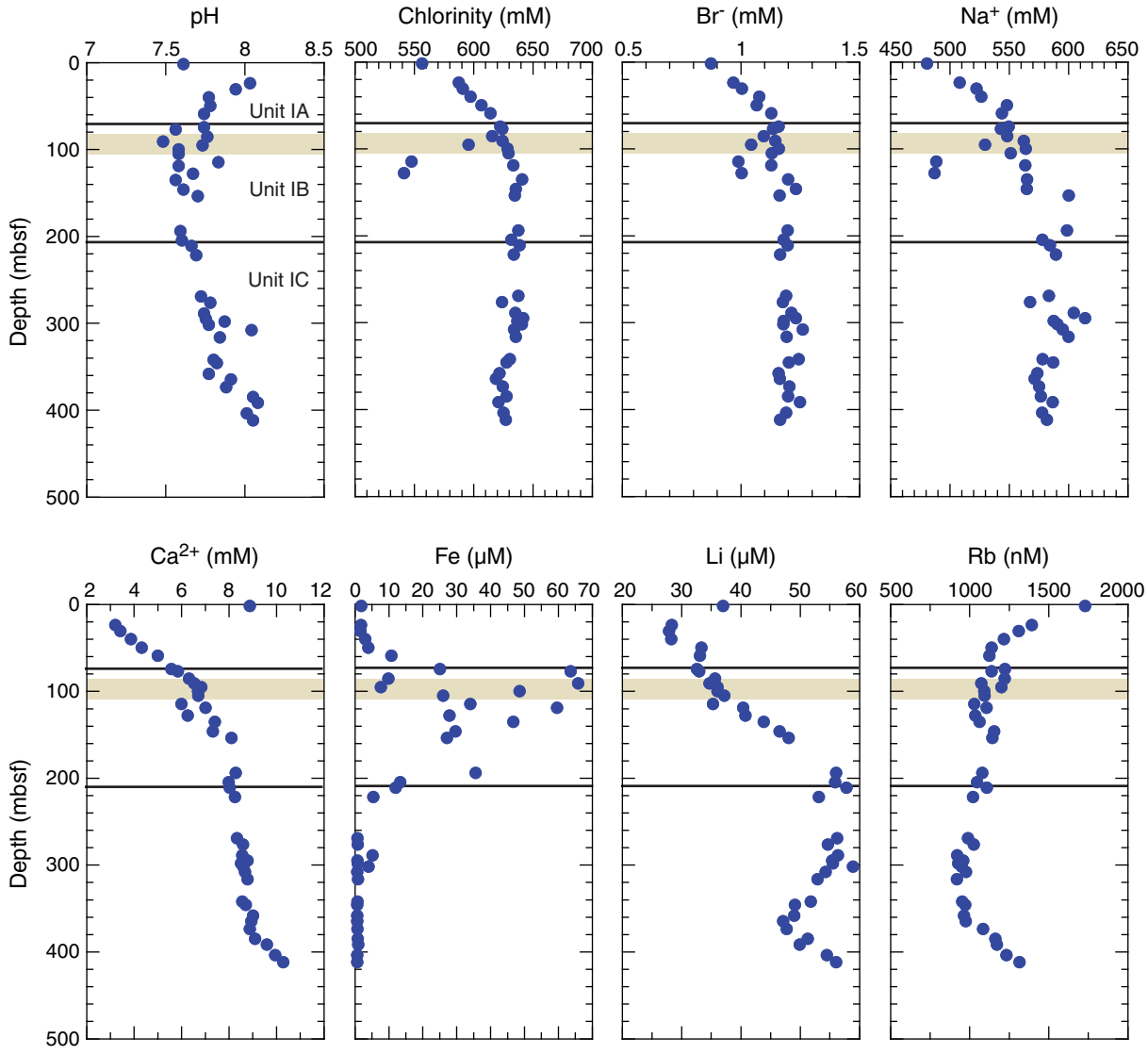

Figure F27. Headspace gas profiles of methane, ethane, and propane, Hole C0022B. Horizontal black lines = lithologic unit boundaries.